Choreographing Dynamical Systems

A thesis presented

by

Hongyi Li

to

The Division of Engineering and Applied Sciences
in partial fulfillment of the requirements
for the degree of

Doctor of Philosophy
in the subject of

Engineering Sciences

Harvard University
Cambridge, Massachusetts

May 2004

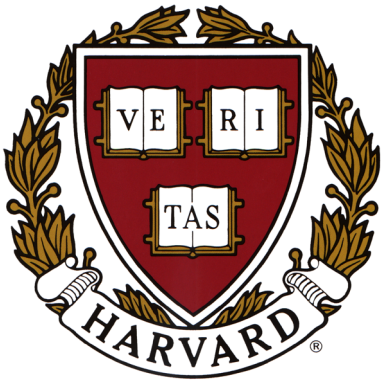

Copyright © 2004 by Hongyi Li. All rights reserved.

Hongyi Li

Professor Roger W. Brockett

Choreographing dynamical systems

Abstract

In this thesis, we address problems relating to the control of motion of dynamical systems from a language point of view. We extend previous works on motion description languages to incorporate systems with momentum. We provide a mathematical foundation for designing control systems that are able to generate motions according choreographic scripts. A useful class of language elements is constructed using phase space specifications of the input space suitable for a second order single pendulum system. We build an experimental apparatus, the HRL single and double pendulum, to test our ideas. A wireless communication module is used to connect the angular position sensors with the host computer such that the pendulum rotates unconstrained. Taking the physical bounds of the control signals into account, a swing-up control of the single pendulum is designed and tested with the experimental apparatus. We compute the region of attraction for unstable, linear control systems with bounded inputs. We formalize the low gain control as an optimization problem and then provide a gradient algorithm searching for local minimal. We presents the linearization problem as an optimization problem for which a linear system and a nonlinear feedback control are selected simultaneously so as to minimize the distance between the nonlinear system with nonlinear feedback and the linear system in a given neighborhood of an equilibrium. Applying this linearization method to the HRL double pendulum, we successfully stabilize it at its up-up position.

To my parents, Shufang Liu and Sheng Li.

Acknowledgments

First, I would like to express my sincere thanks to my thesis adviser, Professor Roger W. Brockett. His passion for research, broad interests, rigorous approaches have guided me through my five-year graduate study at the Harvard Robotics Laboratory. Without his push I would not have finished this thesis. I would also like to thank my thesis committee: Professors Aleksandar Kavcic and Navin Khaneja not only for their evaluation of this thesis, but also the intellectual qualities they and their students brought to the Harvard Robotics Laboratory.

I must also acknowledge the help and support of fellow students and friends. The fellow and former members of the Harvard Robotics Lab have created an environment that was friendly and inspiring. Discussions with colleagues in the office were very helpful in bringing fresh ideas to this work. I would specially like to acknowledge the friendship and support of Manuela Vasconcelos, friendship and collaboration of Magnus Egerstedt and members of the HRL pendulum team: Sam Pfister, Stan Jurga, Drew Carlson, and Richard Hopkirk. I would like to thank Benjamin Pierce and Jason Adaska for their friendship and proof reading my thesis draft. There are of course many more names, too many to distinguish individually. So I thank all of them for five great years: Dimitrios Hristu, Kristi Morgansen, Mark Hoefer, Michael Brody, Aleksandr Rabiner, Michael McElroy, Jian Zou, Su Ying Quek, Mohamed Ali Belabbas, Abdol-Reza Mansouri, and Mark Byrd. I would also thank my friends in the division and in town: Ce Wang, Hanming Rao, Shaohua Yang, Wei Zeng, Guangli Liu, Tong Liu, Yu Sheng, Chen Xin, and Haitong Yang. Special thanks to Ruxiang Chuan and Shengde Lung for making me feel at home in Boston. Thanks Kathleen Lafrance for all help from you.

Finally, I would like to thank my family and relatives, whose love and support have accompanied me throughout my life. Support from my nephews and niece, cousins, aunt and uncles is tremendous. My grandmother's wisdom has benefited me a lot. Brothers and sisters, glad to be with you all while growing up. My father, who is an example of hard working and perseverance through intense adversity. My mother, who shows me caring and patience. Mom and dad, thanks for feeding me up with cookies and love in hungry and dark days, this thesis is dedicated to you.

Contents

List of Figures

Chapter 1

Introduction

The long range goal of the research initiated here is to develop a methodology for symbolic control of dynamical systems that would be appropriate for both animal motion control and robotics. This lofty statement hides many details and, in fact, seems to be highly problem dependent. If we are to have a sound basis for generalization, it is necessary to dig deeply into significant special cases involving nontrivial dynamical effects, limits on the controls, sensor inaccuracies, etc., if we are to have a sound basis for generalization. Although in this thesis we limit ourselves to a detailed description of a specific family of mechanical systems, we will show how a hybrid control strategy provides a natural solution to a class of bounded input control problems. We apply our results to control a pendulum to an upright, inverted position by injecting energy into the system. Once at the inverted position, a locally stabilizing controller is used for stabilizing the system around the inverted position in the presence of control bounds.

This represents a radically new area of theoretical control, the possibilities of which have only recently begun to emerge from the application of high-speed computer control to dynamically unstable systems. The importance of such work can be gauged by examining the large number of examples found in biology and mechanics. Human beings walk by shifting from one unstable state to another. Forward swept wing airplanes, such as Grumman X-29 and Sukhoi S-37, are dynamically unstable and would crash without computerized flight control system. The lowest energy trajectories for lunar exploration and the more general "fly by" trajectories for space exploration also have this flavor. Our goals here are somewhat more ambitious. We investigate the design of a control system that makes it possible to follow trajectories that visit, in sequence, oscillations, stable or unstable equilibria so as to accomplish a task. Our system facilitates the choreography of such systems.

In perusing this research, our mode of operation involves theory, experiment, and software architecture. This thesis describes both the type of theory and the type of experimentation we have done. The development of the software architecture is not discussed here.

The inverted pendulum control has been widely used in control laboratories to demonstrate the effectiveness of control theory and algorithms. The dynamics of the inverted pendulums are complex enough to yield a rich source of nonlinear control problems, yet simple enough to permit considerable mathematical analysis. In the literature of control of inverted pendulums, Furuta's group has a long list of experimental results, see e.g. Furuta et al. (1978, 1980); Yamakita et al. (1993, 1995); Åström and Furuta (1996). Furuta et al. (1978) successfully stabilize a double inverted pendulum at the upright position by using computer control. The controller consists of state feedback and an observer based on its linearized model. Furuta et al. (1980) stabilize a double inverted pendulum on a cart where the cart is placed on an inclined rail. Furuta et al. (1984) stabilize a triple inverted pendulum by introducing redundant controls. One motor is mounted on each of the two upper joints respectively. Yamakita et al. (1993, 1995) swing up a double pendulum by means of a combination of feedforward and feedback controls. The control strategy from the down-down position to the up-up one is a feedforward input until the pendulum reaches the upright position at which point the control is switched to a linear feedback control law around the upright position. Åström and Furuta (1996) and Åström (1999) introduce an energy based swing up strategy. The idea is to define a general energy function for the vertical link of the pendulum, then pick the sign of the control so as to increase the general energy of the pendulum. When the energy is in a certain range, the system evolution will bring the vertical link to the up position.

There is a large literature on the control of pendulums, but we can only mention a few examples here. The pendulum system is not exact feedback linearizable, see Brockett (1978)'s condition for exact feedback linearization. Spong (1995) uses partial feedback linearization and analysis of zero dynamics to swing up an acrobot. He chooses a feedback and state transformation procedure to move all the nonlinear terms to one of the system equations. Wei et al. (1995) stabilize a pendulum using a controller with arbitrarily small horizontal travel. Chung and Hauser (1995) design a swing-up controller by regulating the swing energy while providing internal stability. Angeli (2001) presents a continuous state feedback law for almost global stabilization of an inverted pendulum on a cart. Zhao and Spong (2001) give a hybrid control for global stabilization of the cart-pendulum system. The problem of stabilizing a triple inverted pendulum in experiments has been studied

by Furuta et al. (1984); Meier (1990). They simplify the problem by using two motors to provide the control inputs. Eltohamy and Kuo (1997, 1998) stabilize a triple inverted pendulum with single control input. They use a nonlinear optimal controller design to find a linear feedback law.

Brockett's Motion Description Language (MDL) provides a formal basis for robot programming using behavior, and, at the same time, permits incorporation of kinematic models of robots given in the form of driftless differential equations, Brockett (1988a,b, 1990, 1994b). Behaviors for robots are formalized in term of a kinematic state machine with real-time information from sensors. This formalization allows us to create a mathematical basis for the study of such systems. At its highest level of abstraction, motion control can be viewed as the generation of symbolic inputs to a control system based on sensory information about its current state, desired state, and the state of the environment. These symbolic inputs can be commands such as "move forward", "turn left", "stop". Along with sensor information, these inputs can then be used to generate more complex behaviors such as "go to the refrigerator and get a cup of milk".

Manikonda et al. (1998) extend Brockett's MDL to MDLe (e for extension). The structure of the language MDLe allows descriptions of triggers (generated by sensors) in the language. Feedback and feedforward control laws are selected and executed by the triggering events. These triggers can be viewed as interrupts in CPUs. MDLe is particularly well suited to the demands nonholonomic path planning with limited range sensors. The atoms in MDLe are of the form (u, ξ, T) where the trigger $\xi : Y \longrightarrow \{0, 1\}$ is a Boolean function.

Murray et al. (1992) define robot control primitives. It provides a graph theoretic formalism (tree structure) that codifies the description and control of hierarchically organized robots in contact with their environments. Three primitives are "define", "attach" and "control". Robots are dynamical systems that are recursively "defined" in terms of the properties of their daughter robot nodes. The "attach" primitive reflects geometrical constraints among variables and yields another robot object which accomplishes coordinate transformations. The "control" primitive seeks to direct a robot object to follow a specified desired position/force trajectory using some control algorithm. This approach has a structure which is similar to object oriented programming languages, such as C++.

Neurobiological control systems make computations and exercise control over the motion of animals using methods that are still largely unknown. The available methods for treating nonlinear systems often fail for the type of pulse-like signals that play a dominant role in neurobiological systems. Some aspects of pulse driven systems can be studied by a

topological method, see Brockett (1992, 1994a, 1995). Pulse space is defined as a subset of phase space. Systems driven by pulses respond discretely to pulse-like continuous input. For example, consider the system $\dot{x} = -\sin(x) + u$. By appropriate selection of the pulse space, the state x will increase by 2π after each pulse input.

This thesis arose from the study of Motion Description Language (MDL) and pulse driven dynamical systems as described by Brockett (1988a,b, 1990, 1992, 1994a,b, 1995), as well as the study of pendulum control by Furuta et al. (1978, 1980); Yamakita et al. (1993, 1995); Åström and Furuta (1996); Åström (1999). Language based control deals with systems which are mostly quasi-static. This thesis is an attempt to go beyond the quasi-static domain. We adapt MDL to dynamical systems to facilitate choreography applications. We refer to this adaption as Dynamical Motion Description Language (DMDL). DMDL is a context sensitive language while MDL is context free. A single/double pendulum is built to demonstrate the theory we developed. A radio link connection is used to transfer sensor data to the host computer. We developed a new type of linearization to deal with local stabilization in a lightweight structure having limited control torque.

The following contributions are contained in this thesis. In Chapter 2 a dynamical motion description language (DMDL) is devised. The study of the control of unstable mechanical systems is quite challenging, involving difficult problems caused by limited communication rates, quantization errors, and parasitic dynamics. Trajectories following problems addressed here in a novel way, are particularly difficult and had heretofore not been investigated in a language context. We contrast kinematics with dynamics, MDL with DMDL, and Aristotle $mv = F$ with Newton $m\dot{v} = F$. We define the language atoms of DMDL based on the partition of trajectory space (function space) generated by the state space. Useful descriptions of language elements are defined in the phase space instead of the time domain.

Chapter 3 is about the experimental apparatus and its mathematical model. We built the pendulum system to test our ideas. The integration of electrical and mechanical devices itself is a very productive area of research. At Harvard Robotics Lab (HRL), we developed a vision-based circular single pendulum driven by a servomotor. A digital video camera is used as position sensor for the vertical link. We also built an electrostatic resolver-based circular double pendulum driven by a servomotor. In order to measure the angular positions of the two vertical links, a rotary electrostatic resolver is mounted on each of the joints of the vertical links. The resolvers measure the absolute angular positions and output analog signals. The analog signals are then converted into binary digital data. The

digital data is sent to the host computer through a RS232 radio link. Interesting problems arise concerning ways to increase data rate without increasing delay time. A small packet radio link protocol is used for this purpose. Power consumption, size and weight are also reduced.

In Chapter 4 we discover that good local stabilization is very important in the case where the state space contains unstable equilibria. We show that a hybrid or multi-modal control strategy provides a natural framework for the control of unstable systems. Here we study a single pendulum that we bring to an upright, inverted position by a carefully designed control sequence. The control sequence repeats a four-pulse pattern. It is shown that the energy of the vertical link is increased at the end of each four-pulse pattern while the horizontal link remains at the original position. Once at the inverted position, a locally stabilizing controller that consists of both a closed-loop and an open-loop component is used for stabilizing the system around the inverted position. Experimental results show that our method is practically as well as theoretically sound.

In Chapter 5 a new theory is derived to make stabilization work in a lightweight structure having limited control torque. Stabilization is one of the most important problems in the control of dynamical systems. In most cases, a global stabilization control law is hard to find or does not exist at all (e.g. inverted pendulum). However, in some cases, a local stabilization control law can be constructed. In this case we want the region of attraction to be as large as possible. A new type of linearization method, which we call feedback linear approximation, is derived in studying local stabilization. Here feedback is used to reduce nonlinearities of the original system. The average difference in a given region between the original system and its linear counterpart is minimized. Then a low gain controller design is used to enlarge the domain of attraction. The family of candidate controllers is parameterized. The desired controller is found through a gradient algorithm in the parameter set of candidate controllers. The results are successfully demonstrated in stabilizing the HRL double inverted pendulum.

Chapter 6 applies the theory developed in Chapter 2 to the experimental apparatus described in Chapter 3. It includes stabilization of the HRL double pendulum at its four equilibrium points, generation of periodic orbits, and a transfer from an equilibrium point to a periodic orbit.

Chapter 2

DMDL for choreography

In this Chapter, we describe the mathematical foundation for designing a control system that processes choreographic scripts. The interaction of discrete and continuous objects is one of the fundamental difficulties encountered in application digital computing to understanding or control of physical systems, Brockett (1992). To illustrate, consider controlling a vehicle on Mars from a base station on Earth. It is not a good idea to send a detailed analog command specifying the motor torque or velocity at each time spot, due to the time delay and the limited channel capacity. It is better to send high-level discrete commands such as "move", "turn", "stop", or composite commands such as "avoid the rock". Along this line Brockett defined a language for Kinematic machines, called Motion Description Language (MDL), Brockett (1988a, 1990). Later, Krishnaprasad's group at University of Maryland extended MDL to incorporate interrupts from sensors, which they refered to as MDLe, Manikonda et al. (1998). Sastry's group at UC Berkeley took a graph theoretic approach to the motion control of robots, which they called control primitives. Its structure is similar to object oriented programming languages, such as C++, Murray et al. (1992). It is of equal importance to investigate the inverse problem. Namely, how does one use analog inputs to generate a discrete motion (an element of a cluster of trajectories sharing a number of common properties)? For example, when we speak the word "hello", we produce an acoustic trajectory with time index. If it is close in some metric to the 'normal' acoustic trajectory of "hello" we can recognize the word correctly. Brockett's pulse driven dynamical systems captures this property. A pulse space is defined as a subset of the phase space. The corresponding dynamical system changes discretely under pulse inputs. An analog counter is defined as a pulse driven dynamical system, Brockett (1992).

2.1 Introduction

Kinematic machines are models of the form

$$\dot{x} = G(x)u; \quad y = h(x)$$

where u, x, and y are functions of time. The input u is subject to some regularity condition, say u belongs to the set of m-dimensional bounded piecewise continuous functions U. x has its range in n-dimensional state coordinate space X. y has its range in p-dimensional output space Y. G is a $n \times m$ matrix that depends only on x. $h : X \longrightarrow Y$ is an actuator-to-output coordinate map. The symbolic inputs are called atoms. The atoms of the MDL are triples of the form (u, k, T). If at time t_0 the machine receives an input string (u_1, k_1, T_1), $\cdots$, (u_i, k_i, T_i) , the state x evolves according to

$$\begin{array}{lll} \dot{x} = G(x)(u_1 + k_1(y)); & y = h(x); & t_0 \le t \le t_0 + T_1 \\ \vdots & \vdots & \vdots \\ \dot{x} = G(x)(u_i + k_i(y)); & y = h(x); & t_0 + T_1 + \cdots T_{i-1} \le t \le t_0 + T_1 + \cdots + T_i \end{array}$$

where $k : Y \longrightarrow X$ is a feedback function belonging to a function space K, Brockett (1988a).

The theorem of the completeness of MDL is called expressiveness of Affine Modal Segments in Brockett (1988b). In order to be able to implement a system, which interprets a family of atoms, it is necessary to index the possible atoms in a finite way. A natural choice is to take an affine linear form. By an *affine atom* we understand that (u, k, T) is of the form

$$\begin{bmatrix} v_1 \\ v_2 \\ \vdots \\ v_m \end{bmatrix} = \begin{bmatrix} u_1 \\ u_2 \\ \vdots \\ u_m \end{bmatrix} + \begin{bmatrix} k_{11} & k_{12} & \cdots & k_{1p} \\ k_{21} & k_{22} & \cdots & k_{2p} \\ \vdots & \vdots & \vdots & \vdots \\ k_{m1} & k_{m2} & \cdots & k_{mp} \end{bmatrix} \begin{bmatrix} y_1 - d_1 \\ y_2 - d_2 \\ \vdots \\ y_p - d_p \end{bmatrix}$$

with the u_i, k_{ij}, d_i, and T all being real numbers.

Theorem 2.1.1 (Brockett). *If G is continuous functions of x whose components satisfy a Lipschitz continuity condition, then affine atoms can be used to generate an arbitrarily good approximation to any curve, which the mechanism is capable of generating.*

Proof. Let $\bar{x}(t)$ be any solution of

$$\dot{x} = G(x)\bar{v}(t).$$

The standard Euler approximation to this solution, obtained by solving the difference equation

$$x(nh+h) = x(nh) + hG(x(nh))\bar{v}(nh),$$

converges to the true solution $\bar{x}(t)$, as step size h goes to zero. Let $u_i = \bar{v}(ih)$, $k_i = 0$, and $T_i = h$ we get a system which approximates the original system just like the Euler approximation. As h goes to zero, the solution of the system driven by the (u, k, T)'s approaches the original solution $\bar{x}(t)$. ■

Pulse space and pulse driven systems are studied in Brockett (1992). It appears that in many cases neurobiological systems communicate by means of pulses rather than bilevel signals. One can attempt to define a pulse by imposing specifications directly on the functions of time. However, because of the character of pulse trains and the processes that generate them, it seems to be more efficient to characterize pulses in term of differential inclusions. This means, we put constraints on u and $\dot{u}$ and possible higher order derivatives. In this paper an example of a **double annulus** model of pulse space is constructed. The dynamical system

$$\dot{x} = -\sin(2\pi x) + u; \quad x(0) = 0$$

can count the number of pulses defined by the above pulse space.

2.2 Definition of DMDL

The MDL deals with kinematic systems. The differential equations for a kinematic system have no drift term (i.e. no inertia). However, most physical systems have inertia. They are described by differential equations with drift terms, called dynamical systems. A dynamical system can be approximated by a kinematic system only when its moment of inertia is small and its velocity is low. The language, which deals with dynamical systems, is called Dynamical Motion Description Language (DMDL).

Let's define a control system in the following way. Let X be a n-dimensional differentiable manifold. Let

$$\dot{x} = f(x, u), \quad x \in X \tag{2.1}$$

be a control system on X. By saying a control system can be choreographed, we mean that the system can accept a language as input, and outputs a trajectory choreographed as dictated by the language. In its most narrow sense, the language is a collection of strings of atoms. Each atom describes a cluster of trajectory segments.

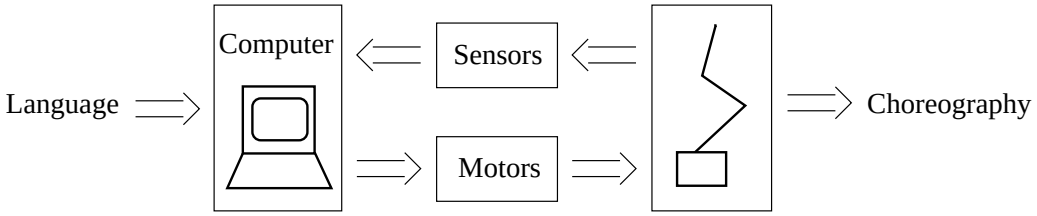

Figure 2.1: A typical control system

A typical diagram of such control system is shown as Figure 2.1. In order to interpret a language, we need to define equivalence classes of trajectories using a certain equivalence relation. These equivalence classes will be our atoms. One can define such equivalence relation based on homotopy.

Definition 2.2.1 . *A feasible trajectory is a trajectory, which can be generated using a feasible control function. An equivalence class of trajectories is a collection of feasible trajectories, which can be deformed from one to another continuously. An atom is a symbol, which defines an equivalence class of trajectories.*

Given a control system with k isolated equilibrium points $p_1, p_2, \cdots, p_k$. Possible atoms include:

- Stay at equilibrium p_i for time t_i,
- Moving around submanifold p_i of type l_i,
- Change from p_i to p_j of type l_i,
- circling around p_i, or a cluster of equilibrium points $p_{i_1} \to p_{i_2} \to \cdots p_{i_s} \to p_{i_1}$.

We can also consider discretization of a function space instead of the state space. The discretization should be fine enough to capture any interesting topology on the function space. First, let's define the trajectory space as

$$\mathcal{S} = \{x([0,T]) | \dot{x} = f(x,u) \quad \text{for some } x(0) = x_0 \text{ and some } u(t) \in \Omega \quad \text{for } t \in [0,T]\}.$$

Thus an element $x([0,T]) \in \mathcal{S}$ can be identified by pair $(x_0, u([0,T]))$ with $u(t) \in \Omega$ for $t \in [0,T]$. It maybe happen that two different $u([0,T])$'s result in same trajectory $x([0,T])$ Thus $\mathcal{S}$ is a subset of $X \times \Omega[0,T]$. In general, $\mathcal{S}$ is a function space of infinite dimension. The motion control problem is then to find an appropriate $u([0,T]) \in \Omega$ and/or initial state $x_0 \in X$ to generate the desired trajectory $x([0,t]) \in \mathcal{S}$. In choreography, we do not need to

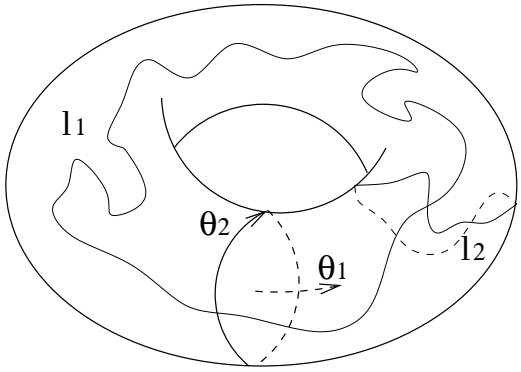

Figure 2.2: Alphabets on a torus

generate a trajectory $x([0,T])$ precisely. We want to reduce the problem to a problem in a finite dimensional space or finite state space. Thus we need to define alphabets on set $\mathcal{S}$.

Definition 2.2.2 . *An* **atom** l *is a subset of trajectory space* $\mathcal{S}$. *An* **Alphabet** $\mathcal{A} = \{l \,|\, l \subset \mathcal{S}\}$ *is a collection of atoms which partitions* $\mathcal{S}$. *We can also say, alphabet* $\mathcal{A}$ *is a quotient space of trajectory space* $\mathcal{S}/\sim$ *where '*$\sim$*' is the equivalence relation defined by the atoms* l*'s. A* **language** $\mathcal{L}$ *is subset of* $\mathcal{A}^*$ *containing empty set* Φ, *where* $\mathcal{A}^*$ *is the free monoid over* $\mathcal{A}$. *We say alphabet* $\mathcal{A}'$ *is* **coarser** *than* $\mathcal{A}$ *(or* $\mathcal{A}$ *is* **finer** *than* $\mathcal{A}'$*) if there is an equivalence relation* $\sim$ *such that* $\mathcal{A}' = \mathcal{A}/\sim$.
Thus we can have a hierarchy structure of alphabets based on coarseness ($\prec$),

$$\mathcal{A}_1 \prec \mathcal{A}_2 \prec \cdots \prec \mathcal{S}.$$

An example. Consider a first order system on a torus $T^2 = S^1 \times S^1$

$$\begin{cases} \dot{\theta}_1 = u_1 \\ \dot{\theta}_2 = u_2, \end{cases}$$

with $(\theta_1, \theta_2) \in T^2$. We can define atoms

$$\begin{aligned} l_1 = &\text{ make a big circle in time } T \ = \{(\theta_1,\theta_2)([0,T])|\, \textstyle\int_0^T d\theta_1 = 2\pi, \int_0^T d\theta_2 = 0\}, \\ l_2 = &\text{ make a small circle in time } T \ = \{(\theta_1,\theta_2)([0,T])|\, \textstyle\int_0^T d\theta_1 = 0, \int_0^T d\theta_2 = 2\pi\}. \end{aligned}$$

They are illustrated in Figure 2.2. More generally, we can define an atom

$$l(\alpha,\beta,T) = \{(\theta_1,\theta_2)([0,T]) \mid \int_0^T d\theta_1 = \alpha, \int_0^T d\theta_2 = \beta\}.$$

Under the atom $l(\alpha, \beta, T)$, the initial and final states are related by

$$(\theta_1, \theta_2)(T) = (\theta_1, \theta_2)(0) + (\alpha, \beta).$$

With a sequence of $l(\alpha, \beta, T)$'s, we can describe almost all the trajectories. Thus we can define an alphabet

$$\mathcal{A} = \{l(\alpha, \beta, T) | \alpha, \beta \in R; \quad T \in R_+\}$$

and a language $\mathcal{S} = \mathcal{A}^*$. Such $\mathcal{S}$ is a finite dimensional language in the sense that $\mathcal{A}$ is homeomorphic to R^3. We can also define a coarse alphabet and languages on the coarse alphabet. For example, define atom

$$l(i, j, k) = \{(\theta_1, \theta_2)([0, k\Delta T]) \mid \int_0^{k\Delta T} d\theta_1 = i\Delta\alpha, \int_0^{k\Delta T} d\theta_2 = j\Delta\beta\}.$$

It captures the properties of state quantization and time discretization.

Consider a simple 2nd order system

$$\ddot{\theta} = u. \tag{2.2}$$

We want to command (2.2) to turn a full circle. Assuming $\dot{\theta}(0) = 0$, we can integrate (2.2) to get the constraint on u to be $x(T) - x(0) = \int_0^T \int_0^t u(\sigma) d\sigma dt = 2\pi$. Then

$$\begin{aligned} x(T) - x(0) &= \int_0^T \int_0^t u(\sigma) d\sigma dt = \int_0^T \int_\sigma^T u(\sigma) dt d\sigma \\ &= \int_0^T u(\sigma)(T - \sigma) d\sigma = \int_0^T u(\sigma) g(\sigma) d\sigma \end{aligned} \tag{2.3}$$

where $g(\sigma) = (T - \sigma)$. By putting a metric $g(t)$ on the input space $\mathcal{U}$, making a full circle in θ space can be down by selecting u such that $\int_0^T u(t) g(t) dt = 2\pi$. $\dot{\theta}(T)$ is still arbitrary. If we want $\dot{\theta}(T) = 0$, then we have another integral constraint, $\int_0^T u(t) dt = 0$. So we need to find candidate solutions from these two constraints.

$$\begin{cases} \int_0^T u(t) g(t) dt = 2\pi \\ \int_0^T u(t) dt = 0 \end{cases} \tag{2.4}$$

Equation (2.4) has at least one solution when g is not a constant. One such u could be a function that has positive value around $t_{max} = \arg\max g(t)$, negative value around $t_{min} = \arg\min g(t)$, and zero elsewhere. For example,

$$u = \begin{cases} \dfrac{\pi}{(g(t_{max}) - g(t_{min}))\Delta t}, & \text{for } t \in [t_{max} - \Delta t, t_{max} + \Delta t], \\ -\dfrac{\pi}{(g(t_{max}) - g(t_{min}))\Delta t}, & \text{for } t \in [t_{min} - \Delta t, t_{min} + \Delta t], \\ 0, & \text{otherwise.} \end{cases}$$

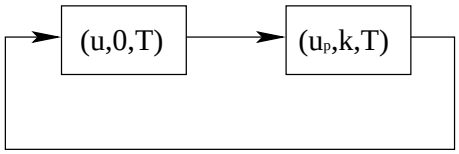

Figure 2.3: Example of the syntax of DMDL

MDL applied to a kinematic machine is a context free language, i.e., any arbitrary string of atoms is in the language. But DMDL is a context sensitive language. We cannot cascade atoms arbitrarily to form a valid string. That is because we need to take the state of the dynamical system into account. One type of *syntax* to form a valid string is to cascade atoms, which share a common stationary point. For example, $(u, 0, T) \longrightarrow (u_p, k, T) \longrightarrow (u, 0, T) \longrightarrow \cdots$, where $(u, 0, T)$ changes the dynamical system from one equilibrium point/periodic orbit to another equilibrium point/periodic orbit and (u_p, k, T) stabilizes the system at one . It changes from one equilibrium point/periodic orbit to another one equilibrium point/periodic orbit ($u_p = 0$ for equilibrium points), shown in Figure 2.3.

2.3 Useful descriptions of language elements

Given a single pendulum, 2nd order system,

$$\ddot{x} + \dot{x} + \sin x = u, \tag{2.5}$$

we want to generate motion by selecting the torque u of the driving motor. The pendulum has two type of isolated equilibria, $(x, \dot{x}) = (2k\pi, 0)$ and $(x, \dot{x}) = ((2k+1)\pi, 0)$, $k \in Z$. The reason to put a damping term in (2.5) is that we want attractive equilibria at $(2k\pi, 0)$ for $k \in Z$. One type of motion we are interested in is to turn a full circle, i.e., change from $x = 2k\pi$ to $(2k+2)\pi$. We are interested in the description of $(u, \dot{u})$ to generate such motion. Suppose the initial state of the system (2.5) is in a neighborhood of $(x, \dot{x}) = (2k\pi, 0,)$, we can use pulse u to reset the initial velocity $\dot{x}$. With the new $\dot{x}$ in a certain range, system will turn a full circle and approach $((2k+2)\pi, \dot{)}$. In order to rest around the new equilibrium $(2k+2)\pi, 0)$, we need to send a negative pulse to bring $\dot{x}$ close to 0. The state x will then rest at the new equilibrium because of its damping term. Figure 2.4 is the sketch of such a u in phase space. It looks like a dumbbell. The following lemma will describe properties

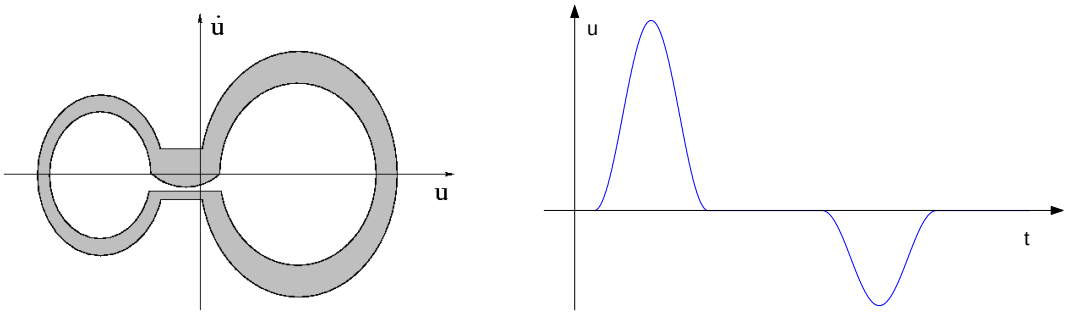

Figure 2.4: Left: Dumbbell phase space. Right: A pulse from the dumbbell phase space.

of pulse generated from the dumbbell phase plot. Let

$$S = (-\alpha_2 - \alpha_3\varepsilon, \alpha_1) \times (-\beta_1\varepsilon, \beta_2\varepsilon)$$

$$d_1(u,\dot{u}) = \begin{cases} 0, & \text{for } u < 0 \text{ or } (u,\dot{u}) \in S \\ 1, & \text{otherwise,} \end{cases}$$

$$d_2(u,\dot{u}) = \begin{cases} 0, & \text{for } u > -\alpha_3\varepsilon \text{ or } (u,\dot{u}) \in S \\ 1, & \text{otherwise.} \end{cases}$$

Definition 2.3.1 *We say that $u : [0,\infty) \to R$ is a dumbbell-pulse train if*

i. $\omega^2\alpha_1^2(1-\varepsilon)^2 < \dot{u}^2 + \omega^2(u-\alpha_1)^2$, *and* $\omega^2\alpha_2^2(1-\varepsilon)^2 < \dot{u}^2 + \omega^2(u-\alpha_2-\alpha_3\varepsilon)^2$, *and* $(u,\dot{u}) \notin [-\alpha_2-\alpha_3\varepsilon, \alpha_1] \times [-\beta_1(\varepsilon-\varepsilon^2), \beta_2(\varepsilon-\varepsilon^2)]$

ii. $\dot{u}^2 + \omega^2(u-\alpha_1)^2 < \omega^2\alpha_1^2$, *or* $\dot{u}^2 + \omega^2(u-\alpha_2-\alpha_3\varepsilon)^2 < \omega^2\alpha_2^2$, *or* $(u,\dot{u}) \in (-\alpha_2-\alpha_3\varepsilon, \alpha_1) \times (-\beta_1\varepsilon, \beta_2\varepsilon)$

iii. $|\ddot{u} + \omega^2 u - \alpha_1\omega^2|d_1(u,\dot{u}) + |\ddot{u} + \omega^2 u + (\alpha_2+\alpha_3\varepsilon)\omega^2|d_2(u,\dot{u}) < \varepsilon$.

Lemma 2.3.1 *(Dumbbell) If $u(\cdot)$ is a dumbbell-pulse train, then:*

i. *The period between successive pulses, T_d, approaches $\frac{4\pi}{\omega} + \frac{\alpha_3}{\beta_1} + \frac{\alpha_3}{\beta_2}$ as ε goes to zero.*

ii. *If $d_k(u(t_1)) = d_k(u(t_2)) = 0$ then the integral*

$$I_k(t_1,t_2) = \int_{t_1}^{t_2} u(t)d_k(u(t))dt$$

approaches $(-1)^{k-1}\frac{2\pi\alpha_k}{\omega}$, $k = 1,2$, times the number of positive and negative pulses in $[t_1,t_2]$ respectively as ε goes to zero.

iii. *If $u(t)$ begins and ends around 0, the time integral*

$$\frac{1}{2\pi}\int \dot{\theta}(t)dt = \frac{1}{2\pi}\int \frac{\ddot{u}(t)u(t) - \dot{u}^2(t)}{u^2(t) + \dot{u}^2(t)}dt$$

is the number of positive (or negative) pulses.

We omit the proof, because it is almost identical to the proof of Lemma 3 in Brockett (1994a). In the region of $d_1(u, \dot{u}) = 1$, u approaches one period of positive pulse $\alpha_1(1 - \cos(\omega t))$ as ε goes to zero. In the region of $d_2(u, \dot{u}) = 1$, u approaches negative pulse $\alpha_2(\cos(\omega t) - 1)$. The two strips in between give the separation time between positive and negative pulses. The 2nd order constraint for the pulse train prevents u from making tiny circles when $|\dot{u}|$ is small. We will find use of this pulses generator in the following theorem and determine those parameters.

Theorem 2.3.1 *Given a 2nd order system*

$$\ddot{x} + \dot{x} + \sin x = u, \quad x(0) = 0, \quad \dot{x}(0) = 0, \tag{2.6}$$

there exist parameters $(\omega, \alpha, \beta, \varepsilon)$ such that any dumbbell-pulse train u will increase x by 2π at the end of each period T_d. More precisely, if $u(0) = u(t_1) = 0$ and $\dot{u}(0) = \dot{u}(t_1) > 0$, then

$$(x,\, \dot{x})(t_1) = (\frac{1}{2\pi}\int_0^{t_1} \frac{\ddot{u}(t)u(t) - \dot{u}^2(t)}{u^2(t) + \dot{u}^2(t)}dt,\, 0) + O(\varepsilon).$$

Proof. We break this problem into four steps. First, we need to reset the initial velocity $\dot{x}$ to a large enough value using a big positive pulse in the region of $d_1(u, \dot{u}) = 1$. Second, We let the system flow by itself, i.e., u is zero or very small which corresponds to the thin strip below u-axis. Third, when $x(t)$ is close to 2π we need to reset $\dot{x}$ to around zero which is done by the small negative pulse in the region of $d_2(u, \dot{u}) = 1$. Last, we let the system flow by itself again corresponding the thick strip above u-axis. See Fig2.5 for the vector field of (2.6) with $u = 0$. The damping term will bring the state to the new equilibrium. The next cycle then starts.

Now we will compute parameters $(\omega, \alpha, \beta, \varepsilon)$ so that the system (2.6) will evolve as expected. Since we don't have the analytic solution to (2.6), we will use an approximation. When $\dot{x}$ is large, we can approximate (2.6) with $u = 0$ by

$$\ddot{x} + \dot{x} = 0 \tag{2.7}$$

We can integrate it to get $\dot{x} + x = const.$ In order to reach point $(x, \dot{x}) = (2\pi, 0)$, we have $\dot{x} + x = 2\pi$. Thus we need $\dot{x}(0) = 2\pi$. We need the large positive pulse u to reset $\dot{x}(0)$. We

can pick a large ω so that the duration of the pulse is very short. Then we can approximate (2.6) by

$$\ddot{x} = u. \tag{2.8}$$

Let $t_1 = \frac{2\pi}{\omega}$. From lemma 2.3.1.ii we then have

$$2\pi = \dot{x}(t_1) - \dot{x}(0) = \int_0^{t_1} u(t)dt = \frac{2\pi\alpha_1}{\omega} + h.o.t.$$

Thus $\alpha_1 = \omega$. Now we need to estimate the time t_2 to reach $x(t_2) = 2\pi$ to get β_1. We can use (2.7) for $x \in [0, \frac{3\pi}{2}]$ and the linearization of (2.6) for $x \in [\frac{3\pi}{2}, \frac{5\pi}{2}]$, i.e.,

$$\ddot{x} + \dot{x} + x - 2\pi = 0 \tag{2.9}$$

With initial $(x(t_1), \dot{x}(t_1)) = (0, 2\pi)$, the solution to (2.7) takes the form of $x(t) = 2\pi(1 - e^{-(t-t_1)})$. At $x(t_{21}) = \frac{3\pi}{2}$, we get $t_{21} = t_1 + \ln(4)$ and $\dot{x}(t_{21}) = 2\pi - x(t_{21}) = \frac{\pi}{2}$. With initial $(x(t_{21}), \dot{x}(t_{21}))$, the solution to (2.9) takes the form of

$$x(t) - 2\pi = e^{-\frac{t-t_{21}}{2}}[-\frac{\pi}{2}\cos(\frac{\sqrt{3}}{2}(t - t_{21})) + \frac{\pi}{2\sqrt{3}}\sin(\frac{\sqrt{3}}{2}(t - t_{21}))].$$

From $x(t_2) = 2\pi$, we get $\tan(\frac{\sqrt{3}}{2}(t_2 - t_{21})) = \sqrt{3}$. Thus

$$t_2 = t_{21} + \frac{2\pi}{3\sqrt{3}} = \frac{2\pi}{\omega} + \ln(4) + \frac{2\pi}{3\sqrt{3}}.$$

Then we need $\beta_1 = \frac{\alpha_3}{t_2 - t_1} = \alpha_3/(\ln(4) + \frac{2\pi}{3\sqrt{3}})$. At t_2, we have $\dot{x}(t_2) = \frac{\pi}{2}e^{-\frac{\pi}{3\sqrt{3}}}$. We need to use the small negative pulse u to bring $\dot{x}(t_2)$ to zero. Combine equation (2.8) and lemma 2.3.1.ii, we have $0 - \dot{x}(t_2) = -\frac{2\pi\alpha_2}{\omega}$. Thus $\alpha_2 = \frac{\omega}{4}e^{-\frac{\pi}{3\sqrt{3}}}$. Then we can select a small enough β_2 so that x will rest at the new equilibrium. Thus, one set of appropriate parameters for the dumbbell-pulse train is

$$(\omega, \alpha_1, \alpha_2, \alpha_3, \beta_1, \beta_2, \varepsilon) = (\omega, \omega, \frac{\omega}{4}e^{-\frac{\pi}{3\sqrt{3}}}, \alpha_3, \alpha_3/(\ln(4) + \frac{2\pi}{3\sqrt{3}}), \beta_2, \varepsilon)$$

where ω is large and $\alpha_3, \beta_2, \varepsilon$ are small. ∎

The dumbbell pulse space has a thin belt below, as shown in Figure 2.4 left. This means dumbbell-pulses are not robust, i.e., they are sensitive to perturbations. To improve on this

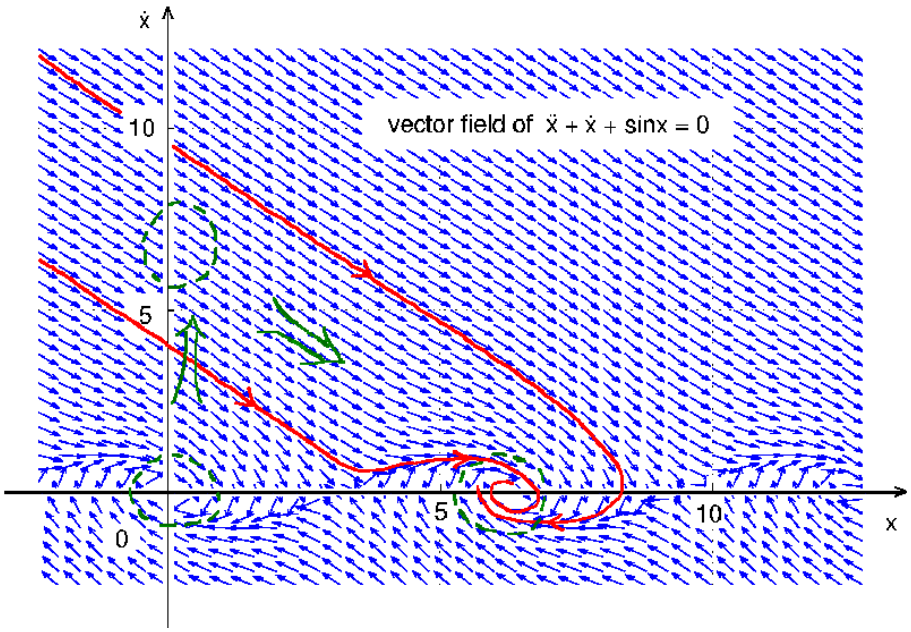

Figure 2.5: Vector field

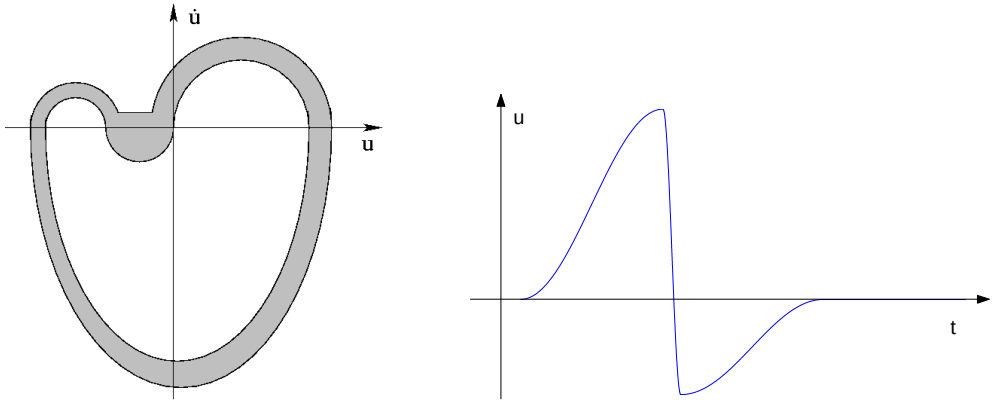

Figure 2.6: Left: Bean phase space. Right: A pulse from the bean phase space.

we construct a bean pulse space that overcomes this shortcoming. Let

$$b_1(u,\dot{u}) = \begin{cases} 0, & \text{for } u<0 \text{ or } \dot{u}<0 \text{ or } (u,\dot{u})\in S \\ 1, & \text{otherwise,} \end{cases}$$

$$b_2(u,\dot{u}) = \begin{cases} 0, & \text{for } u>0 \text{ or } \dot{u}<0 \text{ or } (u,\dot{u})\in S \\ 1, & \text{otherwise.} \end{cases}$$

$$b_3(u,\dot{u}) = \begin{cases} 0, & \text{for } u>0 \text{ or } \dot{u}>0 \text{ or } (u,\dot{u})\in S \\ 1, & \text{otherwise.} \end{cases}$$

Definition 2.3.2 *We say that $u:[0,\infty)\to R$ is a bean-pulse train if*

i. $\omega_1^2\alpha_1^2 < \dot{u}^2+\omega_1^2(u-\alpha_1)^2$ *and* $\omega_1^2\alpha_2^2 < \dot{u}^2+\omega_1^2(u+\alpha_2+2\alpha_3\varepsilon)^2$ *for* $\dot{u}\geq 0$, $\omega_2^2(\alpha_1+\alpha_2+\alpha_3\varepsilon)^2 < \dot{u}^2+\omega_2^2(u-\alpha_1+\alpha_2+\alpha_3\varepsilon)^2$ *or* $\dot{u}^2+\omega_1^2(u+\alpha_3\varepsilon)^2 < \omega_1^2\alpha_3^2\varepsilon^2$ *for* $\dot{u}<0$

ii. $\dot{u}^2+\omega_1^2(u-\alpha_1)^2 < \omega_1^2\alpha_1^2(1+\varepsilon)^2$ *or* $\dot{u}^2+\omega_1^2(u+\alpha_2+2\alpha_3\varepsilon)^2 < \omega_1^2\alpha_2^2(1+\varepsilon)^2$ *or* $\dot{u}^2+\omega_2^2(u-\alpha_1+\alpha_2+\alpha_3\varepsilon)^2 < \omega_2^2(\alpha_1+\alpha_2+(\frac{1}{2}\alpha_1+\frac{1}{2}\alpha_2+\alpha_3)\varepsilon)^2$, *or* $\dot{u}<\beta\varepsilon$ *for* $u\in(-\alpha_2-\alpha_3\varepsilon,\alpha_1)$

iii. $|\ddot{u}+\omega_1^2u-\omega_1^2\alpha_1|b_1(u,\dot{u})+|\ddot{u}+\omega_1^2u+\omega_1^2(\alpha_2+2\alpha_3\varepsilon)|b_2(u,\dot{u})+|\ddot{u}+\omega_2^2u-\omega_2^2(\alpha_1-\alpha_2-\alpha_3\varepsilon)|b_3(u,\dot{u})<\varepsilon$.

Where $\alpha_1,\alpha_2,\alpha_3,\beta,\omega_1,\omega_2,\varepsilon>0$, $2\alpha_3-\alpha_1-\alpha_2>0$, $\omega_2\gg\omega_1$.

Lemma 2.3.2 *(Bean) If $u(\cdot)$ is a bean-pulse train, then:*

i. *The minimal time T_b for a complete pulse approaches* $\frac{3\pi}{\omega_1}+\frac{\pi}{\omega_2}+\frac{\alpha_3}{\beta}$ *as ε goes to zero.*

ii. *If* $b_k(u(t_1),\dot{u}(t_1))=b_k(u(t_2),\dot{u}(t_2))=0$ *then the integral*

$$I_k(t_1,t_2)=\int_{t_1}^{t_2}u(t)s_k(u(t),\dot{u}(t))dt$$

approaches $(-1)^{k-1}\frac{\pi\alpha_k}{\omega_1}$, $k=1,2$, *times the number of positive and negative pulses in $[t_1,t_2]$ respectively as ε goes to zero.*

iii. *If $u(t)$ begins and ends around 0, the time integral*

$$\frac{1}{2\pi}\int\dot{\theta}(t)dt=\frac{1}{2\pi}\int\frac{\ddot{u}(t)(u(t)-\alpha_1)-\dot{u}^2(t)}{(u-\alpha_1)^2(t)+\dot{u}^2(t)}dt$$

is the number of positive (or negative) pulses.

We omit the proof for the same reason as in Lemma 2.3.1.

Theorem 2.3.2 *Given a 2nd order system*

$$\ddot{x} + \dot{x} + \sin x = u, \quad x(0) = 0, \quad \dot{x}(0) = 0, \tag{2.10}$$

there exist parameters $(\omega, \alpha, \beta, \varepsilon)$ *such that any bean-pulse train* u *will increase* x *by* 2π *at the end of each period* T_b. *More precisely, if* $u(0) = u(t_1) = 0$ *and* $\dot{u}(0) = \dot{u}(t_1) > 0$, *then*

$$(x,\, \dot{x})(t_1) = (\frac{1}{2\pi} \int_0^{t_1} \frac{\ddot{u}(t)u(t) - \dot{u}^2(t)}{u^2(t) + \dot{u}^2(t)} dt,\, 0) + O(\varepsilon).$$

The proof is similar to that of Theorem 2.3.1 and is left to reader.

Chapter 3

Experimental apparatus – HRL single/double pendulum

In this chapter, we describe the experimental apparatus used in this thesis. There is a long-standing interest in the control of inverted pendulums, see, e.g., Spong (1995); Åström and Furuta (1996); Åström (1999). The dynamics of the inverted pendulums are complex enough to yield a rich source of nonlinear control problems, yet simple enough to permit a considerable mathematical analysis. In the Harvard Robotics Laboratory, we have built a vision based rotational single pendulum. We then implemented a hybrid swing-up control on the single pendulum, see chapter 4. Later on, we upgraded it to a double inverted pendulum. The vision sensor was replaced by a pair of electrostatic resolvers, which communicate with the computer through a packet based radio link. In chapter 5, feedback linear approximation is used to stabilize the double pendulum at its up-up position. In chapter 6, we describe the implementation of DMDL on the double pendulum.

3.1 Vision-based single pendulum

The experimental apparatus that we use for the experiments consists of a horizontal link, driven by a servo motor, and a vertical link that moves freely in the plane perpendicular to the horizontal link, as shown in Figure 3.1 $\sim$ 3.3. The motor system used is an integrated motion control system with the motion trajectory controller, motor driver electronics, position encoder and motor all contained on one unit. It communicates with the computer using RS-485 at a sample rate 8.3KHz. A $10:1$ ratio gearbox is mounted on top of the motor to increase the torque output. The natural frequency of the free-swinging vertical

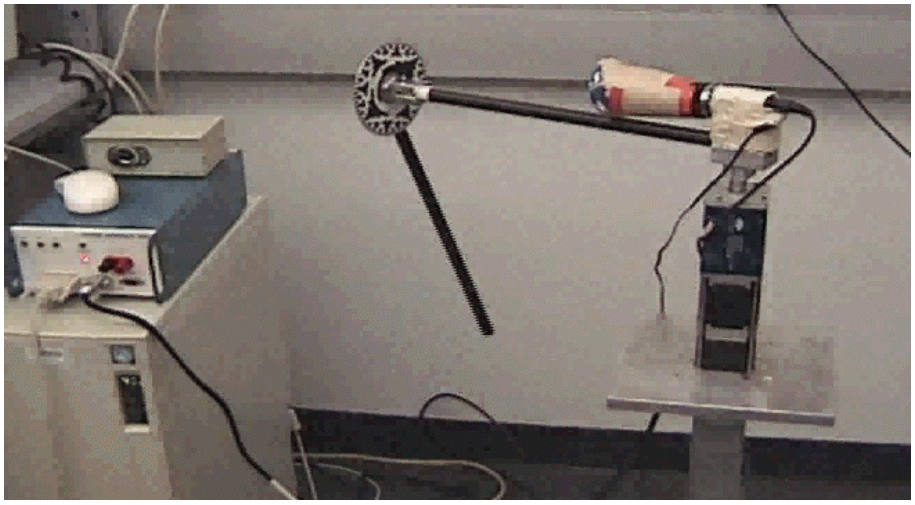

Figure 3.1: The Harvard Robotics Lab single inverted pendulum.

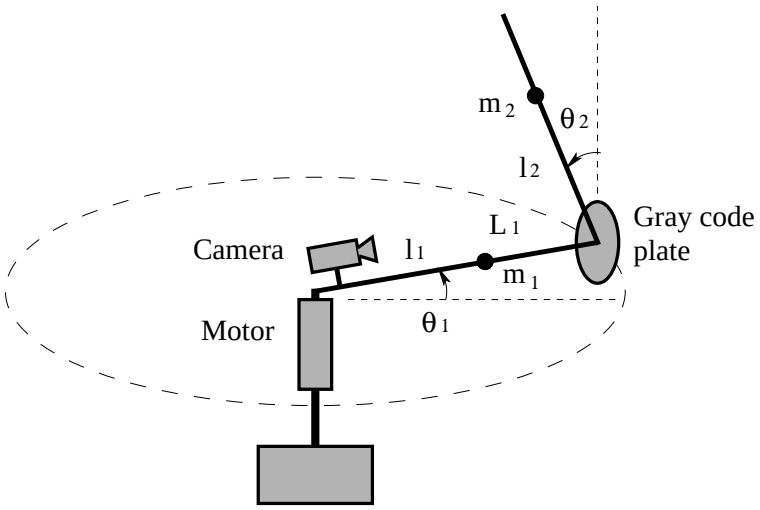

Figure 3.2: A schematic overview of the experimental setup.

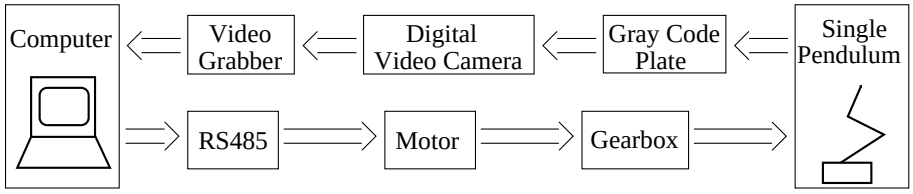

Figure 3.3: Diagram of the vision based single inverted pendulum.

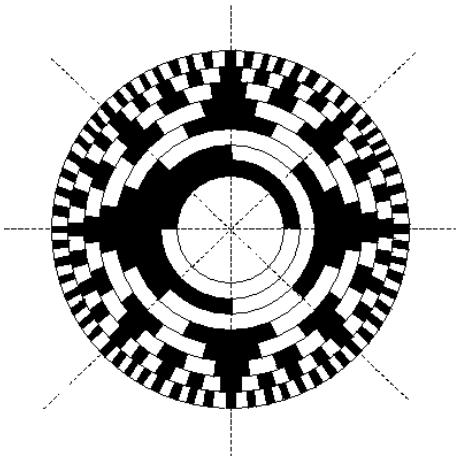

Figure 3.4: The circular disk used for encoding the position of the vertical link.

link is 0.88Hz, and the horizontal link can be controlled at a sample frequency of 60Hz. This is due to the sample rate, 60 frames/sec, of the video camera which is used as a position sensor for the vertical link. The system thus provides us with enough bandwidth for controlling the pendulum.

The Gray code plate

In order to measure the position of the vertical link, a video camera is mounted at the base of the horizontal link, where it grabs images of a circular plate fixed on the vertical link. The camera captures a frame that is 60×80 pixels at a rate of 60 frames/sec. Using black and white blocks, this plate encodes the position of the vertical link which allows readings at 0.28deg angular resolution, as shown in Figure 3.4. There are 8 rings of black and white blocks on the plate. Figure 3.5 shows a typical frame of the camera reading. The image in the top left corner is the grabbed image, which is thresholded into a binary image. The 8 cross points of the thin lines on the image (one horizontal line per ring) form 8bits of angle information. The angle information is encoded using "Gray code". In the binary form, the Gray code changes only one bit for adjacent numbers, e.g., the 4bit Gray code for $0, 1, 2, 3, 4, 5, 6, 7, 8, \cdots$ is $0000, 0001, 0011, 0010, 0110, 0100, 0101, 0111, \cdots$. Thus it is robust to noise. The 8bit Gray code gives us $360/2^8 = 1.4$deg resolution. Each block is of 5 pixel width. We can count the pixel distance from the cross points of the thin lines to the boundary of the block. Thus the resolution is refined to $1.4/5 = 0.28$deg, see Figure 3.6 for a typical sample plot. In the plot, the jumps between neighboring time instances is

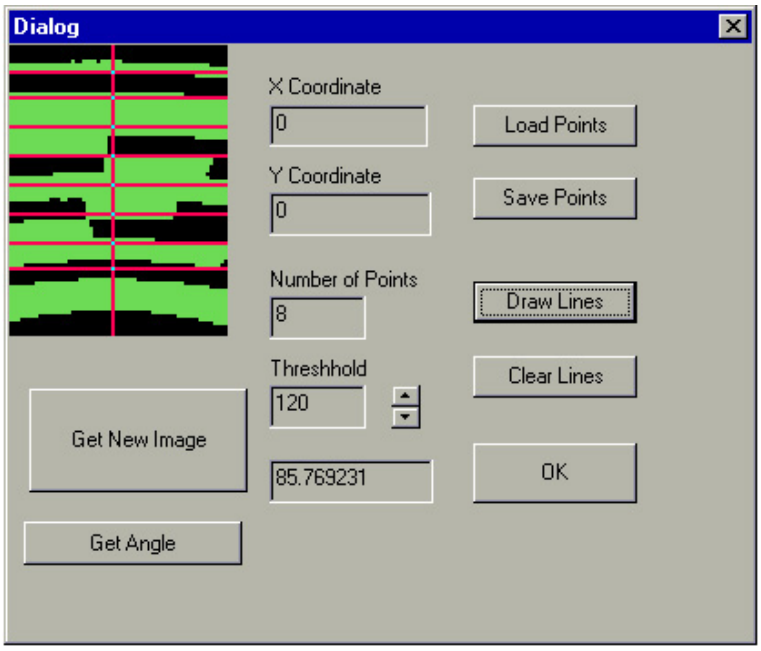

Figure 3.5: A frame of the camera reading.

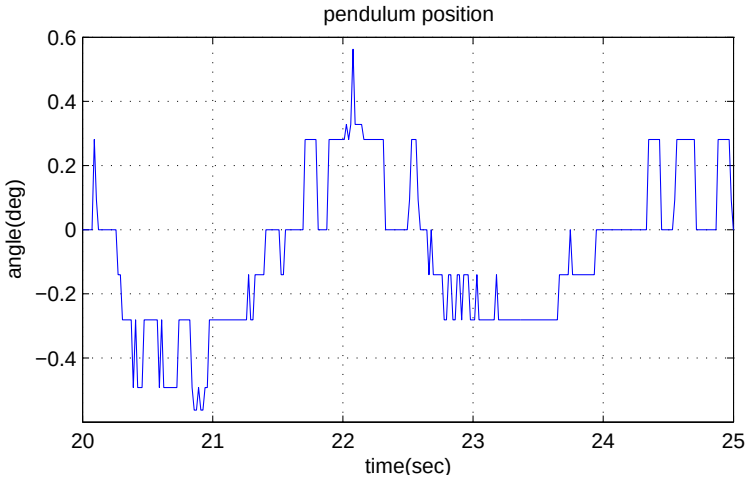

Figure 3.6: A typical sample plot of the vision sensor.

less than 0.3deg.

Control loop

The camera grabs a frame of image of the Gray code plate. Then that frame is sent to the computer through the frame grabber board. The software consists of three modules: the vision module, the control module, and the motor module. The vision module decodes the image to get the current angular position and sends it to the control module. The control module decides the next motor velocity and acceleration, then sends them to the motor module. The motor module packages up the motor control commands and sends them to the motor through RS-485 board. That closes the loop, as shown in Figure 3.2. The motor does not send back its position information. Because it lowers the overall sample rate significantly, from 60Hz to 30Hz. Instead we built a second order motor position estimator inside the control module.

Computing environment

The computer used in this project is a 200MHz dual Pentium processor system with Microsoft Windows NT as its operating system. The software that runs on the computer is written in Microsoft Visual C++ 5.0.

3.2 Electrostatic resolver based double pendulum

The platform that we use for the experiments consists of a horizontal link, driven by a servo motor, and two vertical links that move freely in the plane perpendicular to the horizontal link, as shown in Figure 3.7 and 3.8. In order to measure the position of the vertical links, a rotary electrostatic resolver is mounted on each of the joints of the vertical links. The encoders measure the absolute angular positions (instead of incremental) and outputs analog signals. Then each analog signal is converted into a 12bits binary digital data. The digital data is sent to the host computer through a RS232 radio link, as shown in Figure 3.10. The radio link can send 50 readings of both the encoders per second in real time which limits the sample frequency of the whole system to 50Hz. The sample rate of the motor is 8.3KHz. Each encoder has accuracy of .06deg. The base of the pendulum is leveled with an error of .05deg.

Level the base

The angular position readings of the two vertical links are relative to the horizontal link (the motor link). In order to get accurate readings relative to the ground frame, we need either a leveled horizontal link or a known tilting angle of the horizontal link. We pick the

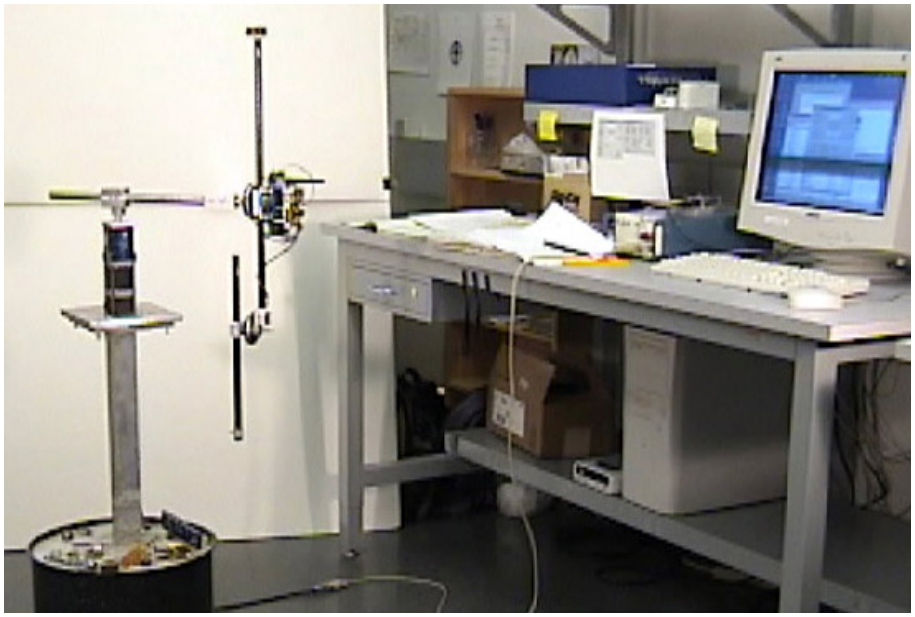

Figure 3.7: HRL double inverted pendulum.

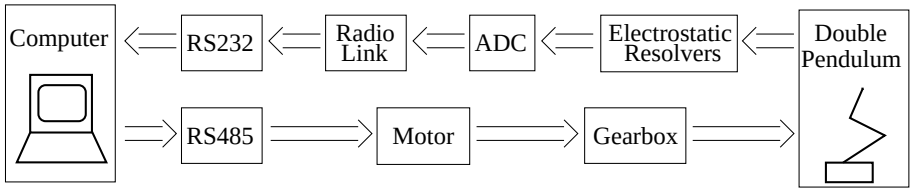

Figure 3.8: Diagram of the electrostatic resolver based double inverted pendulum.

former in these experiments. An adjustable unit is inserted between the motor and the heavy concrete base, as shown in Figure 3.9. We can adjust the level by turning the screws at each of the four corners between two square aluminum plates. The levelness of the base is measured by reading the encoder attached to the first vertical link θ_2 when it points downward (multiple readings to cancel the reading errors), as shown in Table 3.1. Where θ_1 is the motor position and θ_2 is the position of the first vertical link at rest. The maximal error of the levelness of the base is 0.05deg which is good enough for our experiments. Note that the accuracy of the electrostatic resolver is 0.06deg.

Electrostatic resolver and radio module

In order to measure the positions of the two vertical links we need a pair of angular

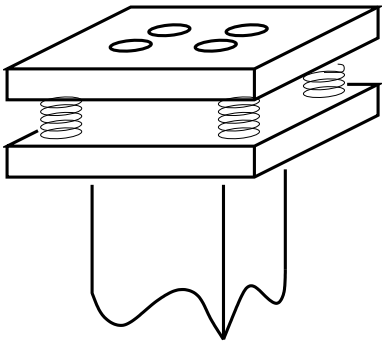

Figure 3.9: Sketch of the level base

θ_1 (deg)	0	90	180	270
θ_2 (deg)	180.00	180.03	180.05	180.04

Table 3.1: Test data for levelness of the base

position encoders. At the same time we do not want loose wires hanging from the vertical links, because that restricts the range of reachable positions. So we use a radio transceiver to send the data to the host computer wirelessly. The design criteria for the encoders and the radio are: small in size, light in weight, 'high' data rate, real time (very small delay), low power consumption. The encoders should have high resolution. The radio should be transparent in the network. The encoder and radio module is shown in Figure 3.10 with its diagram in Figure 3.11. It consists of two electrostatic resolvers, a power amplifier circuit, a 12bits analog to digital converter (ADC), a RS232 radio link, and a power circuit. The electrostatic resolver we used is comprised of an electric field generator, a field receiver, and a dielectric rotor that interacts with the received field. The current collected by the field receiver is processed to provide DC output signals proportional to the sine and cosine of the rotation angle. It provides 15bit absolute reading with 12bit ADC. It consumes 10mA current at 5V. The ADC outputs 12bit data at 19.2kpbs with RS232 interface. It consumes approximately 50mA at 9V. The output range of the encoder is $0 \sim 1$V, while the input range of the ADC is $0 \sim 5$V. So we built a $\times 5$ voltage amplifier in between. The radio works at 19.2kbps with RS232 interface. It has a roughly 10ms time delay. It consumes 60mA at 9V. All together, a 9V and 150mAh battery lasts for 1 hour. It is of a palm size and around 150g. A typical sample plot of each encoder is shown in Figure 3.12.

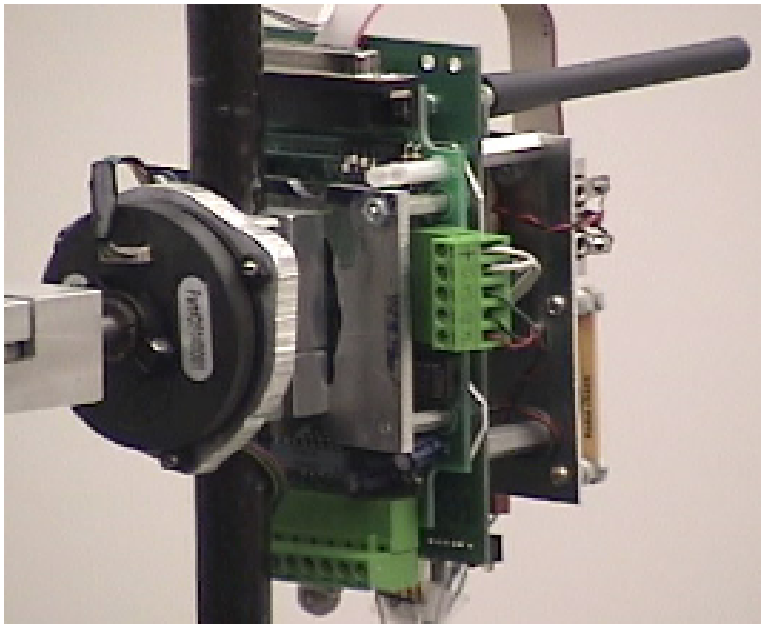

Figure 3.10: Rotary electrostatic resolver and radio link.

Radio transceiver operation

The radio used in the pendulum apparatus is a passive RS232 radio link. The radio works on a fixed frequency, and can only pass data in one direction at a time. The way in which they pass data is controlled by 5 parameters: 'Packet Size', 'CTS De-Assert', 'CTS Asset', 'Preamble Bytes', and 'TX Holdoff Time'.

Using an example on our system, if the computer (connected to radio 1) transmits a message to the ADC (connected to radio 2), radio 1 takes in the message into its buffer. Once radio 1 has received 'Packet Size' bytes it starts the transmission process as follows.

- First it sends 'Preamble Bytes' of blank information. The purpose of this is to allow the receiving radio to lock onto the signal. It is recommended by the designer that this be set to at least 16 bytes.

- Then it encodes and sends all the data that is in its buffer, in the order that the data was received (the buffer is a FIFO queue).

This means that each transmission packet is larger than 'Packet Size' bytes. The buffer size of the buffer in the radio is 180 bytes. Its level is controlled using the Clear To Send (CTS) protocol. When the buffer contains more than 'CTS De-Assert' bytes, the radio

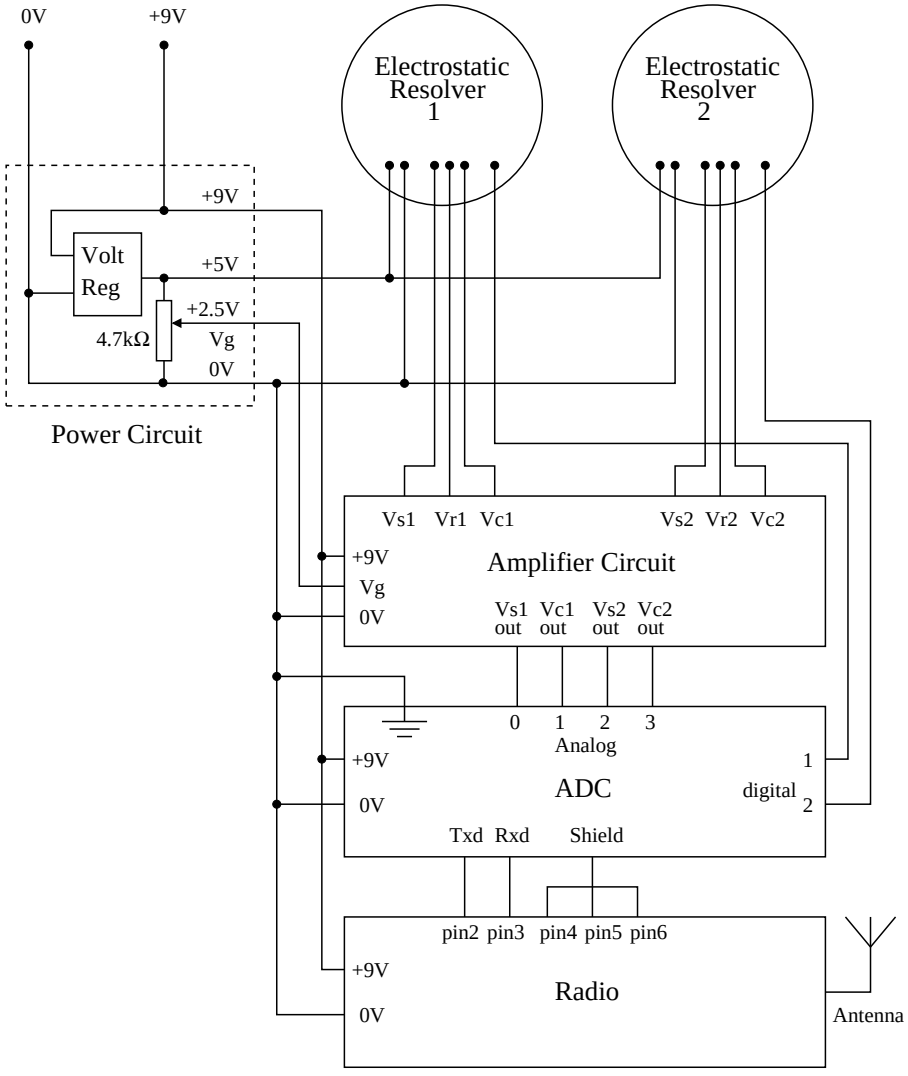

Figure 3.11: Diagram of the position sensoring circuit

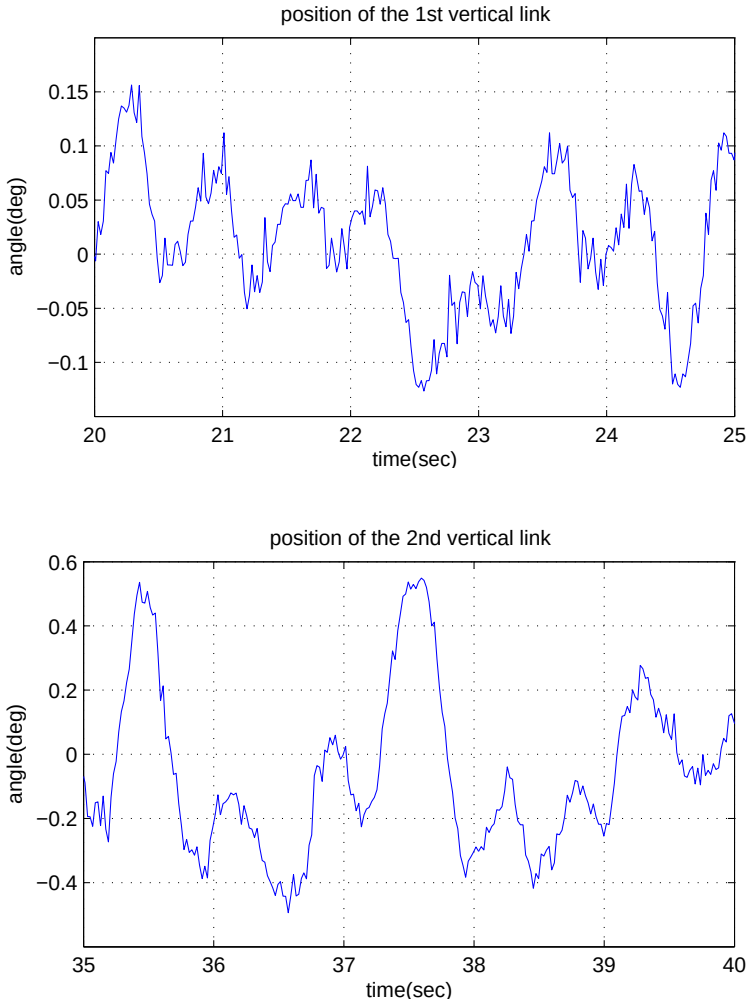

Figure 3.12: A typical sample plot of the electrostatic resolvers.

lowers one of the lines on the RS232 bus, the CTS line. The unit at the other end of the bus is supposed to be monitoring that line, and is meant to cease transmission when CTS is lowered. Once the buffer has dropped back below the level specified in 'CTS Asset', the radio raises the CTS line and the sending unit can recommence sending data. That way the buffer never overflows. Finally, once the receiving radio has finished receiving the data stream, it cannot commence sending data for a fixed period called the 'TX Holdoff Time'. This cannot be set lower than 5ms.

The main problem from our perspective is that our ADC doesn't listen to the CTS line. Thus when the radio transmission cannot keep up with the ADC's data stream (say when

the baud rate is at 56kbps), the ADC just keeps pumping data to the radio even after the CTS line is raised. Instead of ignoring this data, the radio keeps accepting it into its buffer, until the buffer is full. At this point the radio then has to drop bytes. In addition to that, the data that is going over the lines is 180 bytes old anyway, which is 25ms at 56kpbs. We estimate that the radio would successfully transmit the stream at 19.2kbps without dropping any data at all. When the ADC was set at 19.2kbps it was only transmitting 14kbps of data. This allowed for the packet size to be 40 bytes. It appears from analyzing the data input from the radio into the computer that its actual single transmission size is 14 bytes of data. The total delay time is close to 10ms. It accounts for the sum of the time between the receiving data and the beginning transmission (2ms), the time of transmission the preamble bytes, and/or the 'Tx Holdoff Time' (5ms). The preamble bytes are the empty data that the radio puts on the front of each transmission.

Control loop

The electrostatic resolvers read the pair of angular positions of the vertical links and output them in analog signals. The onboard ADC converts the analog signals into digital data. The onboard radio transceiver sends the digital data to the transceiver on the host computer wirelessly. The radio transceiver on the host computer receives the data and sends it to the computer through the RS232 board. The software used here is similiar to that in the single pendulum experiemts in Section 3.1. The control loop is shown in Figure 3.8.

Computing environment

The computer used in this project is an 800MHz Pentium III processor system with Microsoft Windows 2000 as its operating system. The whole project is built with Microsoft Visual C++ 6.0.

3.3 Mathematical model for the double pendulum

We start with the mathematical model for double pendulum. The single pendulum model is a subsystem of the double pendulum model, which is addressed in the next section. For background on the Lagrangian description of dynamical systems see Arnold (1978); Marsden (1992). All the symbols related to the pendulum are shown in Figure 3.13. The pendulum can be described by the Lagrangian

$$L(\theta, \dot{\theta}) = K - U, \tag{3.1}$$

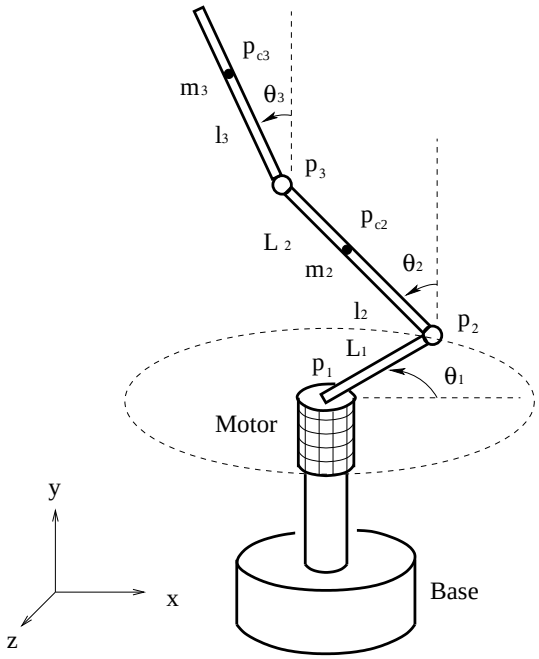

Figure 3.13: Rotational double pendulum.

where $\theta = (\theta_1, \theta_2, \theta_3)^T$ is a vector containing the horizontal and vertical link angles and K and U are the total kinetic and potential energies respectively. K is given by $K = K_1 + K_2 + K_3$, where the kinetic energy of each link is given by the contributions from one linear translation, one rotation component, and one cross product component of translation and rotation:

$$K_i = \frac{1}{2} m_i v_i^T v_i + \frac{1}{2} \omega_i^T \bar{I}_i \omega_i + m_i r_i^T (v_i \times \omega_i), \ i = 1, 2, 3. \tag{3.2}$$

Here v_i is the linear velocity of the link at its joint p_i, ω_i is its angular velocity with respect to its joint space (notice that it is the angular velocity with respect to the **non-rotating frame** attached on the joint p_i), $r_i = p_{ci} - p_i$ is the vector from the joint to the center of mass of the link, m_i is its mass, and $\bar{I}_i$ is the inertia tensor of the link with respect to its joint. For the first link, the kinetic energy is

$$K_1 = \frac{1}{2} I_1 \dot{\theta}_1^2. \tag{3.3}$$

We pick a non-rotational body-fixed frame at the joint p_2 with z pointing to the center p_1 (shown in Fig 3.13). Then $v_2 = (-L_1 \dot{\theta}_1, 0, 0)^T$, $\bar{I}_2 = \text{diag}\{I_2 \cos^2 \theta_2, I_2 \sin^2 \theta_2, I_2\}$, $\omega_2 =$

$(0, \dot{\theta}_1, \dot{\theta}_2)^T$, and $r_2 = (-l_2 \sin\theta_2, l_2 \cos\theta_2, 0)^T$. K_2 takes the form of

$$K_2 = \frac{1}{2} m_2 (L_1 \dot{\theta}_1)^2 + \frac{1}{2} I_2 (\dot{\theta}_2^2 + \dot{\theta}_1^2 \sin^2\theta_2) + m_2 l_2 \dot{\theta}_2 L_1 \dot{\theta}_1 \cos\theta_2. \tag{3.4}$$

If we pick the same frame at p_3, then in the inertial frame at p_1,

$$p_3 = L_1(\cos\theta_1, 0, -\sin\theta_1)^T + L_2(-\sin\theta_2 \sin\theta_1, \cos\theta_2, -\sin\theta_2 \cos\theta_1)^T.$$

Thus

$$v_3 = \dot{p}_3|_{\theta_1 = \frac{\pi}{2}} = (-L_1\dot{\theta}_1 - L_2\dot{\theta}_2 \cos\theta_2, -L_2\dot{\theta}_2 \sin\theta_2, L_2\dot{\theta}_1 \sin\theta_2)^T,$$

$\bar{I}_3 = \mathrm{diag}\{I_3 \cos^2\theta_3, I_3 \sin^2\theta_3, I_3\}$, $\omega_3 = (0, \dot{\theta}_1, \dot{\theta}_3)^T$, and $r_3 = (-l_3 \sin\theta_3, l_3 \cos\theta_3, 0)^T$. Thus

$$\begin{aligned} K_3 \;=\; & \tfrac{1}{2} m_3 ((L_1\dot{\theta}_1 + L_2\dot{\theta}_2 \cos\theta_2)^2 + (L_2\dot{\theta}_2 \sin\theta_2)^2 + (L_2\dot{\theta}_1 \sin\theta_2)^2) \\ & + \tfrac{1}{2} I_3 (\dot{\theta}_3^2 + \dot{\theta}_1^2 \sin^2\theta_3) \\ & + m_3 l_3 (L_2\dot{\theta}_2\dot{\theta}_3 \cos(\theta_2 - \theta_3) + L_2\dot{\theta}_1^2 \sin\theta_2 \sin\theta_3 + L_1\dot{\theta}_1\dot{\theta}_3 \cos\theta_3). \end{aligned} \tag{3.5}$$

Where I_2 and I_3 are the moments of inertia of link 2 and link 3 with respect to their joints p_2 and p_3, respectively. L_1 and L_2 are the lengths of link 1 and link 2, while l_2 and l_3 are the distances from the center of mass to their joints of link 2 and link 3, respectively. We also have the potential energy

$$U = U_2 + U_3 = m_2 g l_2 \cos\theta_2 + m_3 g (L_2 \cos\theta_2 + l_3 \cos\theta_3). \tag{3.6}$$

The coupled equations of motion that describe the dynamics of the pendulum are described by the Euler-Lagrangian equation

$$\frac{d}{dt}\left(\frac{\partial L}{\partial \dot{\theta}_i}\right) - \frac{\partial L}{\partial \theta_i} = F_i, \;\; i = 1, 2, 3, \tag{3.7}$$

where F_i is a generalized force. Combine equation (3.1) $\sim$ (3.7), we get the set of equations

$$\begin{aligned} & (I_1 + I_2 \sin^2\theta_2 + I_3 \sin^2\theta_3 + m_2 L_1^2 + m_3 (L_1^2 + L_2^2 \sin^2\theta_2) + 2 m_3 l_3 L_2 \sin\theta_2 \sin\theta_3) \ddot{\theta}_1 \\ & + (m_2 l_2 + m_3 L_2) L_1 \ddot{\theta}_2 \cos\theta_2 + m_3 l_3 L_1 \ddot{\theta}_3 \cos\theta_3 \\ & + 2 m_3 l_3 L_2 \dot{\theta}_1^2 \cos\theta_2 \sin\theta_3 - (m_2 l_2 + m_3 L_2) L_1 \dot{\theta}_2^2 \sin\theta_2 - m_3 l_3 L_1 \dot{\theta}_3^2 \sin\theta_3 \\ & + (I_2 + m_3 L_2^2) \dot{\theta}_1 \dot{\theta}_2 \sin 2\theta_2 + (I_3 \sin 2\theta_3 + 2 m_3 l_3 L_2 \sin\theta_2 \cos\theta_3) \dot{\theta}_1 \dot{\theta}_3 = u, \end{aligned} \tag{3.8}$$

$$
\begin{aligned}
&(m_2 l_2 + m_3 L_2) L_1 \ddot{\theta}_1 \cos\theta_2 + (I_2 + m_3 L_2^2)\ddot{\theta}_2 + m_3 l_3 L_2 \ddot{\theta}_3 \cos(\theta_2 - \theta_3) \\
&\quad -(\tfrac{1}{2}(I_2 + m_3 L_2^2)\sin 2\theta_2 + m_3 l_3 L_2 \cos\theta_2 \sin\theta_3)\dot{\theta}_1^2 + m_3 l_3 L_2 \dot{\theta}_3^2 \sin(\theta_2 - \theta_3) \qquad (3.9) \\
&\quad -(m_2 g l_2 + m_3 g L_2)\sin\theta_2 = 0,
\end{aligned}
$$

$$
\begin{aligned}
&m_3 l_3 L_1 \ddot{\theta}_1 \cos\theta_3 + m_3 l_3 L_2 \ddot{\theta}_2 \cos(\theta_2 - \theta_3) + I_3 \ddot{\theta}_3 \\
&\quad -(\tfrac{1}{2} I_3 \sin 2\theta_3 + m_3 l_3 L_2 \sin\theta_2 \cos\theta_3)\dot{\theta}_1^2 - m_3 l_3 L_2 \dot{\theta}_2^2 \sin(\theta_2 - \theta_3) \qquad (3.10) \\
&\quad -m_3 g l_3 \sin\theta_3 = 0.
\end{aligned}
$$

In this problem, we can directly control the acceleration of the motor. Thus we can replace (3.8) by $\ddot{\theta}_1 = u$. If we take friction μ_2 and μ_3 into account too, then we will get

$$
\begin{cases}
\ddot{\theta}_1 = u \\
(I_2 + m_3 L_2^2)\ddot{\theta}_2 + m_3 l_3 L_2 \ddot{\theta}_3 \cos(\theta_2 - \theta_3) + \mu_2 \dot{\theta}_2 \\
\quad -(\tfrac{1}{2}(I_2 + m_3 L_2^2)\sin 2\theta_2 + m_3 l_3 L_2 \cos\theta_2 \sin\theta_3)\dot{\theta}_1^2 + m_3 l_3 L_2 \dot{\theta}_3^2 \sin(\theta_2 - \theta_3) \\
\quad -(m_2 g l_2 + m_3 g L_2)\sin\theta_2 = -u(m_2 l_2 + m_3 L_2) L_1 \cos\theta_2 \qquad (3.11) \\
m_3 l_3 L_2 \ddot{\theta}_2 \cos(\theta_2 - \theta_3) + I_3 \ddot{\theta}_3 + \mu_3 \dot{\theta}_3 \\
\quad -(\tfrac{1}{2} I_3 \sin 2\theta_3 + m_3 l_3 L_2 \sin\theta_2 \cos\theta_3)\dot{\theta}_1^2 \\
\quad -m_3 l_3 L_2 \dot{\theta}_2^2 \sin(\theta_2 - \theta_3) - m_3 g l_3 \sin\theta_3 = -u m_3 l_3 L_1 \cos\theta_3.
\end{cases}
$$

In order to determinate the parameters of the pendulum, we measure the torque and the natural frequency. Then we can compute the moment of inertia by $I = mlg/(2\pi f r)^2$. The parameters we used in the double pendulum setup are as follows:

$$
\begin{array}{rclrclr}
g & = & 9.81\text{N/kg}; & & & \text{gravitation constant} & \\
L_1 & = & 0.32\text{m}; & L_2 & = & 0.264\text{m}; & \\
m_2 l_2 & = & -0.0042\text{kgm}; & m_3 l_3 & = & 0.0023\text{kgm}; & m_3 = 0.0795\text{kg}; \\
I_2 & = & 0.0241\text{kgm}^2; & I_3 & = & 7.5642e-4\text{kgm}^2; & \\
\mu_2 & = & 0.0; & \mu_3 & = & 0.0; \text{ the friction coefficients are artificial.} &
\end{array}
$$

Figure 3.14 shows a typical plot of the double pendulum around its down-down position without control. We can see that the coupled motion of the two vertical links is quite complex.

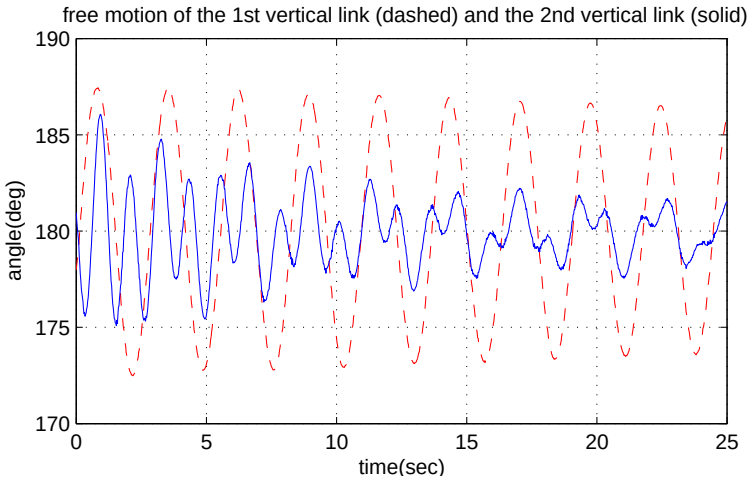

Figure 3.14: A typical sample plot of double pendulum at around down-down position.

We now have a nonlinear model for the dynamics of the pendulum. However, when designing a local, stabilizing control law, a linear model is preferred from a design point of view. There are many stabilization results, e.g. LQ design, which are computational feasible and easy to implement. The next step is thus to show how to linearize the equation (3.11).

We want to stabilize the double pendulum at its invariant positions. We can first linearize (3.11) at one of its four equilibrium points, $\dot{\theta}_1^* = \dot{\theta}_2^* = \dot{\theta}_3^* = 0$, $\theta_1^* \in R$, and $\theta_2^*, \theta_3^* \in \{2k\pi, (2k+1)\pi\}, k \in Z\}$. Let $\delta\theta_i = \theta_i - \theta_i^*$ and $\delta\dot{\theta}_i = \dot{\theta}_i - \dot{\theta}_i^*$. Then the linear approximation of equation (3.11) becomes

$$\begin{cases} \delta\ddot{\theta}_1 = u \\ \\ (I_2 + m_3L_2^2)\delta\ddot{\theta}_2 + m_3l_3L_2\cos(\theta_2^* - \theta_3^*)\delta\ddot{\theta}_3 + \mu_2\delta\dot{\theta}_2 \\ \qquad -(m_2gl_2 + m_3gL_2)\cos\theta_2^*\delta\theta_2 = -u(m_2l_2 + m_3L_2)L_1\cos\theta_2^* \\ \\ m_3l_3L_2\cos(\theta_2^* - \theta_3^*)\delta\ddot{\theta}_2 + I_3\delta\ddot{\theta}_3 + \mu_3\delta\dot{\theta}_3 - m_3gl_3\cos\theta_3^*\delta\theta_3 = -um_3l_3L_1\cos\theta_3^*. \end{cases} \tag{3.12}$$

If we let $x = (\delta\theta_1, \delta\dot{\theta}_1, \delta\theta_2, \delta\dot{\theta}_2, \delta\theta_3, \delta\dot{\theta}_3)$ the linearized system equations become

$$\dot{x} = Ax + bu, \tag{3.13}$$

where

$$A = \begin{pmatrix} 0 & 1 & 0 & 0 & 0 & 0 \\ 0 & 0 & 0 & 0 & 0 & 0 \\ 0 & 0 & 0 & 1 & 0 & 0 \\ 0 & 0 & a_{43} & a_{44} & a_{45} & a_{46} \\ 0 & 0 & 0 & 0 & 0 & 1 \\ 0 & 0 & a_{63} & a_{64} & a_{65} & a_{66} \end{pmatrix}, \qquad b = \begin{pmatrix} 0 \\ 1 \\ 0 \\ b_4 \\ 0 \\ b_6 \end{pmatrix}. \tag{3.14}$$

with

$$\begin{pmatrix} a_{43} & a_{44} & a_{45} & a_{46} \\ a_{63} & a_{64} & a_{65} & a_{66} \end{pmatrix} = M^{-1} \begin{pmatrix} (m_2 g l_2 + m_3 g L_2)\cos\theta_2^* & -\mu_2 & 0 & 0 \\ 0 & 0 & m_3 g l_3 \cos\theta_3^* & -\mu_3 \end{pmatrix}$$

$$\begin{pmatrix} b_4 \\ b_6 \end{pmatrix} = M^{-1} \begin{pmatrix} -(m_2 l_2 + m_3 L_2) L_1 \cos\theta_2^* \\ -m_3 l_3 L_1 \cos\theta_3^* \end{pmatrix}$$

$$M = \begin{pmatrix} I_2 + m_3 L_2^2 & m_3 l_3 L_2 \cos(\theta_2^* - \theta_3^*) \\ m_3 l_3 L_2 \cos(\theta_2^* - \theta_3^*) & I_3 \end{pmatrix}$$

Thus at up-up position, $\theta_2^* = \theta_3^* = 0$,

$$A = \begin{pmatrix} 0 & 1 & 0 & 0 & 0 & 0 \\ 0 & 0 & 0 & 0 & 0 & 0 \\ 0 & 0 & 0 & 1 & 0 & 0 \\ 0 & 0 & 5.6453 & 0 & -0.6328 & 0 \\ 0 & 0 & 0 & 0 & 0 & 1 \\ 0 & 0 & -4.5720 & 0 & 30.6070 & 0 \end{pmatrix}, \qquad b = \begin{pmatrix} 0 \\ 1 \\ 0 \\ -0.1635 \\ 0 \\ -0.8493 \end{pmatrix}.$$

The denominator of the corresponding transfer function is

$$\begin{aligned} p(s) &= \det(sI - A) \\ &= s^2(s^4 - (a_{43} + a_{65})s^2 + a_{43}a_{65} - a_{45}a_{63}) \\ &= s^2(s^4 - 35.98s^2 + 168.5) \\ &= s^2(s^2 - 5.536)(s^2 - 30.44). \end{aligned}$$

The transfer function $G(s)$ for $C = (x_1, x_3, x_5)^T$,

$$G(s) = C(sI - A)^{-1}b$$

$$= \begin{pmatrix} \frac{1}{s^2} \\ \frac{b_4 s^2 - a_{65}b_4 + a_{45}b_6}{s^4 - (a_{43} + a_{65})s^2 + a_{43}a_{65} - a_{45}a_{63}} \\ \frac{b_6 s^2 - a_{63}b_4 + a_{43}b_6}{s^4 - (a_{43} + a_{65})s^2 + a_{43}a_{65} - a_{45}a_{63}} \end{pmatrix} = \begin{pmatrix} \frac{1}{s^2} \\ \frac{-0.164s^2 + 5.4966}{s^4 - 35.9765s^2 + 168.5048} \\ \frac{-0.8414s^2 + 5.4966}{s^4 - 35.9765s^2 + 168.5048} \end{pmatrix}.$$

3.4 Specialization to single pendulum case

The mathematical model for the single pendulum is a subsystem of the model for double pendulum in the previous section, containing (θ_1, θ_2). Following the derivation from equation (3.1) to (3.11), we get

$$\begin{aligned} (I_1 + I_2 \sin^2\theta_2 + m_2 L_1^2)\ddot{\theta}_1 + m_2 l_2 L_1 \ddot{\theta}_2 \cos\theta_2 & \\ -m_2 l_2 L_1 \dot{\theta}_2^2 \sin\theta_2 + I_2 \dot{\theta}_1 \dot{\theta}_2 \sin 2\theta_2 &= u \\ m_2 l_2 L_1 \ddot{\theta}_1 \cos\theta_2 + I_2 \ddot{\theta}_2 - \tfrac{1}{2} I_2 \sin 2\theta_2 - m_2 l_2 g \sin\theta_2 &= 0 \end{aligned} \tag{3.15}$$

With direct acceleration control of the motor, we have

$$\begin{aligned} \ddot{\theta}_1 &= u \\ I_2 \ddot{\theta}_2 - \tfrac{1}{2} I_2 \sin 2\theta_2 - m_2 l_2 g \sin\theta_2 &= -u m_2 l_2 L_1 \cos\theta_2 \end{aligned} \tag{3.16}$$

The parameters we used in the single pendulum setup are:

$g = 9.81\text{N/kg}$ (gravitation constant), $L_1 = 0.452\text{m}$, $m_2 l_2 = 0.0109\text{kgm}$, $I_2 = 0.035\text{kgm}^2$

We now have a nonlinear model for the dynamics of the single pendulum. However, as we have already pointed out in Section 3.3, when designing a local, stabilizing control law, a linear model is preferred. If we let $x = (\theta_1, \dot{\theta}_1, \theta_2, \dot{\theta}_2)$, the linearized system equations become

$$\dot{x} = Ax + bu, \tag{3.17}$$

where

$$A = \begin{pmatrix} 0 & 1 & 0 & 0 \\ 0 & 0 & 0 & 0 \\ 0 & 0 & 0 & 1 \\ 0 & 0 & a_{43} & 0 \end{pmatrix}, \qquad b = \begin{pmatrix} 0 \\ 1 \\ 0 \\ b_4 \end{pmatrix}. \tag{3.18}$$

with $a_{43} = 1 + \frac{m_2 l_2 g}{I_2} = 31.57$ and $b4 = -\frac{m_2 l_2 L_1}{I_2} = -3.116$. The denominator of the corresponding transfer function is

$$p(s) = \det(sI - A) = s^2(s^2 - a_{43}) = s^2(s^2 - 31.57).$$

The transfer function $G(s)$ for $C = (x_1, x_3)^T$ is

$$G(s) = C(sI - A)^{-1}b = \begin{pmatrix} \frac{1}{s^2} \\ \frac{b_4}{s^2 - a_{43}} \end{pmatrix} = \begin{pmatrix} \frac{1}{s^2} \\ -\frac{3.116}{s^2 - 31.57} \end{pmatrix}.$$

Example 3.4.1 *If the horizontal link of the pendulum is fairly long, we can approximate it by a cart base pendulum with direct acceleration control of the cart. After normalizing the masses and link lengths, the dynamics become*

$$\begin{cases} \ddot{\theta}_1 &= u \\ \ddot{\theta}_2 &= \sin\theta_2 + u\cos\theta_2. \end{cases} \tag{3.19}$$

Insights about the controllability of this system have been gained from the following Lie bracket computations based on a reduced order model, see Brockett (1970, 1976) for background. Let, as before, $x = (\theta_1, \dot{\theta}_1, \theta_2, \dot{\theta}_2)$. Equation (3.19) becomes

$$\begin{pmatrix} \dot{x}_1 \\ \dot{x}_2 \\ \dot{x}_3 \\ \dot{x}_4 \end{pmatrix} = \begin{pmatrix} x_2 \\ 0 \\ x_4 \\ \sin x_3 \end{pmatrix} + u \begin{pmatrix} 0 \\ 1 \\ 0 \\ \cos x_3 \end{pmatrix} = f(x) + ug(x).$$

We want to check the Lie bracket directions generated by the drift term f and the control term g.

$$[f,g] = \begin{pmatrix} -1 \\ 0 \\ -\cos x_3 \\ -x_4 \sin x_3 \end{pmatrix}, \quad [f,[f,g]] = \begin{pmatrix} 0 \\ 0 \\ 2x_4 \sin x_3 \\ -x_4^2 \cos x_3 + \cos 2x_3 \end{pmatrix},$$

$$[f,[f,[f,g]]] = \begin{pmatrix} 0 \\ 0 \\ 3x_4^2 \cos x_3 - 2\cos 2x_3 + 1 \\ x_4^3 \sin x_3 - 4x_4 \sin 2x_3 \end{pmatrix},$$

$$[[f,g],g] = \begin{pmatrix} 0 \\ 0 \\ 0 \\ \sin 2x_3 \end{pmatrix}, \quad [[[f,g],g],g] = 0.$$

The linearization of system (3.19) at its inverted position is

$$\dot{x} = Ax + bu, \tag{3.20}$$

with

$$A = \begin{pmatrix} 0 & 1 & 0 & 0 \\ 0 & 0 & 0 & 0 \\ 0 & 0 & 0 & 1 \\ 0 & 0 & 1 & 0 \end{pmatrix}, \quad b = \begin{pmatrix} 0 \\ 1 \\ 0 \\ 1 \end{pmatrix}. \tag{3.21}$$

We can locally stabilize this system using state feedback in a straightforward manner, using $u = -b^T Kx$*, where* K *is the solution to a LQ optimization problem. One choice of feedback law that stabilizes the system could for instance be*

$$K = \begin{pmatrix} 10 & -1 & 0 & 0 \\ -1 & 10 & 0 & -12 \\ 0 & 0 & 20 & 5 \\ 0 & -12 & 5 & 17 \end{pmatrix}, \tag{3.22}$$

which gives that $\mathrm{eig}(A - bb^T K) = \{-0.12 \pm i0.7, -1, -1.7\}$.

Chapter 4

Swing-up control of the single pendulum

In this chapter, we investigate the problem of stabilizing a pendulum to its inverted position. This is a well studied (see for example Åström and Furuta (1996); Spong (1995)) and, some would argue, a well-solved problem, but what is novel in this chapter is that we take the physical bounds on the control signals into account already at the design stage. Since physical constraints always impose limits on what control signals are available, we take the position that any controller that is to be implemented should explicitly address the bounded input problem. Most part of this Chapter is in unpublished manuscript Li and Egerstedt (2002).

The experimental platform that we work with, developed at the Harvard Robotics Laboratory, is a rotational single pendulum, as seen in Figure 3.1∼3.3. It consists of a horizontal link, directly controlled by a servomotor, and a vertical link moving freely in the plane perpendicular to the horizontal link. Even though our discussion will be quite general, this platform will serve as a motivating example as well as a test-bed for evaluating the practical value of our contribution.

Given a Lagrangian system $L(x, \dot{x}, u)$ defined on $M \times TM \times U$, where M is a manifold, TM its tangent space, and $U \subset \mathbb{R}$ a compact set of available control signals from which the generalized forces in the Lagrangian can be derived. If $(x_1, u_1), \ldots, (x_k, u_k)$, where $x_i \neq x_j$ when $i \neq j$, satisfies $L(x_i, 0, u_i) = 0,\ i = 1, \ldots, k$, then we say that $\{(x_1, u_1), \ldots, (x_k, u_k)\}$ are Lagrangian equilibrium points. Furthermore, let $(A_i, b_i),\ i = 1, \ldots, k$, be the linear control systems that characterize the local dynamics around a particular equilibrium point. The problem of swinging up an inverted pendulum can be thought of as driving the system

from one such equilibrium point (e.g. the pendulum is hanging straight down) to another (e.g. upright position) under bounded inputs. A more general formulation of the problem is to drive the system through a list of equilibria. A model that describes such transitions between different equilibria is that of a reachability graph, i.e. a directed graph obtained by associating each equilibrium with a node in the graph. The presence of a directed edge, e_{ij}, between node n_i and n_j is equivalent to the existence of a feasible ($u \in U$) path in $M \times TM$ between $(x_i, 0)$ and $(x_j, 0)$. In this chapter, we investigate what nodes can be reached from each other, and what bounded controllers achieve this, i.e. we design the reachability graph.

In order to make our control strategy robust we do not demand that the system has to reach the equilibrium exactly. Instead we are content if the trajectory intersects a suitable open set around the equilibrium, from which a locally stabilizing controller can be constructed that drives the system to the desired state. However, a stabilizing feedback controller can only be effective on selected parts of the state space when the input is subject to magnitude constraints. In Section 4.1, we compute these regions of attraction for unstable, linear control systems driven by bounded inputs. We then let the stabilizing controller, together with the corresponding region of attraction (which in the hybrid dynamic systems literature is referred to as an *invariant set*) define a *mode* in a multi-modal hybrid system. We thus control the inverted pendulum by introducing different control modes, such as *swing-up* and *stabilization*.

If we now denote the invariant set, or region of attraction, associated with the equilibrium (x_i, u_i) by $E(x_i, u_i) \subset M \times TM$ then, as long as $E(x_i, u_i) \cap E(x_j, u_j) = \emptyset$, the reachability problem is equivalent to finding feasible paths ($u \in U$) between these regions of attraction. Our solution to the problem of driving L between the different nodes in the reachability graph is based on energy control. By injecting energy into the system, a bounded input control strategy with proven reachability properties can be attained. The experimental results are shown in Section 4.3.

4.1 Lemon theorem for the region of attraction

As already mentioned in the introduction, we want to construct a reachability graph for the Lagrangian system $L(x, \dot{x}, u)$, where each node n_i corresponds to an equilibrium (x_i, u_i), and each directed edge e_{ij} represents the existence of a feasible path between n_i and n_j. Around $(x_i, 0, u_i)$, the linear system (A_i, b_i) describes the local behavior of L. Our first task

is to derive the regions of attraction around each equilibrium point where bounded input feedback stabilization is possible.

We investigate how to design a locally stabilizing feedback controller for a linear system under bounded inputs. For the inverted pendulum, this corresponds to constructing a stabilizing controller for the linearized dynamics around the upright position. The solution is to be used in a hybrid control strategy. In order for such a mode to be a useful component in a hybrid system, it must be possible to define its corresponding *guards* and *invariant sets*, i.e. the parts of the state space on which the mode is well defined and locally effective (invariant sets) and the transition rules (guards). (See for example Henzinger (1996); Lygeros et al. (1999).)

We start by considering a linearized version of the pendulum model and then move on to formulate a more general theory. As in Section 3.4, we can approximate the model of the inverted pendulum by the following set of equations:

$$\begin{aligned} \ddot{\theta}_1 &= u, \\ \ddot{\theta}_2 &= \sin\theta_2 + u\cos\theta_2, \end{aligned} \tag{4.1}$$

where the subscripts 1 and 2 denote horizontal and vertical link angle, respectively, as seen in Figure 3.2. If we let the state space be $x = (\theta_1, \dot{\theta}_1, \theta_2, \dot{\theta}_2)^T$, the linearized dynamics around 0 becomes

$$\dot{x} = \begin{pmatrix} 0 & 1 & 0 & 0 \\ 0 & 0 & 0 & 0 \\ 0 & 0 & 0 & 1 \\ 0 & 0 & 1 & 0 \end{pmatrix} x + \begin{pmatrix} 0 \\ 1 \\ 0 \\ 1 \end{pmatrix} u, \tag{4.2}$$

which constitutes an unstable but controllable, linear time-invariant system.

Let us now study this situation in some generality. Consider an unstable, controllable linear system

$$\dot{x} = Ax + bu, \tag{4.3}$$

where $x \in \mathbb{R}^n, u \in \mathbb{R}$, and A, b are constant matrices of compatible dimensions. In the absence of control bounds, we can easily construct an exponentially stabilizing controller

$$u = -b^T K x, \tag{4.4}$$

where K is a symmetric, positive definite matrix solution (we will use $\succ$ to denote positive definiteness) to the Riccati equation, $Ricc(A, b, Q)$,

$$A^T K + KA - 2Kbb^T K + Q = 0, \tag{4.5}$$

given the positive definite matrix Q. (See any textbook on LQ-design, for example Brockett (1970).) If we now let the admissible controls be bounded by

$$|u| \leq 1, \tag{4.6}$$

then the introduction of this bound on the control means that the closed loop control strategy in (4.4) can not be guaranteed to work. Instead we add an open loop term to the controller, and choose to be content with the performance of the controller as long as it drives the system to any stationary point.

The idea is to construct a locally stabilizing affine control law

$$u = -b^T K x + v, \tag{4.7}$$

where K is the symmetric, positive definite matrix solution to $Ricc(A, b, Q)$ and $v \in \mathbb{R}$ is a constant, open-loop term. This gives the closed loop system dynamics as

$$\dot{x} = (A - bb^T K)x + bv, \tag{4.8}$$

with stationary point

$$x_v = -(A - bb^T K)^{-1} bv. \tag{4.9}$$

Here the inverse is well defined since the system is asymptotically stable. This follows from the fact that the real parts of the eigenvalues of $(A - bb^T K)$ are all negative.

Theorem 4.1.1 (Stationary Points Under Bounded Inputs) *Let (A, b) be a controllable pair and let K be the positive definite matrix solution to $Ricc(A, b, Q)$ for some $Q \succ 0$. If $u = -b^T Kx + v$, $|u| \leq 1$, then the set of stationary points, $\mathcal{X}$, is given by*

$$\mathcal{X} = \begin{cases} -(A - bb^T K)^{-1} b(b^T K(A - bb^T K)^{-1} b + 1)^{-1}[-1, 1] & \text{if } b^T K(A - bb^T K)^{-1} b + 1 \neq 0 \\ -(A - bb^T K)^{-1} b\mathbb{R} & \text{otherwise.} \end{cases}$$

Proof: The total control effort necessary for making the system remain at x_v is

$$\begin{aligned} u_v &= -b^T K x_v + v \\ &= b^T K(A - bb^T K)^{-1} bv + v \\ &= (b^T K(A - bb^T K)^{-1} b + 1)v. \end{aligned} \tag{4.10}$$

If $b^T K(A - bb^T K)^{-1}b + 1 = 0$, then $u_v = 0$ for any choice of $v \in \mathbb{R}$. Since $u_v \in [-1, 1]$, we must have that the set of open-loop control values $\mathcal{V}$ that generate stationary points is given by

$$v \in (b^T k(A - bb^T K)^{-1}b + 1)^{-1}[-1, 1] = \mathcal{V}, \tag{4.11}$$

if $b^T K(A - bb^T K)^{-1}b + 1 \neq 0$, and $v \in \mathbb{R} = \mathcal{V}$ otherwise. Here, given the set $S \subset \mathbb{R}^q$, the set $\alpha S = \{z \in \mathbb{R}^q \mid z = \alpha s \text{ for some } s \in S\}$, for $\alpha \in \mathbb{R}$.

The set $\mathcal{X}$ of stationary points to the closed loop system is given by

$$\mathcal{X} = -(A - bb^T K)^{-1}b\mathcal{V}, \tag{4.12}$$

which is equal to

$$\mathcal{X} = \begin{cases} -(A - bb^T K)^{-1}b(b^T K(A - bb^T K)^{-1}b + 1)^{-1}[-1, 1] & \text{if } b^T K(A - bb^T K)^{-1}b + 1 \neq 0 \\ -(A - bb^T K)^{-1}b\mathbb{R} & \text{otherwise,} \end{cases} \tag{4.13}$$

which concludes the proof. ∎

Since the system matrix in (4.2) for the linearized inverted pendulum dynamics has $rank(A) = n - 1$, it is worth investigating this special case in some detail.

Lemma 4.1.1 *Let (A, b) be a controllable pair, and let $K \succ 0$ solve $Ricc(A, b, Q)$ for some $Q \succ 0$. Then the following statements are equivalent:*

(i) $b^T K(A - bb^T K)^{-1}b = -1$

(ii) $Ker(A) = span\{(A - bb^T K)^{-1}b\}$

(iii) $rank(A) = n - 1$.

Proof:

$(i) \Rightarrow (ii)$: Suppose that $b^T K(A - bb^T K)^{-1}b = -1$. Then, from (4.13), it follows that we can place the equilibrium point x_v anywhere on the 1-dimensional subspace $span\{(A - bb^T K)^{-1}b\}$. For a given x, the total control action becomes

$$u = -b^T K \Delta x_v,$$

where $\Delta x_v = x - x_v$, which gives

$$\Delta \dot{x}_v = (A - bb^T K)\Delta x_v + Ax_v. \tag{4.14}$$

Since we have an equilibrium at $x = x_v$, i.e. at $\Delta x_v = 0$, we have that $Ax_v = 0$, or in other words

$$span\{(A - bb^T K)^{-1} b\} \subset Ker(A). \tag{4.15}$$

But, since controllability of (A, b) implies both that $b \neq 0$ and $rank(A) \geq n - 1$, the two subspaces in (4.15) have to be 1-dimensional. Thus the inclusion has to be an equality, which gives that

$$Ker(A) = span\{(A - bb^T K)^{-1} b\}. \tag{4.16}$$

$(ii) \Rightarrow (iii)$: If $dim(Ker(A)) = dim(span\{(A - bb^T K)^{-1} b\}) = 1$, then it directly follows that $rank(A) = n - 1$.

$(iii) \Rightarrow (i)$: Given the controllable linear system (A, b), we can find an invertible state transformation $x = T\bar{x}$ that transforms the system to a control-canonical form, i.e.

$$\dot{\bar{x}} = \bar{A}\bar{x} + \bar{b}u,$$

with

$$\bar{A} = T^{-1}AT = \begin{pmatrix} 0 & 1 & \cdots & 0 \\ \vdots & \vdots & \ddots & \vdots \\ 0 & 0 & \cdots & 1 \\ -a_0 & -a_1 & \cdots & -a_{n-1} \end{pmatrix}, \quad \bar{b} = T^{-1}b = \begin{pmatrix} 0 \\ \vdots \\ 0 \\ 1 \end{pmatrix}. \tag{4.17}$$

Furthermore, it is straight forward to see that $\bar{K} = T^T K T \succ 0$ solves $Ricc(\bar{A}, \bar{b}, \bar{Q})$, where $\bar{Q} = T^T Q T \succ 0$. We denote the element in $\bar{K}$ at row i and column j by k_{ij}.

Now, $rank(A) = n - 1$ implies $a_0 = 0$, which allows us to compute

$$(\bar{A} - \bar{b}\bar{b}^T \bar{K})^{-1} \bar{b} = \begin{pmatrix} -\frac{1}{k_{1n}} \\ 0 \\ \vdots \\ 0 \end{pmatrix}.$$

Since $\bar{A} - \bar{b}\bar{b}^T \bar{K}$ is stable we must have that $k_{1n} \neq 0$, and thus

$$\bar{b}^T \bar{K} (\bar{A} - \bar{b}\bar{b}^T \bar{K})^{-1} \bar{b} = (k_{1n}, \ldots, k_{nn}) \begin{pmatrix} -\frac{1}{k_{1n}} \\ 0 \\ \vdots \\ 0 \end{pmatrix} = -1.$$

This equality is furthermore invariant under the state transformation T

$$\begin{aligned}
&\bar{b}^T\bar{K}(\bar{A}-\bar{b}\bar{b}^T\bar{K})^{-1}\bar{b} \\
&= (T^{-1}b)^T(T^TKT)(T^{-1}AT-T^{-1}b(T^{-1}b)^T(T^TKT))^{-1}T^{-1}b \\
&= b^TK(A-bb^TK)^{-1}b,
\end{aligned}$$

which concludes the proof. ∎

Remark 4.1.1 *This result is independent of K as long as K solves $Ricc(A,b,Q)$ for some $Q \succ 0$.*

This lemma enables us to directly state the following corollary.

Corollary 4.1.1 (Stationary Points when rank(A) = n − 1) *Under the assumptions in Lemma 4.1.1, the set of stationary points $\mathcal{X}$ is the subspace $Ker(A)$.*

We now have a complete characterization of the set of stationary points under control action $-b^TKx+v$, with $v \in \mathcal{V}$, but it does not tell us from what parts of the state space this set can be reached when $|u| \leq 1$. The question thus becomes to find the set of states from which the stabilizing state feedback controller can be used.

Theorem 4.1.2 (Region of Attraction Under Bounded Inputs) *Given the assumptions in Theorem 4.1.1, the region of attraction contains*

$$\mathcal{L} = \bigcup_{v\in\mathcal{V}} \mathcal{E}(K,v),$$

where $\mathcal{E}(K,v)$ is the ellipsoid

$$\mathcal{E}(K,v) = \{x \in \mathbb{R} \mid (x-x_v)^TK(x-x_v) \leq \alpha_v\}$$

and

$$\alpha_v = (b^TKb)^{-1}(1-|u_v|)^2.$$

Proof: Let, as before, $x = x_v + \Delta x_v$, which gives

$$u = -b^TK(x_v+\Delta x_v)+v = u_v - b^TK\Delta x_v, \tag{4.18}$$

or in other words, since $u \in [-1, 1]$,

$$b^T K \Delta x_v \in [-1 + u_v, 1 + u_v]. \tag{4.19}$$

It is clear that K generates a Lyapunov function to the system (4.3) since

$$\begin{aligned} V(\Delta x_v) &= \Delta x_v^T K \Delta x_v > 0, \ \forall \Delta x_v \in \mathbb{R}^n, \ \Delta x_v \neq 0 \\ \dot{V}(\Delta x_v) &= \Delta x_v^T (A^T K + KA - 2Kbb^T K) \Delta x_v < 0, \ \forall \Delta x_v \in \mathbb{R}^n, \ \Delta x_v \neq 0, \end{aligned} \tag{4.20}$$

and K solves $Ricc(A, b, Q)$. Thus, as long as the system starts from a state from which the flow satisfies (4.19) it reaches the stationary point x_v. But, just because (4.19) is satisfied for some initial condition, it does not follow that it is satisfied by the flow as time evolves. However, along solutions, the Lyapunov function is decreasing, so if the system starts from the boundary of an ellipsoid, given by $\Delta x_v^T K \Delta x_v \leq \alpha_v$ for some α_v, that satisfies (4.19) then (4.19) is satisfied by the flow as time evolves as well.

In other words, the boundary of this region can be found by computing the smallest solution to the two quadratic optimization problems

$$\min_{\Delta x_v} \Delta x_v^T K \Delta x_v, \tag{4.21}$$

subject to either

$$b^T K \Delta x_v = -1 + u_v \tag{4.22}$$

or

$$b^T K \Delta x_v = 1 + u_v. \tag{4.23}$$

If we rename the variables as $c = Kb$ and $d_\pm = \pm 1 + u_v$, the Lagrange necessary and sufficient conditions (see for example Luenberger (1969)) for these two quadratic optimization problems are

$$\begin{aligned} K \Delta x_v + c\lambda_v &= 0 \\ c^T \Delta x_v - d_\pm &= 0, \end{aligned} \tag{4.24}$$

where $\lambda_v \in \mathbb{R}$ is the Lagrange multiplier. This gives

$$\begin{aligned} \lambda_v &= -(c^T K^{-1} c)^{-1} d_\pm \\ \Delta x_v &= K^{-1} c (c^T K^{-1} c)^{-1} d_\pm. \end{aligned} \tag{4.25}$$

That is

$$\begin{aligned} \Delta x_v &= K^{-1} Kb (b^T K K^{-1} Kb)^{-1} (\pm 1 + u_v) = b (b^T Kb)^{-1} (\pm 1 + u_v) \\ \Delta x_v^T K \Delta x_v &= (b^T Kb)^{-1} (\pm 1 + u_v)^2, \end{aligned} \tag{4.26}$$

where the inverse $(b^T K b)^{-1}$ exists since K is positive definite and $b \neq 0$ due to the controllability assumption.

If we let α_v be the smallest of the two solutions to (4.21), we directly get that

$$\alpha_v = (b^T K b)^{-1}(1 - |u_v|)^2, \tag{4.27}$$

which gives us the region from which $-b^T K x + v$ stabilizes the system around each x_v as the following ellipsoid

$$\mathcal{E}(K, v) = \{x \in \mathbb{R} \mid (x - x_v)^T K (x - x_v) \leq \alpha_v\}. \tag{4.28}$$

Thus the total region of attraction contains

$$\mathcal{L} = \bigcup_{v \in \mathcal{V}} \mathcal{E}(K, v), \tag{4.29}$$

and the theorem follows. ∎

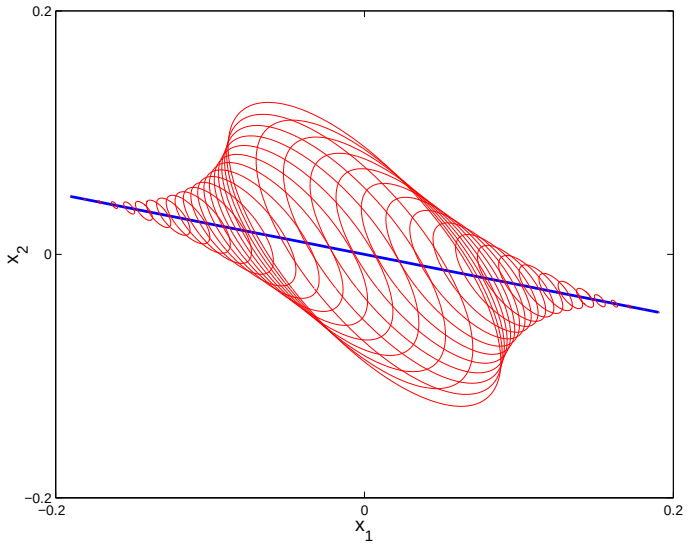

Figure 4.1: The thick, solid line is the set of stationary points achievable for constant inputs of available magnitudes, $\mathcal{X}$, while each ellipsoid, $\mathcal{E}(K, v)$, corresponds to a particular choice of $v \in \mathcal{V}$.

An example of applying Theorem 4.1.2 can be seen in Figure 4.1 where the following system matrices are used

$$A = \begin{pmatrix} 1 & 2 \\ 0 & -1 \end{pmatrix}, \quad b = \begin{pmatrix} 2 \\ 1 \end{pmatrix}, \quad K = \begin{pmatrix} 2 & -1 \\ -1 & 3 \end{pmatrix}. \tag{4.30}$$

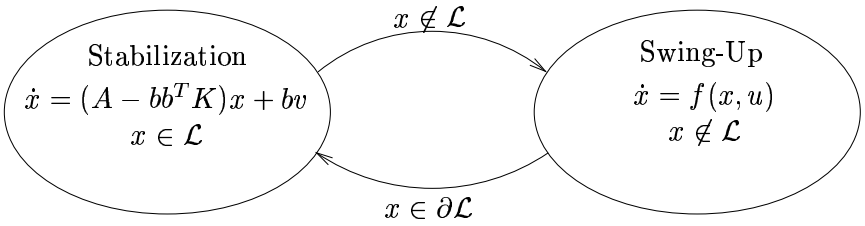

Figure 4.2: Schematic intended to suggest the need for a transition between stable or unstable equilibria and unsustainable transient needed to make a particular transition.

Remark 4.1.2 *If $rank(A) = n - 1$, we have that $u_v = 0$ for all $v \in \mathbb{R}$, and hence that $\alpha_v = (b^T K b)^{-1}$, which is independent of v. Thus $\mathcal{L}$ is a hyper-cylinder along $Ker(A)$. For the linearized model of the inverted pendulum $x_v \in Ker(A) = span\{(1,0,0,0)^T\}$, which means that the only stationary points are those for which $\dot{\theta}_1 = \theta_2 = \dot{\theta}_2 = 0$. But, since θ_1 lives on the quotient space $\mathbb{R}/2\pi\mathbb{Z} = S^1$, we can rewrite $\mathcal{X}$ as $\{(\theta_1, 0, 0, 0)^T \mid \theta_1 \in S^1\}$. Thus, the total region of attraction is compact in $\mathbb{R}^4$, and it furthermore has the structure of $S^1 \times B^3$, i.e. the circle times the 3-dimensional solid ball.*

4.2 Swing-up control

A hybrid system can be modeled as a *hybrid automaton* (see for example Henzinger (1996); Lygeros et al. (1999)), which can be thought of as a directed graph with a specific system dynamics associated with each node. Since we have derived a stabilizing controller and a corresponding region of attraction, or invariant set, one mode in the hybrid pendulum controller is already finished. Hence, our switching rule should be to switch from the swing-up mode to the stabilization mode when $x \in \partial\mathcal{L}$, i.e. we let this condition be the guard relation for the stabilization mode. It should be noted that we, throughout this chapter, assume that the linearized model is adequate on $\mathcal{L}$ for describing the system dynamics.

What remains to be done in the pendulum inversion problem is to design a swing-up controller that drives the system to $\mathcal{L}$ under bounded inputs, i.e. to derive an adequate u in the Swing-Up mode in Figure 4.2. In this case the nonlinear nature of the dynamics must be taken into account since, in the pendulum case, a large part of the state space is covered as the pendulum is swinging back and forth. Such a swing-up controller can be designed in a variety of ways. As an illustration, a naive approach can be seen in Figure 4.3, where the system matrices (the system is linear) are given by (4.30). The control is

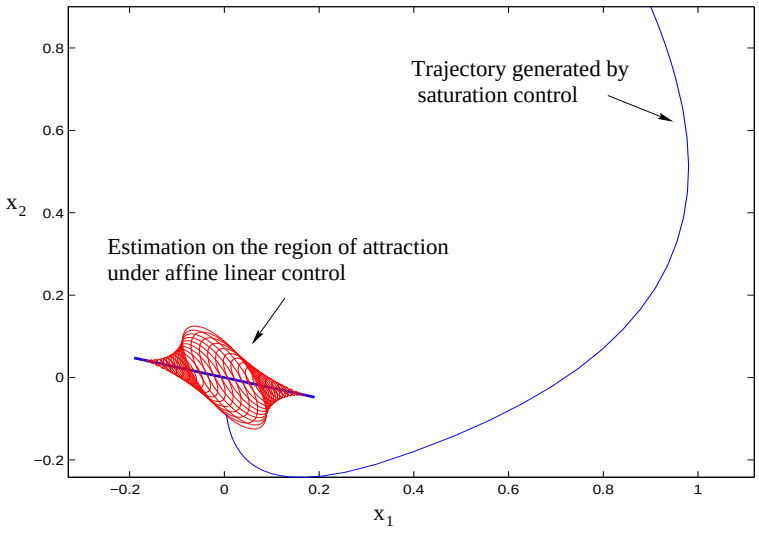

Figure 4.3: A switching example is shown where $v = \text{sat}(-b^T K x)$. This naive approach still results in a satisfactory behavior, and $\partial\mathcal{L}$ from Figure 4.1 is intersected by the trajectory.

simply given by a saturation function

$$u = \text{sat}(-b^T K x), \tag{4.31}$$

where $\text{sat}(\beta) = \beta$ if $\beta \in (-1, 1)$ and $\text{sign}(\beta)$ otherwise.

A Lagrangian mechanical system $L(x, \dot{x}, u)$ can be described by the equation

$$M(x, \dot{x})\ddot{x} + C(x, \dot{x})\dot{x} + \frac{\partial P(x)}{\partial x} = F(x)T(u), \tag{4.32}$$

where x is a vector of generalized coordinates, $M(x, \dot{x})$ the inertia matrix, $C(x, \dot{x})$ the damping matrix, $P(x)$ the potential energy, $F(x)$ an input gain matrix, and $T(u)$ are the external control torques. (See for example Marsden (1992); Spong and Vidyasagar (1989).)

The energy of the system is

$$E = \frac{1}{2}\dot{x}^T M(x, \dot{x})x + P(x),$$

and in Åström (1999) it was shown that

$$\frac{dE}{dt} = \dot{x}^T F(x)T(u).$$

In Åström and Furuta (1996); Åström (1999), it was furthermore pointed out that energy control could be explored for controlling Lagrangian systems.

In the inverted pendulum case, we have

$$\begin{aligned} \ddot{\theta}_1 &= u \\ \ddot{\theta}_2 &= \sin\theta_2 + u\cos\theta_2, \end{aligned} \tag{4.33}$$

and we can associate an energy measure with the movement of the vertical link. Since we want to drive this link to an inverted position it makes sense to inject as much energy into the system as possible.

We see that, if $u = 0$, we have

$$\dot{\theta}_2(\ddot{\theta}_2 - \sin\theta_2) = 0, \tag{4.34}$$

or, in other words, that $1/2\dot{\theta}_2 + \cos\theta_2$ is constant. It is thus possible to define the energy of the vertical link as

$$E(\theta_2, \dot{\theta}_2) = \frac{1}{2}\dot{\theta}_2 + \cos\theta_2, \tag{4.35}$$

which is constant if $u = 0$. Moreover, since

$$\frac{d}{dt}E(\theta_2, \dot{\theta}_2) = u\dot{\theta}_2\cos\theta_2 \tag{4.36}$$

we can easily control this energy since the system is simply an integrator with varying gain.

If we want to increase the energy in the vertical link, which is desirable in the swing-up situation, we can simply choose u such that

$$u\dot{\theta}_2\cos\theta_2 > 0 \tag{4.37}$$

at the same time as the constraint $|u| \leq 1$ is respected. This can always be done except when $\dot{\theta}_2 = 0$ or when $\theta_2 = \frac{\pi}{2} + n\pi,\ n \in \mathbb{Z}$.

However, for our experimental platform it is easier to implement swing-up controllers that are non-zero only when the pendulum is hanging straight down since, by virtue of (4.37), this is where the effect of the control is the most significant.

Since θ_1 and θ_2 are coupled we do not, in general, have control over $(\theta_1, \dot{\theta}_1)$ when the energy of the vertical link is controlled. However, an energy based control sequence that drives the states $x = (\theta_1, \dot{\theta}_1, \theta_2, \dot{\theta}_2)^T$ from any initial state $x_0 = (\theta_{10}, \dot{\theta}_{10}, \theta_{20}, \dot{\theta}_{20})^T$ to an open neighborhood of $x_F = (\theta_{1F}, 0, 0, 0)^T$ can be constructed from the following lemma:

Lemma 4.2.1 (Energy Increments) *Consider the initial state $x(0) = x_0 = (0, 0, -\pi, d)$, where $d > 0$. By applying the control*

$$u(t) = \begin{cases} -1, & \text{for } t \in [0, h) \\ 1, & \text{for } t \in [h, 2h], \end{cases}$$

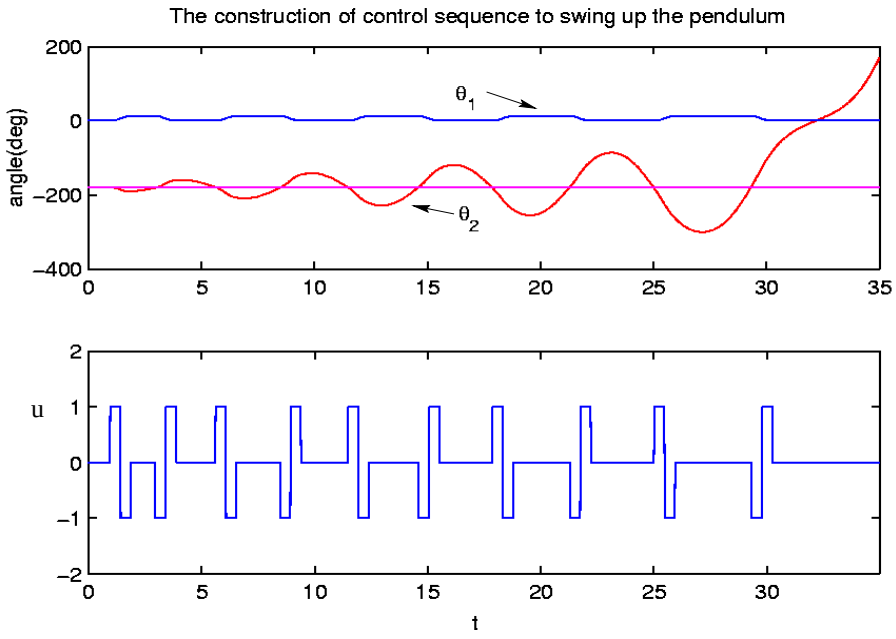

Figure 4.4: The control sequence and the corresponding trajectories in Lemma 4.2.1.

for a small $h \in \mathbb{R}^+$*, we obtain a net energy increase*

$$E(\theta_2(2h), \dot{\theta}_2(2h)) - E(-\pi, d) = h^3 d(d^2 + 1) + \mathcal{O}(h^4).$$

Proof: We first observe that from (4.33) it follows that when we apply the control $u = -1$ followed by $u = 1$ for the same amount of time h we get $\dot{\theta}_1(2h) = 0$. At the same time we will see that we get a net increase in the energy function $E(\theta_2, \dot{\theta}_2)$. Since the exact solution to $\ddot{\theta} = \sin\theta$ involves elliptic functions and is highly dependent on initial conditions we have to look for alternative ways of expressing the solution. Our proof of is based on an approximation of the exponential map

$$y(h) = \exp\{hf\}y_0,$$

where $y = (\theta_2 - \pi, \dot{\theta}_2)^T$, $y_0 = (0, d)^T$, and

$$f(y) = \begin{pmatrix} y_2 \\ -\sin y_1 - u\cos y_1 \end{pmatrix}.$$

Since we do not work around an equilibrium point a linear approximation will not suffice. Instead we can expand $\exp\{hf\}y_0$ in a manner similar to Taylor expansions (see for example Oliver (1993))

$$y(h) = y_0 + hf(y_0) + \frac{h^2}{2}\frac{\partial f}{\partial y}\bigg|_{y_0} f(y_0) + \frac{h^3}{6}\frac{\partial}{\partial y}(\frac{\partial f}{\partial y}f)\bigg|_{y_0} f(y_0) + \mathcal{O}(h^4).$$

By observing that $u = -1$ on $[0, h)$, it is tedious but straight forward to compute

$$y(h) = \begin{pmatrix} 0 \\ d \end{pmatrix} + h\begin{pmatrix} d \\ 1 \end{pmatrix} + \frac{h^2}{2}\begin{pmatrix} 1 \\ -d \end{pmatrix} + \frac{h^3}{6}\begin{pmatrix} -d \\ -d^2 - 1 \end{pmatrix} + \mathcal{O}(h^4).$$

Now, on $[h, 2h]$, we have $u = 1$ and we get

$$\begin{aligned} f(y(h)) &= \begin{pmatrix} d \\ -1 \end{pmatrix} + h\begin{pmatrix} 1 \\ -d \end{pmatrix} + \tfrac{h^2}{2}\begin{pmatrix} -d \\ d^2 - 1 \end{pmatrix} + \mathcal{O}(h^3), \\ \tfrac{\partial f}{\partial y}\Big|_{y(h)} f(y(h)) &= \begin{pmatrix} -1 \\ -d \end{pmatrix} + h\begin{pmatrix} -d \\ d^2 - 1 \end{pmatrix} + \mathcal{O}(h^2), \\ \tfrac{\partial}{\partial y}(\tfrac{\partial f}{\partial y}f)\Big|_{y(h)} f(y(h)) &= \begin{pmatrix} -d \\ d^2 + 1 \end{pmatrix} + \mathcal{O}(h). \end{aligned}$$

As before we can expand the exponential map

$$\begin{aligned} y(2h) &= y(h) + hf(y(h)) + \frac{h^2}{2}\frac{\partial f}{\partial y}\bigg|_{y(h)} f(y(h)) + \frac{h^3}{6}\frac{\partial}{\partial y}(\frac{\partial f}{\partial y}f)\bigg|_{y(h)} f(y(h)) + \mathcal{O}(h^4) \\ &= \begin{pmatrix} 0 \\ d \end{pmatrix} + h\begin{pmatrix} 2d \\ 0 \end{pmatrix} + h^2\begin{pmatrix} 1 \\ -2d \end{pmatrix} + h^3\begin{pmatrix} -4/3d \\ d^2 - 1 \end{pmatrix} + \mathcal{O}(h^4). \end{aligned}$$

Now, since

$$\cos(y_1(2h)) = 1 - 2h^2d^2 - 2h^3d + \mathcal{O}(h^4),$$

the difference in energy ($E(y) = 1/2y_2^2 - \cos y$ due to the change of variables) becomes

$$\begin{aligned} E(y(2h)) - E(y_0) &= \frac{1}{2}y_2^2(2h) - \cos(y_1(2h)) - \frac{1}{2}d^2 + 1 \\ &= \frac{1}{2}(d - 2h^2d + h^3(d^2 - 1))^2 - 1 + 2h^2d + 2h^3d - \frac{1}{2}d^2 + 1 + \mathcal{O}(h^4) \\ &= h^3d(d^2 + 1) + \mathcal{O}(h^4), \end{aligned}$$

which concludes the proof. ∎

Remark 4.2.1 *In a similar manner it is possible to derive that when $d = 0$ we get a net energy increase of $1/2h^4 + \mathcal{O}(h^5)$.*

With the help of Lemma 4.2.1, we can now state the main swing-up theorem.

Theorem 4.2.1 (Swing-Up Control) *Given a pendulum with initial conditions* $x_0 = (\theta_{10}, \dot{\theta}_{10}, \theta_{20}, \dot{\theta}_{20})^T$, *a control sequence based on Lemma 4.2.1 can be constructed, as seen in Figure 4.2, that drives the initial state to any given open neighborhood of* $x_F = (\theta_{1F}, 0, 0, 0)^T \in S^1$.

Proof:

Case1: Let $x_0 = (0, 0, -\pi, 0)^T$, $x_F = (0, 0, 0, 0^T)$. From Lemma 4.2.1 it follows that we can increase the energy $E(\theta_2, \dot{\theta}_2)$ by a factor $h^3\dot{\theta}_2(\dot{\theta}_2^2 + 1)$ when $\dot{\theta}_2 > 0$ (or $1/2h^4$ when $\dot{\theta}_2 = 0$.) When $\dot{\theta}_2 < 0$ we can change the control to $u(t) = 1$ for $t \in [0, h)$ and $u(t) = -1$ for $t \in [h, 2h]$ to get the same amount of energy increase. We can thus apply this control sequence, as seen in Figure 4.2, whenever $\theta_2(t)$ passes $-\pi$ until the energy is $\geq 1 - \delta$, for any $\delta \geq 0$. (The engergy at the inverted position is 1.) By setting $u = 0$ the state will eventually flow into the neighborhood of $(\theta_1, \dot{\theta}_1, 0, 0)^T$ by itself once the right energy is obtained due to the conservation of energy. Since $\ddot{\theta}_1 = u$ the pairs $(\theta_1, \dot{\theta}_1)$ will remain in the interval $[-2h, 0] \times [-h, h]$ for all times. By reducing h and δ we can thus make the open neighborhood of $x_F = (0, 0, 0, 0)^T$ arbitrarily small.

Case 2: Suppose that the system starts at $x_0 = (0, 0, \theta_{20}, \dot{\theta}_{20})$. If the initial energy $E(\theta_{20}, \dot{\theta}_{20})$ is less than $1-\delta$ we can use the control sequence in Case 1. If $E(\theta_{20}, \dot{\theta}_{20}) > 1+\delta$, we need to "flip" the control in order to decrease the energy, i.e. $u(t) = 1$ for $t \in [t_i, t_i + h)$ and -1 for $t \in [t_i + h, t_i + 2h]$, where $\dot{\theta}_2(t_i) > 0$ when $\theta_2(t_i)$ passes $-\pi$. If the energy is still greater 1 at time $t_i + 2h$, we can expect θ_2 to pass 0 at some t_{i+1}. We can then apply the same type of "flipped" control at time t_{i+1}. In this way we can keep reducing the energy until we have $E(\theta_2, \dot{\theta}_2) < 1 + \delta$, as in Case 1. We can furthermore guarantee that $(\theta_1, \dot{\theta}_1) \in [-2h, 2h] \times [-h, h]$ for all times and thus the pendulum reaches the open neighborhood of $x_F = (0, 0, 0, 0)^T$.

Case 3: For arbitrary initial conditions $x_0 = (\theta_{10}, \dot{\theta}_{10}, \theta_{20}, \dot{\theta}_{20})^T$ and final conditions $x_F = (\theta_{1F}, 0, 0, 0)^T$ we can first send $(\theta_1, \dot{\theta}_1)$ to $(\theta_{1F}, 0)$ using a bounded u without difficulty and then apply the controller in Case 2. ∎

As we will see in Section 4.3, this control sequence is a good candidate for the swing-up mode in our multi-modal hybrid control design.

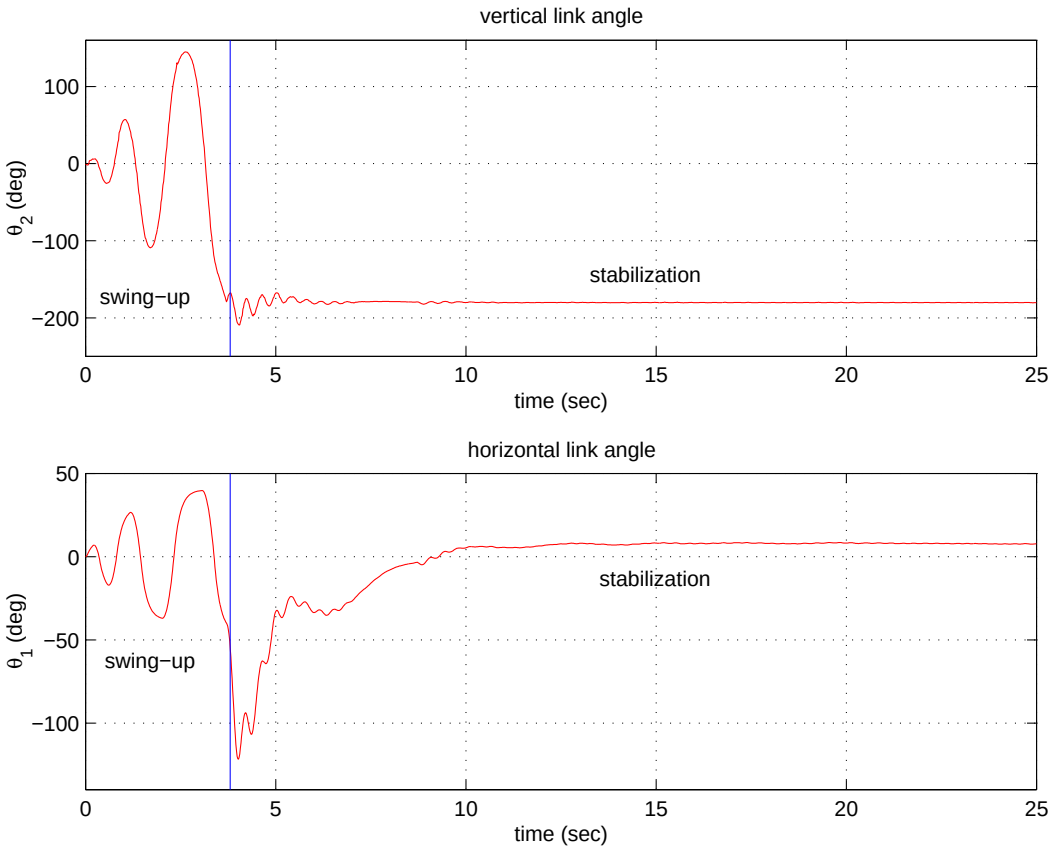

Figure 4.5: Swing-Up and Stabilization. The top figure shows the vertical link angle, while the horizontal link angle is depicted in the bottom figure. The mode transition from Swing-Up to Stabilization occurs after 3.8 seconds.

4.3 Experimental results

An example of applying the theory developed in Section 4.1 and Section 4.2 to the platform in Section 3.4 is shown in Figure 4.5. Here, the bounded input stabilization is combined with an energy-based swing-up controller. Since we can choose any $u \in [-1, 1]$ such that the energy in the system is increased as the pendulum swings back and forth, we choose to work with the provenly correct control sequence in Theorem 4.2.1.

In Figure 4.6, a case where the pendulum is perturbed at its inverted position is shown. The figure clearly illustrates that, even though the available inputs are bounded, our solution is quite robust to external disturbances.

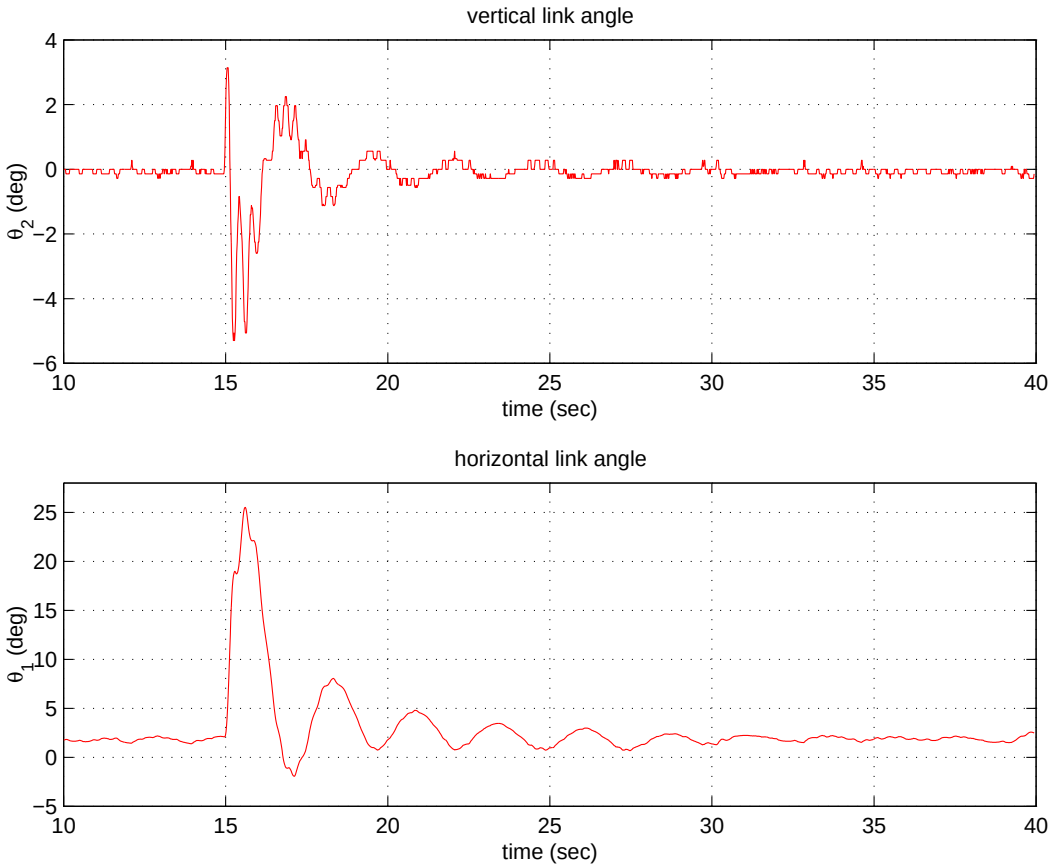

Figure 4.6: An example when the vertical link is perturbed at its inverted position is shown.

Chapter 5

Results on stabilization

5.1 Introduction

The usual application of feedback stabilization is based on linearization and the assumption of linear controllability. Least squares optimal control is often used to determine a set of feedback gains that will stabilize the system. In addition to the commonly acknowledged challenges arising when this methodology is applied to open-loop unstable systems with significant nonlinearities, there are also other significant problems that are not given prominence in the literature. These include the role of high gain feedback in exciting vibrations in unmodeled modes and the possibility of lightly damped oscillatory modes accentuating the effect of the nonlinearities. In this chapter we report some experimental results relating to these points and suggest some techniques for dealing with them. Significant parts of this chapter are reported in Brockett and Li (2003).

This chapter describes an experimental effort concerned with the stabilization of a rotary double link pendulum. This problem, and several related ones, has a long history going back several decades. In the literature the name of Furuta stands out because of his early interest in these problems and the steady stream of experimental results reported by his group Furuta et al. (1978); Yamakita et al. (1993); Åström (1999). Our approach differs from those previously reported not in terms of the basic form of the mechanics, but rather in terms of important aspects of the experimental apparatus. Most notably, we are working with a system with the following attributes:

1. All measurement signals are transmitted over a wireless link delivering 50 samples per second. This removes the need for wires connecting the moving parts to a fixed platform but introduces some latency in the data path and limits the sampling fre-

quency.

2. The apparatus is light weight and has low inertia. This results in a structure with low stiffness and a tendency to vibrate.

3. The motor is a low torque, completely integrated amplifier/motor/controller unit rather than a high performance direct drive motor. This makes it necessary to design around the possibility of torque saturation.

In attempting to further develop the rotary link double pendulum stabilization technology, several challenges present themselves. The principal ones are.

1. The emergence of vibrational modes associated with unmodeled dynamics associated with the elasticity of the structure.

2. The problem of avoiding high feedback gains which can lead to torque saturation, noise amplification, and undesirable vibration.

3. A reduction in the size of the domain of asymptotic stability.

The general problem of stabilization via feedback has received considerable attention in both a linear and nonlinear context. Indeed, one of the central questions in classical control theory is the problem of avoiding instability in feedback systems. In this chapter we are concerned with the problem of designing a control law that provides an adequate domain of attraction for a nonlinear system of the form

$$\dot{x} = f(x) + g(x)u \tag{5.1}$$

under the hypothesis that $f(0) = 0$; $g(0) \neq 0$. We assume that f and g are smooth functions and that the linearized system is controllable. Such questions are widely studied in the literature, being motivated by a variety of concrete problems including experimental work on stabilizing various types of open loop unstable mechanical systems.

Because we assume that the linearization of the system at $x = 0$ is controllable, in theory there always exists a linear control law that stabilizes the null solution. Moreover, there exists a change of coordinates valid in a neighborhood of the origin that makes g equal to a constant vector so we can carry out the first step in the feedback linearization procedure. A precise question along these lines can be formulated as follows.

Linear Feedback Stabilization Problem: Given a system of the form $\dot{x} = f(x) + G(x)u$ with $f(0) = 0$ and $g(0) \neq 0$, find the linear time invariant control law $u = Kx$ such

that the null solution of $\dot{x} = f(x) + G(x)Kx$ is asymptotically stable and the domain of attraction of 0 is as large as possible in the sense that it contains a ball of the form $||x|| \leq a$ with a maximal.

5.2 A hierarchy of mechanical systems

Our ultimate goal is to shed further light on the problem of enlarging the domain of attraction for nonlinear control systems. Both the rotary double pendulum system, as shown in Figure 3.7, and several other simpler mechanical systems have been extensively studied in the literature. In order to maximize the usefulness of this chapter and to put our results in a broader context, we compare this system with a general version of the well-known ball and beam system and the double pendulum on a cart system. We will see that these form a progression with the ball and beam being the least complex, the double pendulum being of intermediate complexity and the rotary pendulum being the most complex. For more about classical mechanics, see Whittaker (1937).

The ball, beam, cart. This is the least complicated system in our hierarchy. Consider the ball and beam on a cart system as shown in Figure 5.1. The kinetic energy is

$$\begin{aligned} K = \tfrac{1}{2}m_5[(\dot{x}_5 + \dot{x}_1\cos x_3)^2 + (x_5\dot{x}_3 - \dot{x}_1\sin x_3)^2] \\ + \tfrac{1}{2}I_5(\frac{\dot{x}_5}{r_5} - \dot{x}_3)^2 + \tfrac{1}{2}m_3\dot{x}_1^2 \\ + \tfrac{1}{2}I_3\dot{x}_3^2 - m_3 l_3\dot{x}_1\dot{x}_3\cos x_3 \end{aligned}$$

Where x_5 is the position of the center of the ball relative to the joint of the beam. r_5 is the radius of the ball. x_3 is the angular position of the beam. x_1 is the position of the cart. All x_i's are on the same vertical plane. m_3, m_5, I_3, and I_5 are the mass and momentum of inertia of the ball and beam respectively. We assume to have direct control over the acceleration of the cart, i.e., $\ddot{x}_1 = u$. The potential energy is

$$V = m_5 g x_5 \sin x_3 + m_3 g l_3 \cos x_3.$$

The Euler-Lagrangian equations take the form

$$F(x)\ddot{x} + G(x,\dot{x}) + V(x) = ub(x) \tag{5.2}$$

with $x = [x_1, x_3, x_5]^T$

$$F(x) = \begin{bmatrix} 1 & 0 & 0 \\ 0 & m_5 x_5^2 + I_5 + I_3 & -\frac{I_5}{r_5} \\ 0 & -\frac{I_5}{r_5} & m_5 + \frac{I_5}{r_5^2} \end{bmatrix}$$

$$G(x, \dot{x}) = \begin{bmatrix} 0 \\ 2m_5 x_5 \dot{x}_3 \dot{x}_5 \\ -m_5 x_5 \dot{x}_3^2 \end{bmatrix}$$

$$V(x) = \begin{bmatrix} 0 \\ -m_3 l_3 g \sin x_3 + m_5 g x_5 \cos x_3 \\ m_5 g \sin x_3 \end{bmatrix}$$

and $b(x)$ is given by

$$b(x) = \begin{bmatrix} 1 \\ m_3 x_5 \sin x_3 + m_3 l_3 \cos x_3 \\ -m_5 \cos x_3 \end{bmatrix}$$

The linearization of the Ball-Beam on Cart is

$$F\ddot{x} + Vx = ub \tag{5.3}$$

with

$$F = \begin{bmatrix} 1 & 0 & 0 \\ 0 & I_5 + I_3 & -\frac{I_5}{r_5} \\ 0 & -\frac{I_5}{r_5} & m_5 + \frac{I_5}{r_5^2} \end{bmatrix}$$

$$V = \begin{bmatrix} 0 & 0 & 0 \\ 0 & -m_3 l_3 g & m_5 g \\ 0 & m_5 g & 0 \end{bmatrix}, \qquad b = \begin{bmatrix} 1 \\ m_3 l_3 \\ -m_5 \end{bmatrix}.$$

The transfer function $G(s)$ from u to x can be most easily obtained from the linearization in second order form,

$$Fs^2 X(s) + VX(s) = U(s)b \tag{5.4}$$

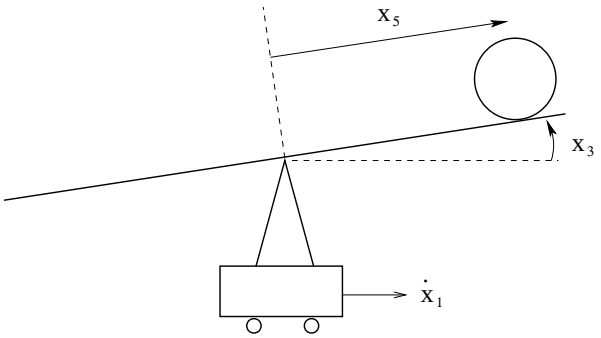

Figure 5.1: Ball, Beam, Cart

This yields the transfer function

$$G(s) = \begin{bmatrix} \frac{1}{s^2} \\ \frac{p_{22}s^2 + p_{20}}{q_4 s^4 + q_2 s^2 + q_0} \\ \frac{p_{32}s^2 + p_{30}}{q_4 s^4 + q_2 s^2 + q_0} \end{bmatrix} \tag{5.5}$$

with

$$\begin{aligned} p_{22} &= -m_5 r_5 I_5 + m_3 l_3 (m_5 r_5^2 + I_5) \\ p_{20} &= -m_5^2 r_5^2 g \\ p_{32} &= -m_5 r_5^2 (I_3 + I_5) + m_3 l_3 I_5 \\ p_{30} &= 2 m_3 m_5 l_3 r_5 g \\ q_4 &= m_5 r_5^2 (I_3 + I_5) + I_3 I_5 \\ q_2 &= 2 m_5 r_5 I_5 g - m_3 l_3 g (m_5 r_5^2 + I_5) \\ q_0 &= -m_5^2 r_5^2 g \end{aligned}$$

Cart with a double pendulum. The coupled equations of motion that describe the dynamics of the pendulum, as shown in Figure 5.2, are described by the Euler-Lagrangian equation

$$F(\theta)\ddot{\theta} + G(\theta, \dot{\theta}) + V(\theta) = ub(\theta) \tag{5.6}$$

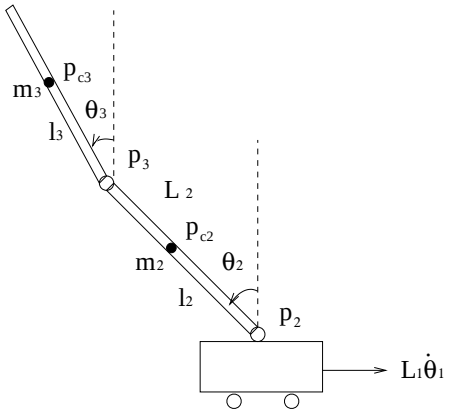

Figure 5.2: The double pendulum on a cart

with $\theta = [\theta_1, \theta_2, \theta_3]^T$

$$F(\theta) = \begin{bmatrix} 1 & 0 & 0 \\ 0 & I_2 + m_3 L_2^2 & m_3 l_3 L_2 \cos(\theta_2 - \theta_3) \\ 0 & m_3 l_3 L_2 \cos(\theta_2 - \theta_3) & I_3 \end{bmatrix}$$

$$G(\theta, \dot{\theta}) = \begin{bmatrix} 0 \\ m_3 l_3 L_2 \dot{\theta}_3^2 \sin(\theta_2 - \theta_3) \\ -m_3 l_3 L_2 \dot{\theta}_2^2 \sin(\theta_2 - \theta_3) \end{bmatrix}$$

$$V(\theta) = \begin{bmatrix} 0 \\ -(m_2 g l_2 + m_3 g L_2) \sin\theta_2 \\ -m_3 g l_3 \sin\theta_3 \end{bmatrix}$$

and $b(\theta)$ given by

$$b(\theta) = \begin{bmatrix} 1 \\ -(m_2 l_2 + m_3 L_2) \cos\theta_2 \\ -m_3 l_3 \cos\theta_3 \end{bmatrix},$$

where I_2 and I_3 are the moments of inertia of link 2 and link 3 with respect to their joints p_2 and p_3, respectively. L_2 is the length of link 2, while l_2 and l_3 are the distance from the center of mass to their joints of link 2 and link 3 respectively. In this problem, we can directly control the acceleration of the motor. Thus the motor equation is simply a double

integrator $\ddot{\theta}_1 = u$. Its linearization is identical to the rotary double pendulum as describe in the following subsection if the motor position θ_1 is replaced by $L_1\theta_1$.

Rotary double pendulum.

We rewrite the double pendulum equations in Section 3.3 to compare with those in the previous two subsections. The coupled equations of motion that describe the dynamics of the pendulum, as shown in Figure 3.13, are described by the Euler-Lagrangian equation

$$F(\theta)\ddot{\theta} + G(\theta, \dot{\theta}) + V(\theta) = ub(\theta) \tag{5.7}$$

with $\theta = [\theta_1, \theta_2, \theta_3]^T$

$$F(\theta) = \begin{bmatrix} 1 & 0 & 0 \\ 0 & I_2 + m_3 L_2^2 & m_3 l_3 L_2 \cos(\theta_2 - \theta_3) \\ 0 & m_3 l_3 L_2 \cos(\theta_2 - \theta_3) & I_3 \end{bmatrix}$$

$$G(\theta, \dot{\theta}) = \begin{bmatrix} 0 \\ g_2(\theta, \dot{\theta}) \\ g_3(\theta, \dot{\theta}) \end{bmatrix}$$

$$V(\theta) = \begin{bmatrix} 0 \\ -(m_2 g l_2 + m_3 g L_2)\sin\theta_2 \\ -m_3 g l_3 \sin\theta_3 \end{bmatrix}$$

and $b(\theta)$ is given by

$$b(\theta) = \begin{bmatrix} 1 \\ -(m_2 l_2 + m_3 L_2) L_1 \cos\theta_2 \\ -m_3 l_3 L_1 \cos\theta_3 \end{bmatrix},$$

where

$$\begin{aligned} g_2(\theta, \dot{\theta}) &= -[\tfrac{1}{2}(I_2 + m_3 L_2^2)\sin 2\theta_2 + m_3 l_3 L_2 \cos\theta_2 \\ &\qquad \sin\theta_3]\dot{\theta}_1^2 + m_3 l_3 L_2 \dot{\theta}_3^2 \sin(\theta_2 - \theta_3) \\ g_3(\theta, \dot{\theta}) &= -(\tfrac{1}{2} I_3 \sin 2\theta_3 + m_3 l_3 L_2 \sin\theta_2 \cos\theta_3)\dot{\theta}_1^2 \\ &\qquad -m_3 l_3 L_2 \dot{\theta}_2^2 \sin(\theta_2 - \theta_3). \end{aligned}$$

Here, the notations are the same as those in Section 3.3.

Associated with this nonlinear model is its linearization about $\theta_i = 0, \dot{\theta}_i = 0$. The corresponding terms are given by

$$F\ddot{\theta} + V\theta = ub \tag{5.8}$$

with

$$F = \begin{bmatrix} 1 & 0 & 0 \\ 0 & I_2 + m_3 L_2^2 & m_3 l_3 L_2 \\ 0 & m_3 l_3 L_2 & I_3 \end{bmatrix}$$

$$V = \begin{bmatrix} 0 & 0 & 0 \\ 0 & -(m_2 g l_2 + m_3 g L_2) & 0 \\ 0 & 0 & -m_3 g l_3 \end{bmatrix}$$

$$b = \begin{bmatrix} 1 \\ -(m_2 l_2 + m_3 L_2) L_1 \\ -m_3 l_3 L_1 \end{bmatrix}$$

The transfer function from u to θ is

$$G(s) = \begin{bmatrix} \frac{1}{s^2} \\ \frac{p_{22} s^2 + p_{20}}{q_4 s^4 + q_2 s^2 + q_0} \\ \frac{p_{32} s^2 + p_{30}}{q_4 s^4 + q_2 s^2 + q_0} \end{bmatrix} \tag{5.9}$$

with

$$\begin{aligned} p_{22} &= -(m_2 l_2 + m_3 L_2) I_3 L_1 \\ p_{20} &= (m_2 l_2 g + m_3 L_2 g + m_3 l_3 L_2) m_3 l_3 L_1 \\ p_{32} &= -(I_2 + m_3 L_2^2)(m_2 l_2 + m_3 L_2) L_1 \\ p_{30} &= (m_2 l_2 g + m_3 L_2 g + m_3 l_3 L_2)(m_2 l_2 + m_3 L_2) L_1 \\ q_4 &= (I_2 + m_3 L_2^2) I_3 \\ q_2 &= -[(I_2 + m_3 L_2^2) m_3 l_3 + (m_2 l_2 + m_3 L_2) I_3] g \\ q_0 &= (m_2 l_2 g^2 + m_3 L_2 g^2 - m_3 l_3 L_2^2) m_3 l_3. \end{aligned}$$

5.3 Feedback linear approximation

In this section, we work with a type of optimization problems in which we linearly approximate the double pendulum at its equilibrium points. Given a scalar input nonlinear system

$$\dot{x} = f(x) + ug(x), \qquad x \in \mathbb{R}^n,\ u \in \mathbb{R}, \tag{5.10}$$

with $f(0) = 0$, i.e., $x = 0$ is an equilibrium point. We can linearize it at its equilibrium point in the standard way to get

$$\dot{x} = \frac{\partial f(0)}{\partial x} x + ug(0). \tag{5.11}$$

It leads to theorems on local controllability and, via least squares theory, to feedback control laws resulting in asymptotic stability. However, in this case there are many stabilizing control laws and if the goal is to design a controller that will have a large domain of convergence, conventional linearization may not provide the best solution. The region in which (5.11) accurately approximates (5.10) is usually very small. Brockett (1978) proposed an exact feedback linearization and its conditions. In many cases, those conditions are not satisfied. Here we develop an alternative, which we have found effective in controlling the rotary double pendulum.

Let $\mathcal{D}$ represent an open set in $\mathbb{R}^n$ that contains origin. If we wish to find a matrix $A \in \mathbb{R}^{n\times n}$ such that Ax approximates $f(x)$ on the set $\mathcal{D}$ then we might choose A so as to minimize

$$\eta_1 = \int_{\mathcal{D}} ||f(x) - Ax||^2 dx \tag{5.12}$$

Of course if $\mathcal{D}$ is very small the minimizing value of A will be close to $\left.\frac{\partial f}{\partial x}\right|_0$ but if $\mathcal{D}$ is large it can be rather different. If we work with the Euclidean norm then the optimal value of A is easily seen to be

$$A^* = \int_{\mathcal{D}} f(x)x^T dx \left(\int_{\mathcal{D}} xx^T dx\right)^{-1} \tag{5.13}$$

However, the possibility exists for improving the accuracy of this approximation through the use of feedback. Consider a refinement of the above procedure in which we select both $(A \in \mathbb{R}^{n\times n}, b \in \mathbb{R}^n)$ and a feedback function $\alpha(\cdot) \in \mathbb{C}^\infty$ with $\alpha(0) = 0$ so as to minimize

$$\eta_1 = \int_{\mathcal{D}} \|f(x) - \alpha(x)g(x) - Ax\|^2 dx, \tag{5.14}$$

in a given domain $\mathcal{D}$ of x containing zero, called $\mathcal{D}_f$*-optimal problem*, and to minimize

$$\eta_2 = \int_{\mathcal{D}} \|g(x) - b\|^2 dx. \tag{5.15}$$

separately, called $\mathcal{D}_g$-*optimal problem.* In this case we can see that for a given value of A the best choice of α is the choice that cancels the error $f(x) - Ax$ in the direction of $g(x)$. Having done so,

$$\dot{x} = Ax + ub$$

becomes the "best" linear approximation of

$$\dot{x} = f(x) - \alpha(x)g(x) + ug(x).$$

in domain $\mathcal{D}$. We need the following assumption for the remainder of the chapter.

Assumption 5.3.1 $\|g(x)\| > 0$ *for all* $x \in \mathcal{D}$.

In order to solve the $\mathcal{D}_f$-optimal problem, we consider two sub cost functions first,

$$\eta_{11}(A) = \int_{\mathcal{D}} \|f(x) - Ax\|^2 dx, \qquad \eta_{12}(\alpha) = \int_{\mathcal{D}} \|f(x) - \alpha(x)g(x)\|^2 dx.$$

Using first order perturbation analysis, we have

$$\begin{aligned} \eta_{11}(A + \delta A) &= \textstyle\int_{\mathcal{D}} \|f(x) - Ax - \delta Ax\|^2 dx \\ &= \textstyle\int_{\mathcal{D}} \|f(x) - Ax\|^2 - 2\langle f(x) - Ax, \delta Ax\rangle + \|\delta Ax\|^2 dx \\ &= \eta_{11} - 2\textstyle\int_{\mathcal{D}} \langle f(x) - Ax, \delta A\rangle dx + h.o.t. \end{aligned}$$

If A minimizes η_{11}, then

$$\int_{\mathcal{D}} \langle f(x) - Ax, \delta Ax\rangle dx = 0 \qquad \text{for any} \quad \delta A,$$

$\Longrightarrow$

$$\begin{aligned} 0 &= \textstyle\int_{\mathcal{D}} (f(x) - Ax)^T \delta Ax \; dx \\ &= \textstyle\int_{\mathcal{D}} \mathrm{trace}(f(x) - Ax)(\delta Ax)^T dx \\ &= \mathrm{trace}(\textstyle\int_{\mathcal{D}} (f(x) - Ax)x^T dx \, \delta A^T). \end{aligned}$$

Since δA is arbitrary, we have

$$\int_{\mathcal{D}} (f(x) - Ax)x^T dx = 0.$$

$\Longrightarrow$

$$A = \int_{\mathcal{D}} f(x)x^T dx \left(\int_{\mathcal{D}} xx^T dx\right)^{-1}. \tag{5.16}$$

Note that $xx^T \geq 0$. We can always find a polytope region $\mathcal{D}_1 = \{x \in R^n \mid |x_i| \leq d_i\}$ inside the domain $\mathcal{D} \in 0$. Integration of xx^T over $\mathcal{D}_1$ results in a positive diagonal matrix.

$$\int_{\mathcal{D}_1} xx^T dx = \mathrm{diag}\{\int_{\mathcal{D}_1} x_1^2 dx, \cdots, \int_{\mathcal{D}_1} x_n^2 dx\} = \frac{1}{3}\mathrm{Vol}(\mathcal{D}_1)\mathrm{diag}\{d_1^2, \cdots, d_n^2\}. \tag{5.17}$$

Hence, $\int_{\mathcal{D}} xx^T dx \geq \int_{\mathcal{D}_1} xx^T dx > 0$ if $Vol(\mathcal{D}) > 0$. $\int_{\mathcal{D}} xx^T dx$ is positive definite even for $\mathcal{D} \not\ni 0$. Thus we can invert $\int_{\mathcal{D}} xx^T dx$ in (5.16). Use first order perturbation analysis again, we have

$$\begin{aligned}
&\eta_{12}(\alpha + \delta\alpha) \\
&= \int_{\mathcal{D}} \|f(x) - \alpha(x)g(x) - \delta\alpha(x)g(x)\|^2 dx \\
&= \int_{\mathcal{D}} \|f(x) - \alpha(x)g(x)\|^2 - 2\langle f(x) - \alpha(x)g(x), \delta\alpha(x)g(x)\rangle + \|\delta\alpha(x)g(x)\|^2 dx \\
&= \eta_{12}(\alpha) - 2\int_{\mathcal{D}} \langle f(x) - \alpha(x)g(x), \delta\alpha(x)g(x)\rangle dx + h.o.t.
\end{aligned}$$

If α minimizes η_{12}, we have

$$\begin{aligned}
0 &= \int_{\mathcal{D}} \langle f(x) - \alpha(x)g(x), \delta\alpha(x)g(x)\rangle dx \\
&= \int_{\mathcal{D}} \langle f(x) - \alpha(x)g(x), g(x)\rangle \delta\alpha(x) dx.
\end{aligned}$$

Since $\delta\alpha(x)$ is arbitrary, we have

$$\langle f(x) - \alpha(x)g(x), g(x)\rangle = 0,$$

i.e.,

$$\alpha(x) = \frac{\langle f(x), g(x)\rangle}{\langle g(x), g(x)\rangle} \qquad \text{for} \quad x \in \mathcal{D}. \tag{5.18}$$

Combining these two cases, we have

Theorem 5.3.1 *The $\mathcal{D}_f$-optimal pair $(\alpha^\star, A^\star)$ satisfies*

$$\alpha^\star(x) = \frac{\langle f(x) - A^\star x, g(x)\rangle}{\langle g(x), g(x)\rangle} = \alpha(x) - \frac{\langle A^\star x, g(x)\rangle}{\langle g(x), g(x)\rangle}, \tag{5.19}$$

and

$$A^\star = \int_{\mathcal{D}} (f(x) - \alpha^\star(x)g(x))x^T dx (\int_{\mathcal{D}} xx^T dx)^{-1} = A - \int_{\mathcal{D}} \alpha^\star(x)g(x)x^T dx (\int_{\mathcal{D}} xx^T dx)^{-1}. \tag{5.20}$$

Where $\alpha(x)$ and A are defined by (5.18) and (5.16), respectively.

We can solve the $\mathcal{D}_g$-optimal problem in the same way.

Theorem 5.3.2 *The $\mathcal{D}_g$-optimal $b^\star$ is given by*

$$b^\star = Vol(\mathcal{D})^{-1} \int_{\mathcal{D}} g(x) dx. \tag{5.21}$$

Proof. Using the first order perturbation to the cost function η_2, we have

$$\begin{aligned}
\eta_2(b + \delta b) &= \int_{\mathcal{D}} \|g(x) - b - \delta b\|^2 dx \\
&= \int_{\mathcal{D}} \|g(x) - b\|^2 dx - 2\int_{\mathcal{D}} \langle g(x) - b, \delta b\rangle dx + h.o.t.
\end{aligned}$$

If b minimizes η_2, we must have

$$\int_{\mathcal{D}} \langle g(x) - b, \delta b \rangle dx = 0, \quad \text{for arbitrary } \delta b.$$

Thus

$$\int_{\mathcal{D}} g(x)dx = \int_{\mathcal{D}} b\, dx = b \int_{\mathcal{D}} dx = b\, \mathrm{Vol}(\mathcal{D}).$$

■

The next question we need to answer is the existence of the $\mathcal{D}_f$-optimal pair $(\alpha^\star, A^\star)$. The space $\mathbb{C}^\infty[\mathcal{D}] \ni \alpha$ is of infinite dimension. The minimal cost (5.14) may not be achievable. If that is the case, we can only find a sequence $\{(\alpha_i, A_i)\}$ to approach the minimal cost (5.14). But $\{(\alpha_i, A_i)\}$ doesn't converge in $\mathbb{C}^\infty[\mathcal{D}]$. Fortunately, we can reduce it in to a finite dimensional optimization problem. Hence the minimal is achievable. We rewrite the $\mathcal{D}_f$-optimal problem (5.14) as follows

$$\min_{\varphi \in \Phi} |\!|\!| f - \varphi |\!|\!|, \tag{5.22}$$

where $|\!|\!| f |\!|\!| = \left(\int_{\mathcal{D}} \|f(x)\|^2 dx \right)^{\frac{1}{2}}$ defines a norm on vector field $f \in \mathbb{C}_n^\infty[\mathcal{D}]$, and

$$\Phi = \{\varphi \in \mathbb{C}_n^\infty[\mathcal{D}] \mid \varphi(x) = \alpha(x)g(x) + Ax, \alpha \in \mathbb{C}^\infty[\mathcal{D}], \text{and } A \in \mathbb{R}^{n\times n}\}.$$

Clearly Φ with inner product defined by $\langle\!\langle \varphi_1, \varphi_2 \rangle\!\rangle = \int_{\mathcal{D}} \langle \varphi_1(x), \varphi_2(x) \rangle dx$ is a Hilbert space of infinite dimension. Norm $|\!|\!| \cdot |\!|\!|$ is induced by inner product $\langle\!\langle \cdot, \cdot \rangle\!\rangle$. Let

$$E_{ij} = \begin{pmatrix} 0 & \cdots & 0 & 0 & 0 & \cdots & 0 \\ & & & \cdots & & & \\ 0 & \cdots & 0 & 1 & 0 & \cdots & 0 \\ & & & \cdots & & & \\ 0 & \cdots & 0 & 0 & 0 & \cdots & 0 \end{pmatrix}$$

where only the (i,j)-th entry is 1. Then matrix $A^\star = \left(a_{ij}^\star\right) = \sum_{i,j} a_{ij}^\star E_{ij}$. We rewrite equation (5.19) in theorem 5.3.1 as

$$\alpha^\star(x) = \alpha(x) - \frac{\langle \sum_{i,j} a_{ij}^\star E_{ij} x, g(x) \rangle}{\langle g(x), g(x) \rangle} = \alpha(x) - \sum_{i,j} a_{ij}^\star \frac{\langle E_{ij} x, g(x) \rangle}{\langle g(x), g(x) \rangle}$$

Let $\varphi_{ij}(x) = \dfrac{\langle E_{ij} x, g(x) \rangle}{\langle g(x), g(x) \rangle}$. We get

$$\alpha^\star(x) = \alpha(x) - \sum_{i,j} a_{ij}^\star \varphi_{ij}(x). \tag{5.23}$$

We need the projection theorem to prove the existence of the solution to (5.22).

Lemma 5.3.1 *(The classic projection theorem) Let H be a Hilbert space and M a closed subspace of H. Corresponding to any vector $x \in H$, there is a unique vector m_0 such that $\|x - m_0\| \leq \|x - m\|$ for all $m \in H$. Further more, a necessary and sufficient condition that $m_0 \in M$ be the unique minimizing vector is that $x - m_0$ be orthogonal to M.*

See Luenberger (1969) p.51 for the proof.

Theorem 5.3.3 *The $\mathcal{D}_f$-optimal problem (5.22)*

$$\min_{\varphi \in \Phi} \|\!| f - \varphi |\!\|,$$

is equivalent to the following problem

$$\min_{\varphi \in \Phi_1} \|\!| f - \alpha - \varphi |\!\|, \tag{5.24}$$

where $\Phi_1 = span\{\varphi_{11}, \varphi_{12}, \cdots, \varphi_{nn}\}$ on domain $\mathcal{D}$. Dimension of Φ_1 is at most n^2. Furthermore, there is a unique solution $\varphi^\star \in \Phi_1$ to (5.24).

Φ_1 is a finite dimensional subspace of Hilbert space Φ and is hence closed. We identify H with $\mathbb{C}_n^\infty[\mathcal{D}]$, M with Φ_1, x with $f - \alpha$, and m with φ. Thus we can apply the projection theorem to prove the last part of theorem 5.3.3.

The projection theorem also provides us a way to find the minimal $\varphi^\star$, hence the minimal pair $(\alpha^\star, A^\star)$. Let $\varphi^\star(x) = \sum_{i,j} a_{ij}^\star \varphi_{ij}(x)$. Then the orthogonal condition

$$\langle\!\langle f - \alpha - \varphi^\star, \varphi \rangle\!\rangle = 0$$

for any $\varphi \in \Phi_1$ is equivalent to

$$\sum_{i,j} a_{ij}^\star \langle\!\langle \varphi_{ij}, \varphi_{kl} \rangle\!\rangle = \langle\!\langle f - \alpha, \varphi_{kl} \rangle\!\rangle \qquad \text{for } k, l = 1, 2, \cdots, n. \tag{5.25}$$

It has n^2 unknowns and n^2 linear equations. Once all the inner products in (5.25) are provided, we can solve it for $A^\star = \left(a_{ij}^\star\right)$ via standard LS method. The corresponding $\alpha^\star(x)$ can be computed via equation (5.19).

Remark 5.3.1 *While solution $\varphi \in \Phi_1$ is unique, the corresponding $\mathcal{D}_f$-optimal pair $(\alpha^\star, A^\star)$ may not be unique. The pair $(\alpha^\star, A^\star)$ is unique only when $\{\varphi_{11}, \varphi_{12}, \cdots, \varphi_{nn}\}$ form a basis for Φ_1, i.e., Φ_1 is of dimension n^2.*

In order to find a solution to equation (5.25), we need to compute the inverse (pseudo-inverse when it is singular) of the coefficient matrix of size $n^2 \times n^2$. When $n = 6$, the size of the coefficient matrix is already 36×36. We will show that the optimization problem (5.14) is convex. Moreover, we will propose a simple descent algorithm to solve problem (5.14).

Lemma 5.3.2 *The cost function*

$$\eta_1(\alpha, A) = \int_{\mathcal{D}} \|f(x) - \alpha(x)g(x) - Ax\|^2 dx$$

is convex with respect to $\alpha(\cdot) \in \mathbb{C}^\infty[\mathcal{D}]$ *and* $A \in \mathbb{R}^{n\times n}$. *Thus the minimal cost* η_1 *is unique.*

Proof. The space of smooth functions $\mathbb{C}^\infty[\mathcal{D}]$ over domain $\mathcal{D}$ is a linear space. So is the Cartesian product space $\mathbb{C}^\infty[\mathcal{D}] \times \mathbb{R}^{n\times n}$. For any $0 < \gamma < 1$,

$$\begin{aligned}
&\eta_1(\gamma\alpha_1 + (1-\gamma)\alpha_2, \gamma A_1 + (1-\gamma)A_2) \\
&= \textstyle\int_{\mathcal{D}} \|f(x) - (\gamma\alpha_1(x) + (1-\gamma)\alpha_2(x))g(x) - (\gamma A_1 + (1-\gamma)A_2)x\|^2 dx \\
&= \textstyle\int_{\mathcal{D}} \|\gamma(f(x) - \alpha_1(x) - A_1x) + (1-\gamma)(f(x) - \alpha_2(x)g(x) - A_2x)\|^2 dx \\
&\le \textstyle\int_{\mathcal{D}} \gamma^2\|f(x) - \alpha_1(x) - A_1x\|^2 + (1-\gamma)^2\|f(x) - \alpha_2(x)g(x) - A_2x\|^2 dx \\
&\le \textstyle\int_{\mathcal{D}} \gamma\|f(x) - \alpha_1(x) - A_1x\|^2 + (1-\gamma)\|f(x) - \alpha_2(x)g(x) - A_2x\|^2 dx \\
&= \gamma\eta_1(\alpha_1, A_1) + (1-\gamma)\eta_1(\alpha_2, A_2)
\end{aligned}$$

Thus $\eta_1(\alpha, A)$ is a convex function. ∎

Now, we can construct a converging sequence of $\alpha_k(x)$ and A_k by

$$\begin{aligned}
&A_0 = A, \qquad \alpha_0(x) = \alpha(x), \\
&A_k = A_0 - \textstyle\int_{\mathcal{D}} \alpha_{k-1}(x)g(x)x^T dx (\int_{\mathcal{D}} xx^T dx)^{-1}, \\
&\alpha_k(x) = \alpha_0(x) - \frac{\langle A_k x, g(x)\rangle}{\langle g(x), g(x)\rangle},
\end{aligned} \tag{5.26}$$

for $k = 1, 2, \cdots$. It is easy to verify that

$$\eta_1(\alpha_{k-1}, A_{k-1}) \ge \eta_1(\alpha_{k-1}, A_k) \ge \eta_1(\alpha_k, A_k), \qquad \text{for } k = 1, 2, \cdots.$$

Combined with the convexity of the cost function η_1, we have

Theorem 5.3.4 *The sequence* $\{\alpha_k, A_k\}$ *in (5.26) will converge to the solution of the coupled equations (5.19) and (5.20) as* $k \longrightarrow \infty$.

Proof. The cost $\{\eta_1(\alpha_k, A_k)\}$ decreases monotonously and η_1 is non-negative. Thus $\{\eta_1(\alpha_k, A_k)\}$ converges. Let $A_k = \left(a_{ij}^k\right)$. From equation (5.23), we rewrite $\alpha_k(x)$ in equation (5.26) as

$$\alpha_k(x) = \alpha_0(x) - \sum_{i,j} a_{ij}^k \varphi_{ij}(x).$$

Thus $(\alpha_k, A_k) \in (\alpha_0 + \Phi) \times \mathbb{R}^{n\times n}$ which is a finite dimensional variety hence closed. So the gradient algorithm (5.26) converges to a local extreme. The $\mathcal{D}_f$-optimal problem is convex. It only has a minimal cost η_1. ∎

Let's consider a special case. Define the radius of domain $\mathcal{D}$ to be $\rho(\mathcal{D}) \stackrel{\triangle}{=} \max_{x\in\mathcal{D}} \|x\|$.

Lemma 5.3.3 *When the radius $\rho(\mathcal{D}) \longrightarrow 0$, (A, b) approaches $(\frac{\partial f(0)}{\partial x}, g(0))$.*

Proof. Note that $f(0) = 0$. Using Taylor expansion of $f(x)$ at $x = 0$, from (5.16) we have

$$\begin{aligned} A &= \textstyle\int_{\mathcal{D}} (\frac{\partial f(0)}{\partial x} x + h.o.t.) x^T dx (\int_{\mathcal{D}} x x^T dx)^{-1} \\ &= \textstyle\frac{\partial f(0)}{\partial x} \int_{\mathcal{D}} x x^T dx (\int_{\mathcal{D}} x x^T dx)^{-1} + h.o.t. \\ &= \textstyle\frac{\partial f(0)}{\partial x} + h.o.t. \end{aligned}$$

Thus A approaches $\frac{\partial f(0)}{\partial x}$, as $\rho(\mathcal{D}) \longrightarrow 0$. Similarly, $b \longrightarrow g(0)$, as $\rho(\mathcal{D}) \longrightarrow 0$. ∎

The above sequence (5.26) becomes

$$A_1 = \frac{\partial}{\partial x}(f(x) - \alpha_0(x) g(x))|_{x=0} = \frac{\partial f(0)}{\partial x} - g(0)\frac{\partial \alpha_0(0)}{\partial x} = A - \frac{1}{b^T b} b b^T A = BA.$$

Where $B = I - \frac{1}{b^T b} b b^T$. Property of B,

$$B^2 = (I - \frac{1}{b^T b} b b^T)^2 = I - 2\frac{1}{b^T b} b b^T + \frac{1}{(b^T b)^2} b b^T b b^T = I - \frac{1}{b^T b} b b^T = B.$$

Thus we have

$$A_2 = B A_1 = B^2 A = BA.$$

Corollary 5.3.1 *The sequence $\{\alpha_i, A_i\}$ converges to $\{\alpha^\star, A^\star\}$ in two steps,*

$$A^\star = BA, \qquad \alpha^\star(x) = \frac{\langle f(x) - A^\star x, g(x)\rangle}{\langle g(x), g(x)\rangle} \tag{5.27}$$

when radius $\rho(\mathcal{D}) \longrightarrow 0$.

For the rotary double pendulum it is possible to "regularize" the drift vector field f through of a preliminary feedback as described here. In our experiments, this was an essential step in arriving at a stable system.

5.4 Low gain control

The High Gain Dilemma. A major source of difficulty in achieving stability for the rotary double pendulum to be described below is the possibility of oscillations corresponding to unmodeled dynamics. For our system these are generally in the range of 6 to 8Hz and are strongly destabilizing. It was observed experimentally that these oscillations could be avoided if the gains could be kept low. Sepulchre has several interesting examples on the high gain dilemma Sepulchre (2003).

However, when stabilizing open loop unstable systems there are limitations on how low the gains can be. Letting $p(s) = \det(Is - A)$, the effect of the feedback term is to replace $p(s)$ by $p(s) + q(s)$. Suppose that $p(s) = s^n + p_{n-1}s^{n-1} + ... + p_0$ has real coefficients and that we want to find the "smallest" polynomial $q(s) = q_{n-1}s^{n-1} + q_{n-2}s^{n-2} + ... + q_0$ such that $p(s) + q(s)$ has all its roots in the left half-plane. Because the different entries in q have different units we adopt a flexible characterization of size involving a scaling vector α. Consider

$$|q|_\alpha \stackrel{\triangle}{=} \sum \alpha_i |q_i|$$

with the components of α being positive numbers.

Recall that for a lossless mechanical system, $p(D)$ is automatically an even function of D.

Fact 1. $p(s)$ is Hurwitz if and only if the zeros of $p_e(s) = (p(s) + p(-s)$ and the zeroes of $p_o(s) = p(s) - p(-s)$ are purely imaginary and interlace.

Fact 2. $p(s)$ is Hurwitz with all roots real and negative if and only $p(s^2)$ has all its roots on the imaginary axis. If this is the case, and if p' denotes the derivative of p then $p(s^2)+p'(s^2)$ is Hurwitz.

Example 5.4.1 *Consider the polynomial $s^2(s^4-3s^2+2)$. What polynomials can we add to this to get a polynomial that has all purely imaginary roots? Consider adding $as^4 + bs^2 + c$. Conditions on the coefficients are*

$$i) a - 3 \geq 0 \ ; \ (a-3)^2 - 4b - 8 \geq 0$$

Possible solutions include $a = 3$, $b = -2$ (minimal for $\alpha_i = 1$ for all i's) and $b = -1$, $a = 3 + \sqrt{6}$, etc.

This analysis shows that there is a lower bound on the minimum gain required to stabilize an unstable mechanical system and that this can be characterized in terms of its determinantal polynomial.

In the chapter 4, the feedback gain is obtained by solving a Riccati equation $Ricc(A, b, Q)$, where Q is a weighting pattern between control and states. There is no systematic way of selecting Q to derive a desired feedback vector/matrix k in general. Typically, one picks a branch of Q, solves the Riccati equation, and then choose a relatively good k, Eltohamy and Kuo (1998). An alternative approach is selecting k with small norm. Let's call it low gain feedback. Low gain is good, if we can achieve the same performance by low gain instead of high gain. Low gain can lower the magnitude of control. Consider the scalar control $u = -kx$, then $|u| \leq \|k\|_2\|x\|_2$. Thus for domain $\mathcal{D} = \{x \,|\, \|x\|_2 \leq 1\}$, let $u_{max} = \max_{x\in\mathcal{D}}\{|u|\} = \|k\|_2$. Then low gain implies small u_{max}. Low gain is preferable for the pendulum system, because large control input u will cause vibration and camera sensor failure. Large control input will produce extremely large acceleration, which is not safe. Low gain is a way reduce u for the same domain $\mathcal{D}$ of states.

Definition 5.4.1 *Given a controllable scalar input linear system*

$$\dot{x} = Ax + bu, \qquad x \in \mathbb{R}^n, \tag{5.28}$$

the minimal gain design is to find k with minimal gain ($= \|k\|_2$), such that the closed-loop system under feedback $u = -kx$ is σ-exponential stable for some $\sigma < 0$, i.e., $\|x(t)\| \leq e^{\sigma t}\|x(0)\|$.

Recall that for the controllable single-input linear system (5.28) we can find a linear transformation $x = T\bar{x}$ such that

$$\dot{\bar{x}} = \bar{A}\bar{x} + \bar{b}\bar{x} \tag{5.29}$$

is the controllable companion form, where $\bar{A} = T^{-1}AT$, $b = T^{-1}b$, $T = [q; qA; \cdots; qA^{n-1}]^{-1}$, and q is the nth row of $[b, Ab, \cdots, A^{n-1}b]^{-1}$. We have that $u = -kx = -kT\bar{x}$. Let $\bar{k} = [k_1, \cdots, k_n] = kT$. Then, the closed-loop system becomes

$$\dot{\bar{x}} = (\bar{A} - \bar{b}\bar{k})\bar{x}. \tag{5.30}$$

The characteristic polynomial of the closed-loop system is

$$f(s) = det(sI - (\bar{A} - \bar{b}\bar{k})) = s^n + (a_{n-1} + k_n)s^{n-1} + \cdots + (a_1 + k_2)s + a_0 + k_1, \tag{5.31}$$

and $f(s)$ is σ-exponential stable iff $f(s + \sigma)$ is stable. We can expand $f(s + \sigma)$ and rewrite it in a matrix form

$$\begin{aligned} f(s+\sigma) &= (s+\sigma)^n + (a_{n-1} + k_n)s^{n-1} + \cdots + (a_1 + k_2)(s+\sigma) + a_0 + k_1 \\ &= s^n + p_{n-1}s^{n-1} + \cdots + p_1 s + p_0, \end{aligned} \tag{5.32}$$

where

$$p = (p_0, p_1, \cdots, p_{n-1}) = p_\sigma + (a + \bar{k})\Sigma = p_\sigma + (a + kT)\Sigma \tag{5.33}$$

with $p_\sigma = (\sigma^n, \binom{n}{n-1}\sigma^{n-1}, \cdots, \binom{n}{1}\sigma)$, $a = (a_0, a_1, \cdots, a_{n-1})$, and

$$\Sigma = \begin{pmatrix} 1 & 0 & \cdots & 0 & 0 \\ \sigma & 1 & \cdots & 0 & 0 \\ & & \cdots & & \\ \sigma^{n-2} & \binom{n-2}{1}\sigma^{n-3} & \cdots & 1 & 0 \\ \sigma^{n-1} & \binom{n-1}{1}\sigma^{n-2} & \cdots & \binom{n-1}{n-2}\sigma & 1 \end{pmatrix}. \tag{5.34}$$

Definition 5.4.2 *Given a polynomial*

$$p(s) = s^n + p_{n-1}s^{n-1} + \cdots + p_1 s + p_0, \tag{5.35}$$

the set $\mathcal{P}$ of parameters corresponding to stable polynomials is defined as

$$\mathcal{P} = \{(p_0, p_1, \cdots, p_{n-1}) \in R^n \mid \textit{the real parts of } p(s)\textit{'s roots are all negative}\}. \tag{5.36}$$

Then the minimal gain problem can be formulated as

Theorem 5.4.1 *Given $\sigma < 0$, the minimal gain feedback k^* such that the closed-loop system is σ-exponentially stable exists and*

$$k^* = [(p^* - p_\sigma)\Sigma^{-1} - a]T^{-1} \tag{5.37}$$

where

$$p^* = \arg\min_{p \in \mathcal{D}} \{\|[(p - p_\sigma)\Sigma^{-1} - a]T^{-1}\|_2\}, \tag{5.38}$$

with $\mathcal{D} = \mathcal{B} \cap \overline{\mathcal{P}}$, $\mathcal{B} = \{p \in \mathbb{R}^n \mid \|[(p - p_\sigma)\Sigma^{-1} - a]T^{-1}\|_2 \leq \|(p_\sigma\Sigma^{-1} + a)T^{-1}\|_2\}$, and $\overline{\mathcal{P}}$ the closure of $\mathcal{P}$. $k^* = 0$ when A is σ-exponential stable by itself.

Proof. By definition, k^* is the solution, if it exists, of the following minimization problem

$$\inf_{k \in R^n} \{\|k\|_2\}$$

subjecting to $p = p_\sigma + (a + kT)\Sigma \in \overline{\mathcal{P}}$. From 5.33, we have that

$$k = [(p - p_\sigma)\Sigma^{-1} - a]T^{-1}, \quad p \in \overline{\mathcal{P}}. \tag{5.39}$$

Let $p = 0$, then $k^0 = -(p_\sigma\Sigma^{-1} + a)T^{-1}$ is a σ-exponential stable controller with roots of closed-loop system are all σ. Thus we only need to search for k in the closed ball

$\mathcal{K} = \{k \in \mathbb{R}^n \mid \|k\|_2 \leq \|k^0\|_2\}$, which is equivalent to searching for p in $\mathcal{D} = \mathcal{B} \cap \overline{\mathcal{P}}$. $\mathcal{D}$ is compact, thus we can replace the inf by min. Thus the theorem follows. ∎

So far, we still do not know how to search in $\overline{\mathcal{P}}$ to find the minimal gain k. Is the minimal gain unique? It is easy to show that for $n = 2$ the minimal k is unique. But for higher dimension, we do not know yet. There may exist many local minimums. The rest of this section will focus on *steepest descent algorithm* for searching the minimal gain controller k.

Lemma 5.4.1 *Given a polynomial*

$$p(s) = s^n + p_{n-1}s^{n-1} + \cdots + p_1 s + p_0,$$

the set of parameters corresponding to stable polynomials $\mathcal{P}$ forms a simply connected set in $\mathbb{R}^n_+ = \{(p_0, p_1, \cdots, p_{n-1}) \in \mathbb{R}^n \mid p_i > 0, \quad \text{for } i = 0, 1, \cdots, n-1.\}$.

Proof. For any polynomial $p(s)$, we can factorize it into a product of first-order and/or second-order polynomials. Say $n = 6$, we can find q_i's and r_i's in $\mathbb{R}$, such that

$$p(s) = (s^2 + q_1 s + r_1)(s^2 + q_2 s + r_2)(s^2 + q_3 s + r_3). \tag{5.40}$$

Thus, the roots of $p(s)$ are the collection of root of $s^2 + q_i s + r_i$. The real parts of root of $s^2 + q_i s + r_i$ are negative iff $q_i > 0$ and $r_i > 0$. Therefore $p(s)$ is stable iff $(q_1, q_2, q_3, r_1, r_2, r_3) \in \mathbb{R}^n_+$. We can expand $p(s)$ as

$$\begin{aligned} p(s) = \quad & s^6 + (q_1 + q_2 + q_3)s^5 + (q_1q_2 + q_2q_3 + q_3q_1 + r_1 + r_2 + r_3)s^4 \\ & + (q_1q_2q_3 + q_1r_2 + q_1r_3 + q_2r_3 + q_2r_1 + q_3r_1 + q_3r_2)s^3 \\ & + (q_1q_2r_3 + q_2q_3r_1 + q_3q_1r_2 + r_1r_2 + r_2r_3 + r_3r_1)s^2 \\ & + (q_1r_2r_3 + q_2r_3r_1 + q_3r_1r_2)s + r_1r_2r_3 \\ = \quad & s^6 + p_5s^5 + \cdots + p_1 s + p_0. \end{aligned} \tag{5.41}$$

Thus $q = (q_1, \cdots, r_3) \in \mathbb{R}^6_+$ is a parameterization of $p(q) = (p_0, p_1, \cdots, p_5) \in \mathcal{P}$. The map $p : \mathbb{R}^6_+ \longrightarrow \mathcal{P}$ is a multi-linear surjective map, thus smooth. $\mathbb{R}^6_+$ is simply connected, so is $\mathcal{P}$. Since the signs of $p(q)$'s components are all positive and $q \in \mathbb{R}^6_+$, $p = p(q)$ is still in $\mathbb{R}^6_+$. This argument is valid for arbitrary n. ∎

With the parameterization of $p \in \mathcal{P}$ by $q \in \mathbb{R}^n_+$, we can instead search for the minimal k in $q \in \overline{\mathbb{R}^n_+}$. Let $g(q) = [(p(q) - p_\sigma)\Sigma^{-1} - a]T^{-1}(T^{-1})^T[(p(q) - p_\sigma)\Sigma^{-1} - a]^T$, then $g = \|k\|_2^2$. Since we use the Euclidean norm, the steepest-descent method is just the gradient method of Hiriart-Urruty and Lemaréchal (1991),

$$q_{k+1} = q_k - h * \nabla g(q_k), \tag{5.42}$$

the step-size $h > 0$ being given by a line-search, and

$$\nabla g(q_k) = 2[(p(q_k) - p_\sigma)\Sigma^{-1} - a]T^{-1}(T^{-1})^T(\Sigma^{-1})^T(\nabla p(q_k))^T. \tag{5.43}$$

The calculation of the map $p(q)$ and $\nabla p(q)$ takes some time, but is rather straight forward, e.g. for $n = 6$

$$\begin{aligned} p(q) \;=\; & (r_1r_2r_3,\ q_1r_2r_3 + q_2r_3r_1 + q_3r_1r_2, \\ & q_1q_2r_3 + q_2q_3r_1 + q_3q_1r_2 + r_1r_2 + r_2r_3 + r_3r_1, \\ & q_1q_2q_3 + q_1r_2 + q_1r_3 + q_2r_3 + q_2r_1 + q_3r_1 + q_3r_2, \\ & q_1q_2 + q_2q_3 + q_3q_1 + r_1 + r_2 + r_3,\ q_1 + q_2 + q_3), \end{aligned} \tag{5.44}$$

$$\nabla p(q) = \begin{pmatrix} 0 & r_2r_3 & q_2r_3 + q_3r_2 & q_2q_3 + r_2 + r_3 & q_2 + q_3 & 1 \\ 0 & r_3r_1 & q_3r_1 + q_1r_3 & q_3q_1 + r_3 + r_1 & q_3 + q_1 & 1 \\ 0 & r_1r_2 & q_1r_2 + q_2r_1 & q_1q_2 + r_1 + r_2 & q_1 + q_2 & 1 \\ r_2r_3 & q_2r_3 + q_3r_2 & q_2q_3 + r_2 + r_3 & q_2 + q_3 & 1 & 0 \\ r_3r_1 & q_3r_1 + q_1r_3 & q_3q_1 + r_3 + r_1 & q_3 + q_1 & 1 & 0 \\ r_1r_2 & q_1r_2 + q_2r_1 & q_1q_2 + r_1 + r_2 & q_1 + q_2 & 1 & 0 \end{pmatrix}. \tag{5.45}$$

In each step, we need to make sure that $q \in \mathbb{R}^n_+$. We can force the direction pointing out of $\mathbb{R}^n_+$ to zero, i.e. move on the boundary hyper-surface of $\mathbb{R}^n_+$.

Remark 5.4.1 *(1) Because the set $\mathcal{P}$ need not be convex, it is not necessarily easy to search for k directly, so we need to perform a Routh test for each set of the parameters p. It is rather easy to search in the parameterization space of the parameters of the polynomial, which is $\overline{\mathbb{R}^n_+}$. But we introduce redundancy by doing so, since interchanging (q_i, r_i) with (q_j, r_j) will result in the same polynomial $p(s)$. Thus it may introduce extraneous minimal points. (2) It is necessary to fix $\sigma < 0$ before the minimization procedure, because, otherwise, the characteristic polynomial of the closed-loop system will have zero as a root.*

Example 5.4.2 *In this example, we try to show that the minimal gain design method described above can find a much smaller k compared with the LQR method. Consider the linearization (A, b) of the double pendulum with*

$$A = \begin{pmatrix} 0 & 1 & 0 & 0 & 0 & 0 \\ 0 & 0 & 0 & 0 & 0 & 0 \\ 0 & 0 & 0 & 1 & 0 & 0 \\ 0 & 0 & 59.0 & 0 & -221.1 & 0 \\ 0 & 0 & 0 & 0 & 0 & 1 \\ 0 & 0 & -247.2 & 0 & 181.3 & 0 \end{pmatrix}, \quad b = \begin{pmatrix} 0 \\ 1 \\ 0 \\ 1.8 \\ 0 \\ -3.1 \end{pmatrix},$$

let pick $Q = \mathrm{diag}\{20, 10, 400, 20, 1000, 40\}$, *then we have*

$$k = b' * Ricc(A, b, Q) = (-4.8, -5.0, 141.6, 13.2, -249.3, -10.2).$$

We have the exponential stable rate $\sigma = \max\{Re[\mathrm{eig}(A - b*k)]\} = -0.93$ *and* $\|k\|_2 = 287.3$. *For the minimal gain design with* $\sigma = -0.93$, *we have*

$$\begin{aligned} q &= (0, 3.8, 0, 0, 51.2, 0), \\ p &= (0, 0, 0, 0, 51.2, 3.8), \\ k^* &= (-0.0009, -0.0042, 82.1, -2.6, -56.9, -4.5), \end{aligned}$$

with $\|k^*\|_2 = 100$, *which is much smaller than* k.

5.5 Application to the double pendulum

Example 5.5.1 *Let's look at an example to get some idea about the* $\mathcal{D}_f$*-optimal approximations. Consider the 2nd order system*

$$\begin{aligned} \dot{x}_1 &= \sin x_2 + u \cos x_1 \\ \dot{x}_2 &= -\sin x_1 + u \cos x_2 \end{aligned} \tag{5.46}$$

The standard linear approximation gives us

$$\dot{x} = Ax + ub$$

with $A = \begin{pmatrix} 0 & 1 \\ -1 & 0 \end{pmatrix}$ *and* $b = \begin{pmatrix} 1 \\ 1 \end{pmatrix}$. *Follow the procedure for feedback linear approximation for* $\rho(\mathcal{D}) \longrightarrow 0$, *we have*

$$A^\star = (I - \frac{1}{b^T b} bb^T)A = \frac{1}{2}\begin{pmatrix} 1 & 1 \\ -1 & -1 \end{pmatrix}, \quad b^\star = b = \begin{pmatrix} 1 \\ 1 \end{pmatrix},$$

and

$$\alpha^\star(x) = \frac{\langle f(x) - A^\star x, g(x)\rangle}{\langle g(x), g(x)\rangle} = -\frac{\sin(x_1 - x_2) + \frac{1}{2}(x_1 + x_2)(\cos x_1 - \cos x_2)}{\cos^2 x_1 + \cos^2 x_2}.$$

For the double pendulum application, our laboratory experience leads us to believe that it is more important to accurately approximate the system (3.11) in coordinates (θ_2, θ_3) than in θ_1. So we use weighted norm $\|\cdot\|_W$ instead of the Euclidean norm. Then Corollary 5.3.1 changes slightly. Note that the equality $(I - \frac{1}{b^T W b} bb^T W)^2 = I - \frac{1}{b^T W b} bb^T W$ still holds. Thus we have

Corollary 5.5.1 *The solution* $\{\alpha^\star, A^\star\}$ *to the weighted* $\mathcal{D}$*-optimal problem satisfies*

$$A^\star = (I - \frac{1}{b^T W b} b b^T W) A, \qquad \alpha^\star(x) = \frac{\langle f(x) - A^\star x, g(x)\rangle_W}{\langle g(x), g(x)\rangle_W} \tag{5.47}$$

when radius $\rho(\mathcal{D}) \longrightarrow 0$.

Let $W = \mathrm{diag}\{\varepsilon, \varepsilon, 1, 1, 1, 1\}$, where $\varepsilon > 0$. Following the above derivation for $\varepsilon \longrightarrow 0$, we have

$$A^\star = (I - \frac{1}{b^T W b} b b^T W) A = \begin{pmatrix} 0 & 1 & 0 & 0 & 0 & 0 \\ 0 & 0 & -3.9315 & 0 & 34.5878 & 0 \\ 0 & 0 & 0 & 1 & 0 & 0 \\ 0 & 0 & 6.2939 & 0 & -6.2939 & 0 \\ 0 & 0 & 0 & 0 & 0 & 1 \\ 0 & 0 & -1.2269 & 0 & 1.2269 & 0 \end{pmatrix}, \qquad b = \begin{pmatrix} 0 \\ 1 \\ 0 \\ -0.1635 \\ 0 \\ -0.8493 \end{pmatrix}.$$

Figure 6.4 shows a plot of the double pendulum at its inverted position with feedback control law computed from its feedback linear approximation $(\alpha^\star(x), A^\star, b)$. This plot is put in Chapter 6 for comparison with other stabilization results. The linear feedback gain we used after feedback linear approximation is

$$k = [0.7 \quad 2.18 \quad 200 \quad 79.2 \quad -126 \quad -27.4]$$

and

$$\mathrm{eig}(A - bk) = \{-3.4682 \pm 0.5019i,\ -2.2113,\ -1.3882 \pm 2.3793i,\ -0.5776\}.$$

Chapter 6

Implementation of the DMDL on the double pendulum

This chapter describes a series of experiments that were performed in order to demonstrate the DMDL proposed in chapter 2 and stabilization results in chapter 5.

6.1 Stabilization

The HRL rotary double pendulum described in Chapter 3 has four equilibrium states: down-down, down-up, up-down, up-up, as shown in its dynamical equations (3.11). We have successively stabilized the double pendulum at all of these four equilibrium points. The up-up stabilization is achieved using the feedback linear approximation and stabilization results in Chapter 5. The rest are done using LQ controller design based on its standard linearized model (3.12). The difficulty of stabilization increases in the order of down-down, up-down, down-up, up-up. Indeed, there is no difficulty at down-down position! For this position, we only need to change it from bounded-input bounded-state stability to asymptotic stability. The down-up stabilization is more difficult than up-down, because the control of the second vertical link has to "pass through" the first vertical link. Up-up stabilization is the most difficult, because the two vertical links need to be kept upward simultaneously while the associated coupling effects tend to be destabilizing. Limited torque, limited communication rate, vibration, sensoring inaccuracy, and other unmodeled effects also need to be overcome. A photograph and a plot shows stabilization at each of the four equilibrium states, see Figure 6.1$\sim$6.4. What follows is a list describing our approach in each case.

1. For down-down control, the weighting matrix in LQ optimization is

$$Q_{dd} = 100\,\mathrm{diag}\{1 \quad 1 \quad 1 \quad 1 \quad 1 \quad 1\},$$

and the resulting linear feedback gain and closed-loop eigenvalues are

$$k_{dd} = [10 \quad 12.7907 \quad 16.1927 \quad 1.3920 \quad 50.6430 \quad 4.5563]$$

and

$$\mathrm{eig}(A_{dd} - b_{dd}k_{dd}) = \{-12.3343, \quad -1.5798 \pm 4.7460i, \quad -1.0051, \quad -0.2111 \pm 2.3303i\}.$$

2. For the down-up stabilization

$$Q_{du} = \mathrm{diag}\{0.01 \quad 0.02 \quad 1 \quad 0.1 \quad 10 \quad 0.1\},$$

$$k_{du} = [-0.1, \quad -0.5082, \quad 10.5262, \quad 1.3055, \quad -77.6966, \quad -14.0438],$$

and

$$\mathrm{eig}(A_{du} - b_{du}k_{du}) = \{-5.5322 \pm 0.2077i, \quad -0.2338 \pm 0.2116i, \quad -0.0495 \pm 2.3602i\}.$$

3. For the up-down one

$$Q_{ud} = \mathrm{diag}\{0.01 \quad 0.02 \quad 1 \quad 0.1 \quad 10 \quad 1\},$$

$$k_{ud} = [-0.1 \quad -0.5582 \quad -81.8311 \quad -34.4866 \quad 6.4736 \quad 1.2933],$$

and

$$\mathrm{eig}(A_{ud} - b_{ud}k_{ud}) = \{-0.5019 \pm 5.5149i, \quad -2.3599 \pm 0.0271i, \quad -0.2338 \pm 0.2116i\}.$$

4. For the up-up stabilization, the control law is computed from its feedback linear approximation in Chapter 5. The results are repeated here for comparison only. The linear feedback gain used after feedback linear approximation is

$$k = [0.7 \quad 2.18 \quad 200 \quad 79.2 \quad -126 \quad -27.4].$$

The resulting eigenvalues are

$$\mathrm{eig}(A - bk) = \{-3.4682 \pm 0.5019i,\ -2.2113,\ -1.3882 \pm 2.3793i,\ -0.5776\}.$$

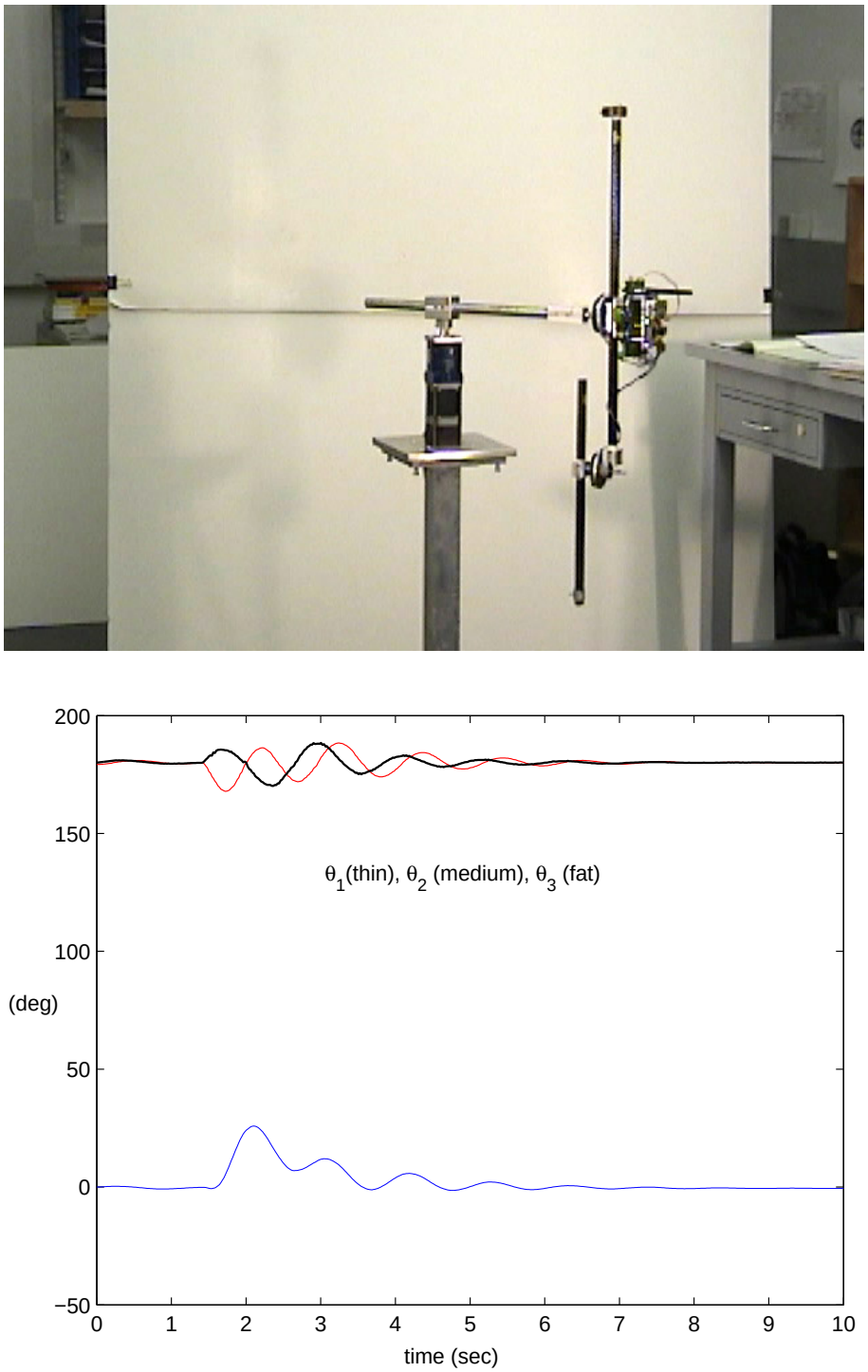

Figure 6.1: Top: Photograph of down-down stabilizing control. Bottom: Plot of experimental data of down-down stabilizing control.

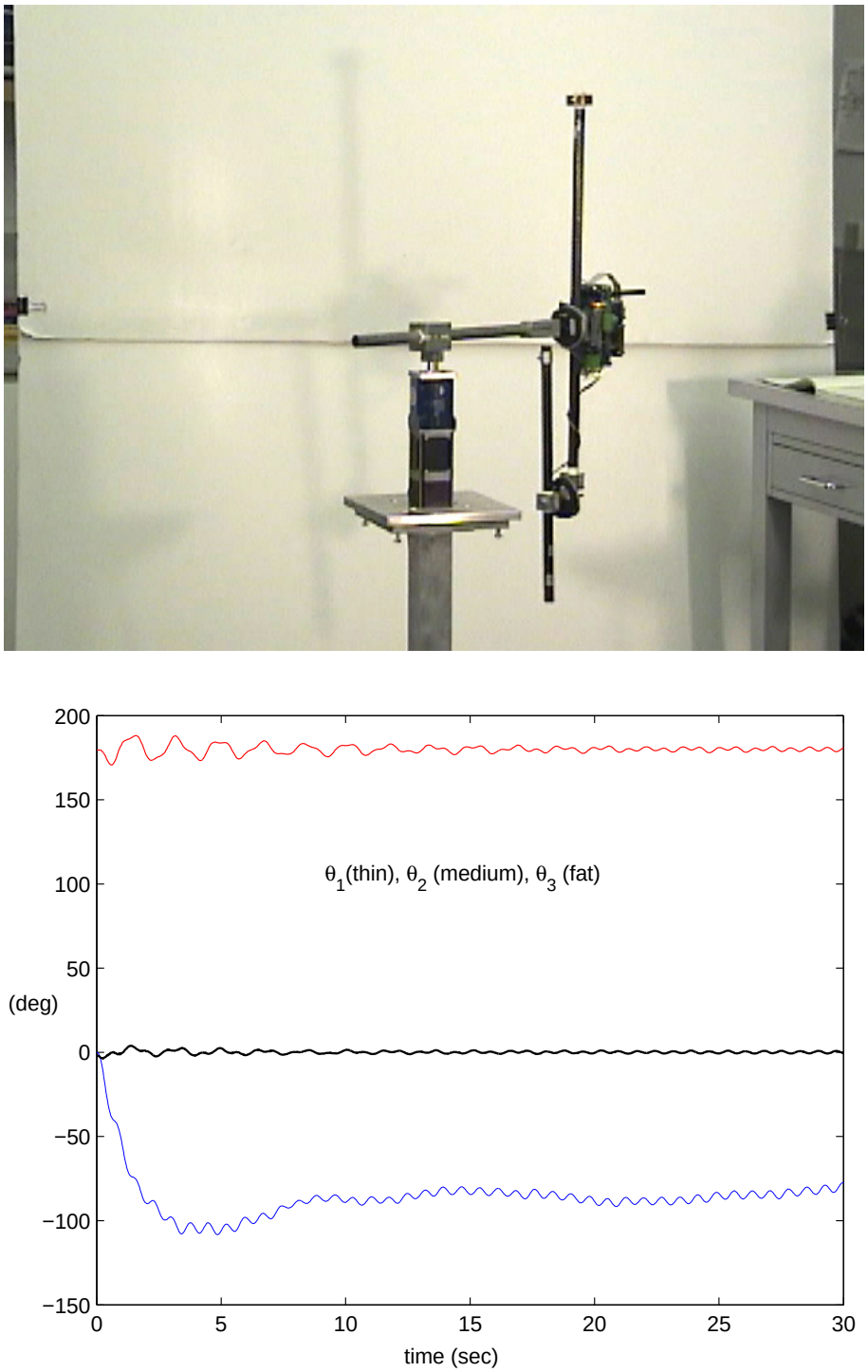

Figure 6.2: Top: Photograph of down-up stabilizing control. Bottom: Plot of experimental data of down-up stabilizing control.

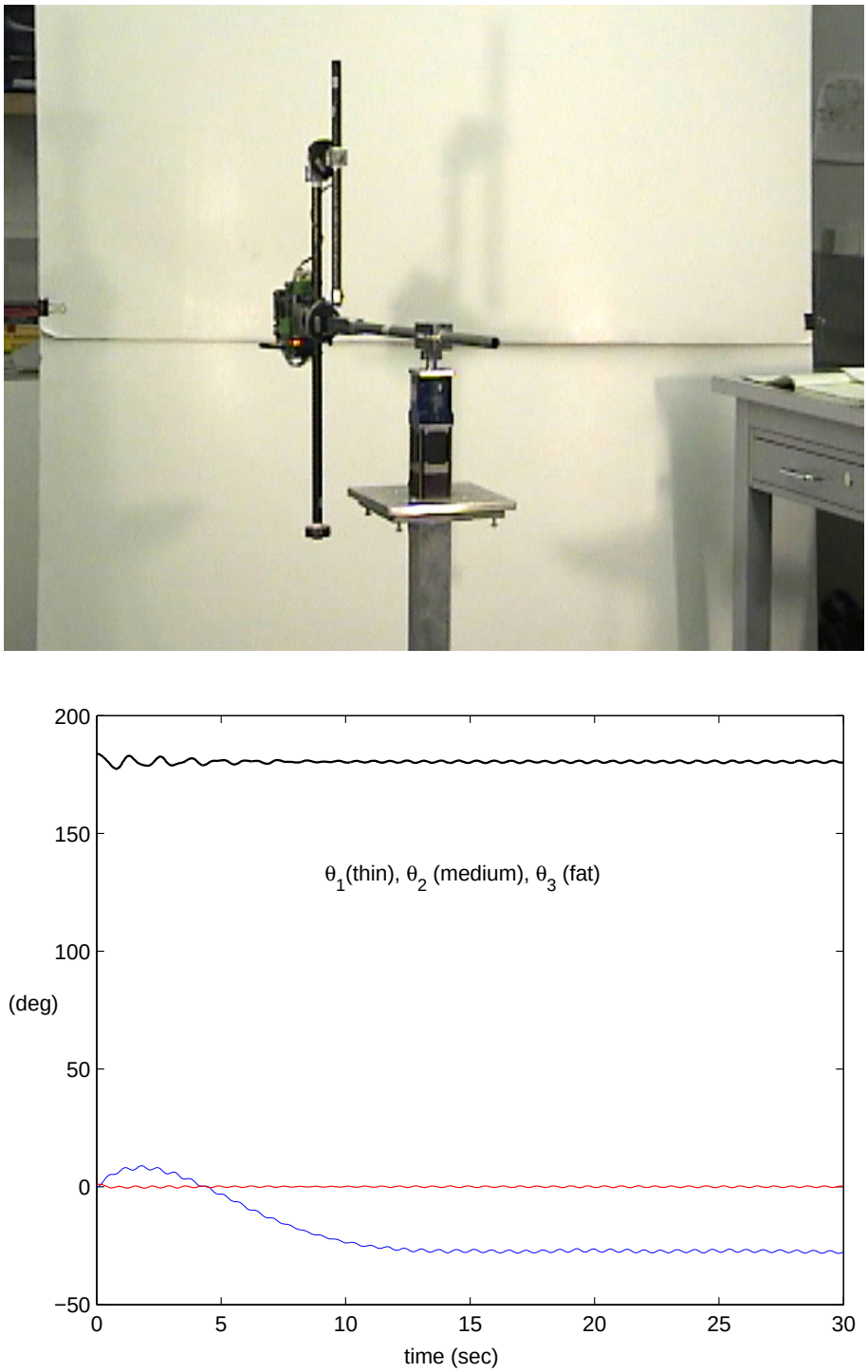

Figure 6.3: Top: Photograph of up-down stabilizing control. Bottom: Plot of experimental data of up-down stabilizing control.

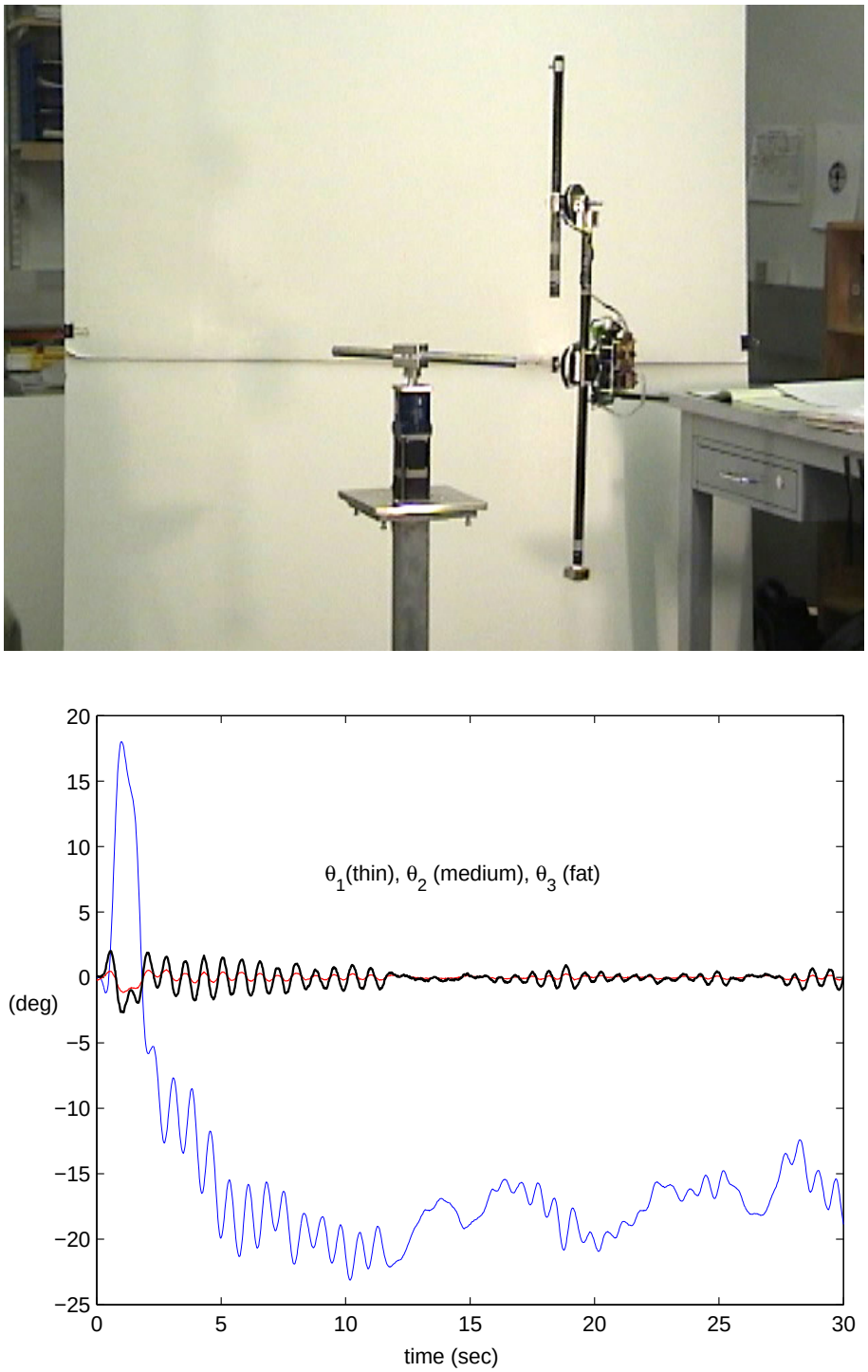

Figure 6.4: Top: Photograph of up-up stabilizing control. Bottom: Plot of experimental data of up-up stabilizing control.

6.2 Generate circling orbits

In Figure 6.5 and 6.6, the top link circles while the other links oscillate. In addition to developing algorithms for stabilization, we also consider the generation of this periodic motion. This result together with an oscillation transition enlarge our "vocabulary" in that they represent motion states that can be used as pieces in a more elaborate motion script.

The control used is negative feedback for the motor link and the first vertical link plus a positive feedback control for the 2nd vertical link. The positive feedback for the 2nd vertical link acts as a periodic feedforward control.

$$u = k_1 x_1 + k_2 x_2 + k_3 x_3 + k_4 x_4 + \gamma \text{sign}(x_6) \cos x_5.$$

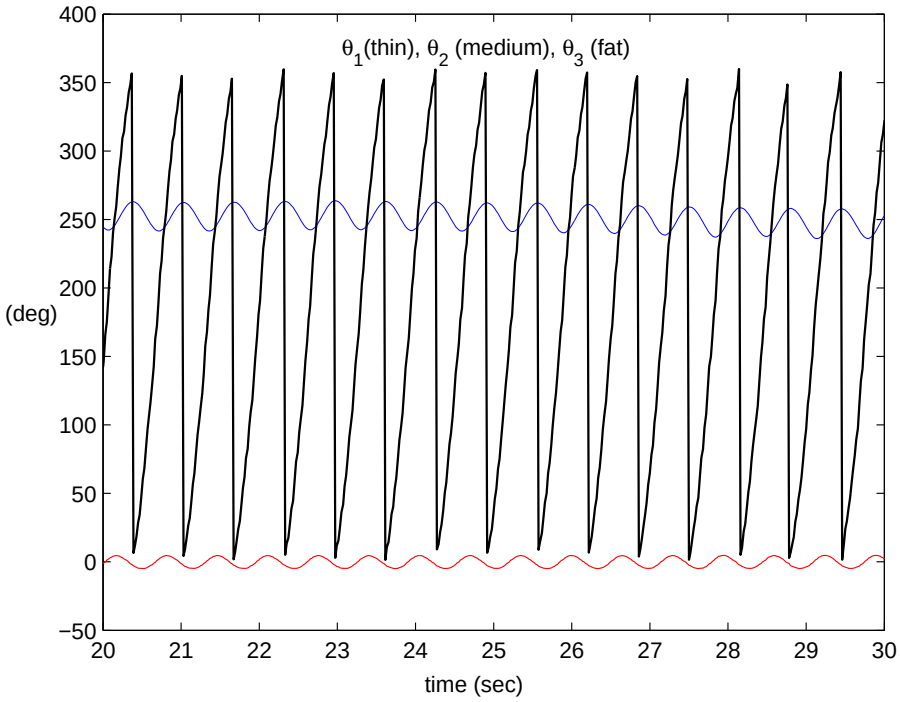

Figure 6.5: Plot of top link circling other links oscillating.

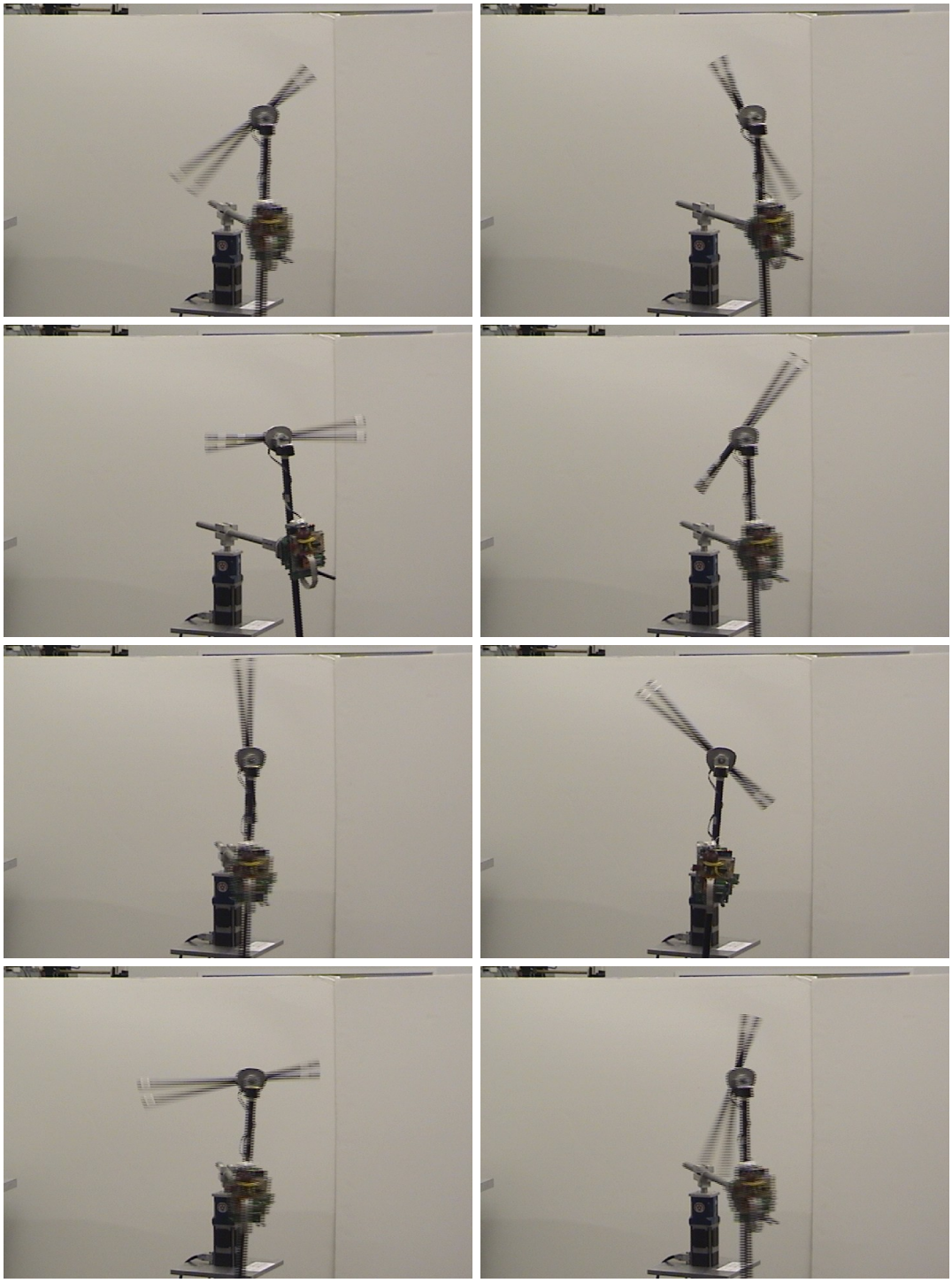

Figure 6.6: From left to right and top to bottom are a series of photographs of top link circling other links oscillating.

6.3 Transition between equilibria and circling orbits

Finally we describe a transition which takes the system from up-down stabilization to top link circling other links oscillating, in Figure 6.7∼6.10.

We start the system using the up-down stabilization control, and then switch the control to negative feedback for the motor link and first vertical link and positive feedback for the second vertical link.

$$u = u = k_1x_1 + k_2x_2 + k_3x_3 + k_4x_4 - k_5x_5 - k_6x_6.$$

Once the second vertical link reaches its upright position, we switch to the control for circling orbits described in Section 6.2.

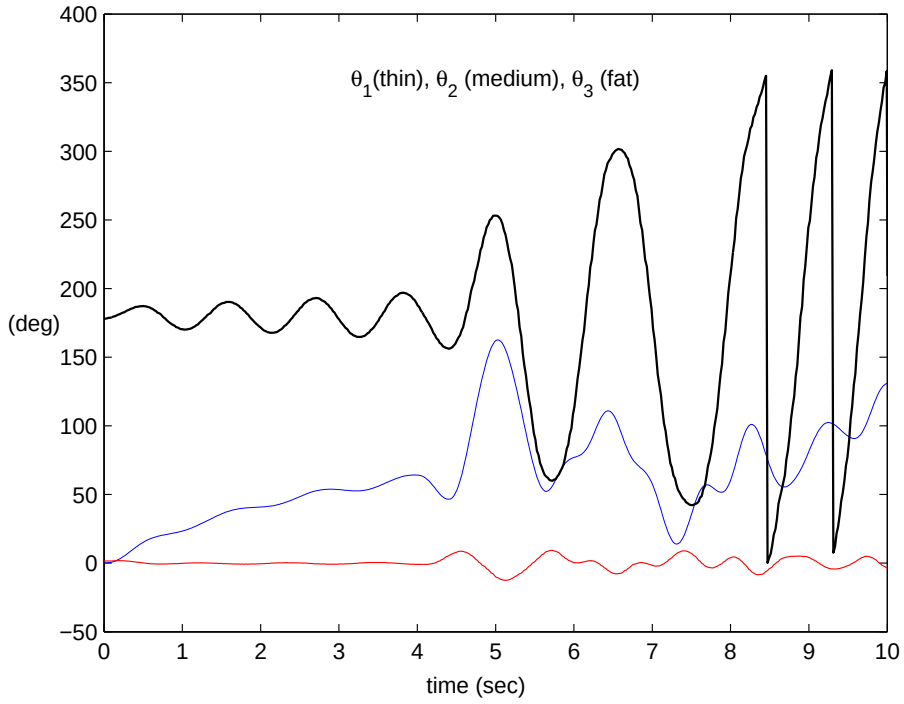

Figure 6.7: Plot of the transition from up-down state to top link circling other links oscillating.

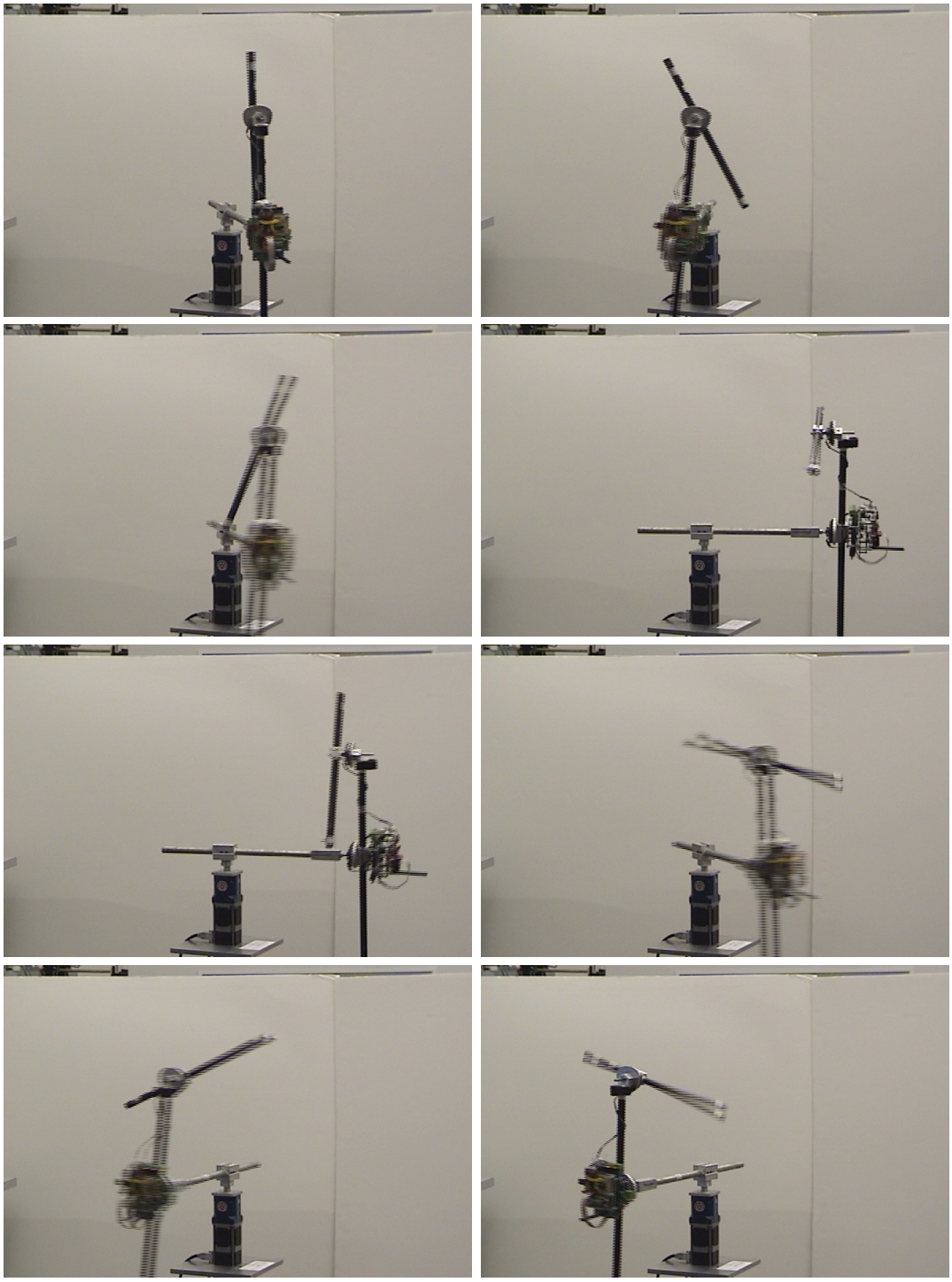

Figure 6.8: From left to right and top to bottom are a series of photographs of the transition from up-down state to top link circling other links oscillating (Part I).

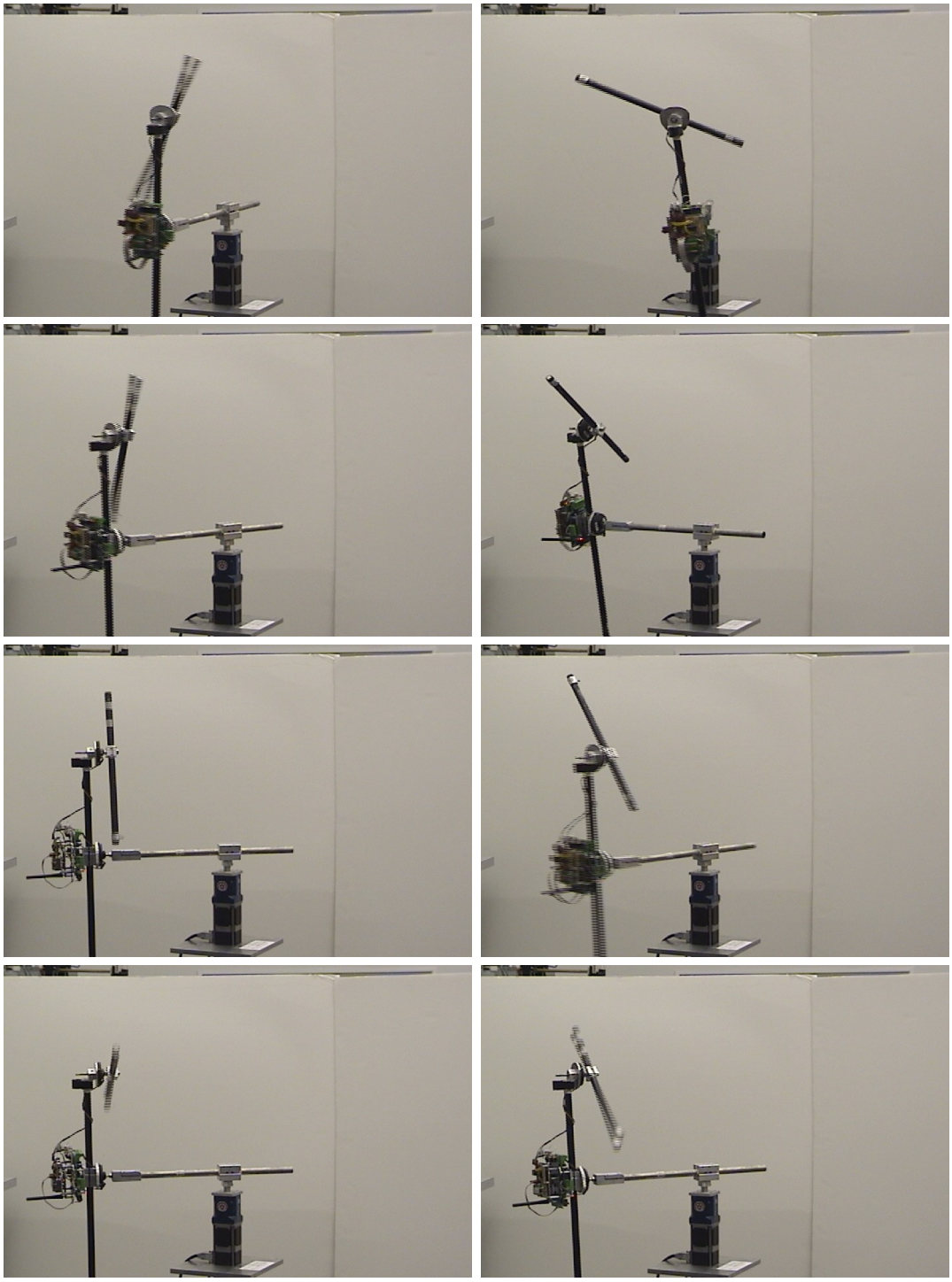

Figure 6.9: From left to right and top to bottom are a series of photographs of the transition from up-down state to top link circling other links oscillating (Part II).

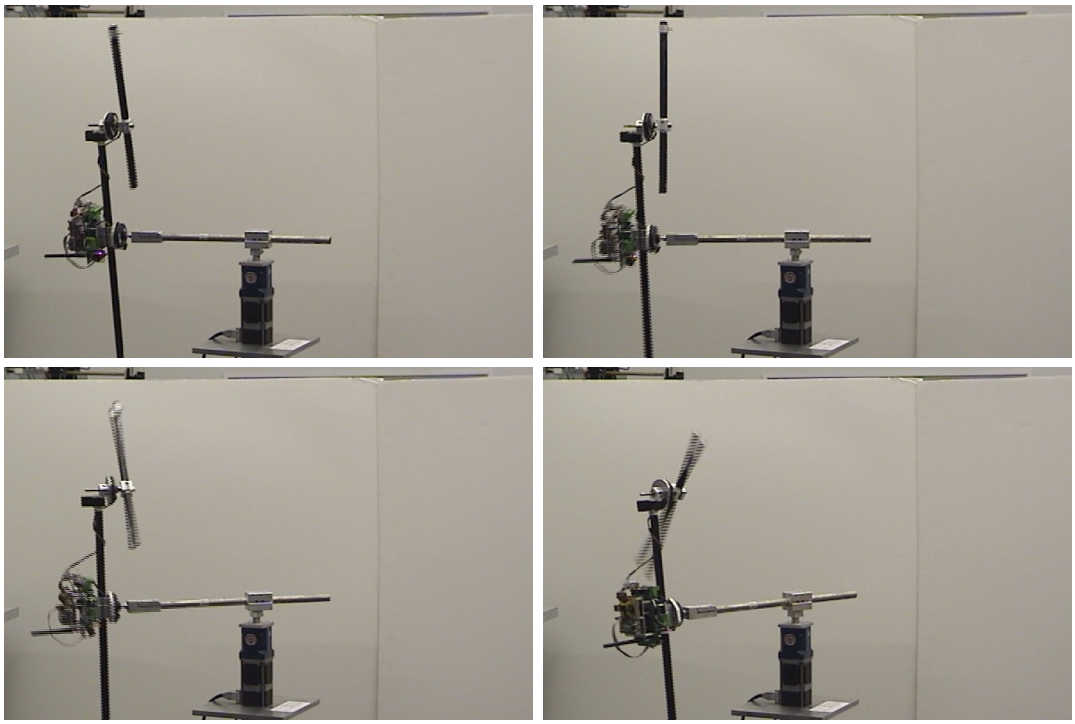

Figure 6.10: From left to right and top to bottom are a series of photographs of the transition from up-down state to top link circling other links oscillating (Part III).

Chapter 7

Conclusions

We have outlined a program for extending MDL to Dynamic situations (DMDL), although this extension is difficult and in some ways imperfect. The study of the control of unstable mechanical systems is quite challenging, involving difficult problems caused by limited communication rates, quantization errors, and parasitic dynamics. Trajectories following problems, of the type investigated here are particularly difficult and have previously not been investigated from the motion control language point of view. We have provided a mathematical foundation for designing control systems capable of processing choreographic scripts. The language atoms are defined based on a discretization of a function space which includes the possible trajectories of the dynamical system under consideration. The class of dynamical systems considered here can model systems with momentum and this has the effect of making our motion control languages context sensitive.

A useful class of language elements (atoms) was constructed using phase space characterizations of the input space appropriate for a second order single pendulum system. Two types of phase space characterization were given: the dumbbell phase space and the bean phase space. We can identify these with pulse trains and then showed that under either type of pulse train, the pendulum will turn one full circle after each pulse.

We built an experimental apparatus to explore the utility of our ideas. The HRL single pendulum that we used for the experiments consists of a horizontal link, driven by a servomotor, and a vertical link that moves freely in the plane perpendicular to the horizontal link. A digital camera based angular position sensor was used to measure the angular position of the vertical link of the pendulum. The HRL double pendulum consists of a horizontal link, driven by a servomotor, and two vertical links that move freely in the plane perpendicular to the horizontal link. In order to measure the position of the

vertical links, a rotary electrostatic resolver is mounted on each of the vertical link joints and communicates with the host computer wirelessly.

Taking the physical bounds of the control signals into account, a swing-up control of the single pendulum was designed and tested with the experimental apparatus. In order to make our swing-up control strategy robust we did not demand that the system reach the equilibrium exactly. A locally stabilizing controller drives the system to the desired state after the swing-up procedure places the system near the equilibrium point. We computed the regions of attraction for unstable, linear control systems driven by bounded inputs.

One way to stabilize a wide class of nonlinear system is to linearize the systems around its equilibrium and to apply a linear feedback control of the linearized system to the original, nonlinear system. In some cases, a low gain controller can be designed in this way. Low gain is desirable because of the limited torque of our motor. This design was used as a way of enlarging the domain of attraction. We formalized the low gain control as an optimization problem, and then provided a gradient algorithm which provides a partial solution.

We developed a new type of nonlocal linearization to deal with local stabilization in a lightweight structure with limited control torque. We presented the linearization problem as an optimization problem for which a linear system and a feedback control are selected simultaneously such that the distance between the nonlinear system with nonlinear feedback and the linear system is minimized in a neighborhood of an equilibrium. We have called this procedure feedback linear approximation. The optimization problem is reduced to the solution of two coupled equations involving the feedback control function and the matrix corresponding the linear approximation. The pair is solved using the projection theorem. Although a formal explicit solution is available it is more convenient to use an iterative algorithm which we have derived. Applying this linearization method to the HRL double inverted pendulum, we successfully stabilized it at its up-up position.

We now offer some suggestions for future work. It would be desirable to have better stabilization algorithms and a more complete knowledge of the limits on the domain of stabilization. One of the basic problems here involves the relationship between the stabilizable set and magnitude and bandwidth limitations of the actuators. That is to say, typically the control u is bounded both in the time and frequency domain. This is also related to the currently unknown "Fundamental Theorem of Robotics", which would place precise limits on the achievable paths, in terms of the capabilities of the sensors and actuators.

Optimal control of unstable Lagrangian systems is an element in the study of DMDL. Optimality is a subgoal but expressiveness is more important. We want to find an efficient

way to move from one equilibrium to another. This could mean a minimal time transfer or a minimal energy transfer. The theory of geometric control as applied to smooth nonlinear systems offers some techniques for answering those problems.

Eventually we want to produce a modulized prototype software package, capable of incorporating a more or less arbitrary sensing and control algorithms. It should also be able to accept descriptions of tasks, decompose the task into a sequence of trajectories, and select the appropriate control sequence to accomplish the task.

Control and optimization the DMDL level also needs to be investigated. In DMDL we define language atoms in terms of quantization of trajectory space instead of state space. This gives us an opportunity to do control and optimization in the quantized trajectory space. This approach may not always yield the very best performance but control and approximate optimization could be much easier on this higher level than on the dynamical system level. The performance can be expected to depend on the construction of atoms. Finer atoms will improve the performance but will also increase the implementation cost.

Bibliography

Åström, K. J. (1999). Hybrid control of inverted pendulums. In Yamamoto and Hara, editors, *Learning, Control, and Hybrid Systems*, pages 150–163. Springer-Verlag.

Åström, K. J., and Furuta, K. (1996). Swinging up a pendulum by energy control. In *Proceedings of IFAC 13th World Congress*, San Francisco, CA.

Angeli, D. (2001). Almost global stabilization of the inverted pendulum via continuous state feedback. *Automatica*, 37(7):1103–1108.

Arnold, V. I. (1978). *Mathematical Methods of Classical Mechanics*. Springer, New York.

Brockett, R. W. (1970). *Finite Dimensional Linear Systems*. John Wiley and Sons, New York.

Brockett, R. W. (1976). Nonlinear systems and differential geometry. In *Proceedings of the IEEE*, volume 64, pages 61–72.

Brockett, R. W. (1978). Feedback invariants for nonlinear systems. In *Proceedings of the 1978 IFAC Congress*, Helsinki, Finland. Pergamon Press.

Brockett, R. W. (1988a). *Lecture Notes on (k,k,T)*. Cambridge, MA.

Brockett, R. W. (1988b). On the computer control of movement. In *Proc. IEEE Conf. on Robotics and Automation*, pages 534–540, Philadelphia, PA.

Brockett, R. W. (1990). Formal languages for motion description and map making. In R. Brockett, editor, *Proceedings of Symposia in Applied mathematics*, volume 41, pages 181–193, Providence, RI. American Mathematical Society.

Brockett, R. W. (1992). Pulse driven dynamical systems. In A. Isidori and T. J. Tarn, editors, *Systems, Models and Feedback: Theory and Applications*, pages 73–79. Birkhauser, Boston, MA.

Brockett, R. W. (1994a). Dynamical systems and their associated automata. In U. Helmke and R. Mennicken, editors, *Systems and Networks: Mathematical Theory and Applications – Proceedings of the 1993 MTNS*, volume 77, pages 49–69, Berlin, German. Akademie-Verlag.

Brockett, R. W. (1994b). Language driven hybrid systems. In *Proc. 33rd Conf. Dec. and Control*, pages 4210–4214, Lake Buena Vista, FL.

BROCKETT, R. W. (1995). Pulses, periods, and cohomological terms in functional expansion. In B. Francis and A. Tannenbaum, editors, *Feedback Control, Nonlinear Systems, and Complexity*, volume 202 of *Springer Lecture Notes in Control and Information Sciences*, pages 24–35. Springer.

BROCKETT, R. W., and LI, H. (2003). Feedback stabilization: Maximizing the domain of attraction. In *Proc. 42nd IEEE Conf. Dec. and Control*, pages 3299 – 3304, Hyatt Regency Maui, Hawaii.

CHUNG, C. C., and HAUSER, J. (1995). Nonlinear control of a swinging pendulum. *Automatica*, 31(6):851–862.

ELTOHAMY, K. G., and KUO, C.-Y. (1997). Real-time stabilization of a triple link inverted pendulum using single control input. *Proceedings of IEEE*, 144:498–504.

ELTOHAMY, K. G., and KUO, C.-Y. (1998). Nonlinear optimal control of a triple link inverted pendulum with single control input. *Int. J. Control*, 69(2):239–256.

FURUTA, K., KAJIWARA, H., and KOSUGE, K. (1980). Digital control of a double inverted pendulum on an inclined rail. *Int. J. Control*, 32:907–924.

FURUTA, K., OCHIAI, T., and ONO, N. (1984). Attitude control of a triple inverted pendulum. *Int. J. Control*, 39:1351–1356.

FURUTA, K., OKUTANI, T., and STONE, H. (1978). Computer control of a double inverted pendulum. *Computer and Electrical Engineering*, 5:67–84.

HENZINGER, T. A. (1996). The theory of hybrid automata. In *Proceedings of the 11th Annual Symposium on Logic in Computer Science*, pages 278–292. IEEE Computer Society Press.

HIRIART-URRUTY, J.-B., and LEMARÉCHAL, C. (1991). *Convex Analysis and Minimization Algorithms I.* Springer-Verlag.

LI, H., and EGERSTEDT, M. (2002). Hybrid control of bounded input control systems. (Unpublished manuscript).

LUENBERGER, D. G. (1969). *Optimization by Vector Space Methods.* John Wiley and Sons, New York.

LYGEROS, J., TOMLIN, C., and SASTRY, S. (1999). Controllers for reachability specifications for hybrid systems. *Automatica*, pages 349–370.

MANIKONDA, V., KRISHNAPRASAD, P. S., and HENDLER, J. (1998). Languages, behaviors, hybrid architectures, and motion control. In J. Baillieul and Y. Willems, editors, *Mathematical Control Theory*, pages 199–226. Springer-Verlag.

MARSDEN, J. E. (1992). *Lectures on Mechanics.* Cambridge University Press, Cambridge, U.K.

MEIER, H. (1990). Discrete computer control of a triple-inverted pendulum. *Optimal Control Applications and Methods*, 11:157–171.

MURRAY, R., DENO, D., and SASTRY, S. (1992). Control primitive for robot systems. *IEEE Tans. on Systems, Man and Cybernetics*, 22:183–193.

OLIVER, P. (1993). *Applications of Lie Groups to Differential Equations (2nd Ed).* Springer-Verlag.

SEPULCHRE, R. (2003). Are basin of attraction easy to enlarge by feedback? preprint.

SPONG, M. W. (1995). The swing up control problem for the acrobot. *IEEE Control Systems Magazine*, 15(1):49–55.

SPONG, M. W., and VIDYASAGAR, M. (1989). *Robot Dynamics and Control.* John Wiley & Sons, New York.

WEI, Q., DAYAWANSA, W. P., and LEVINE, W. S. (1995). Nonlinear controller for an inverted pendulum having restricted travel. *Automatica*, 31(6):841–850.

WHITTAKER, E. T. (1937). *A Treatise on the Analytical Dynamics of Particles and Rigid Bodies.* Cambridge University Press, Cambridge, U.K., 4th edition.

YAMAKITA, M., NONAKA, K., and FURUTA, K. (1993). Swing up control of a double pendulum. In *Proceedings of 1993 American Control Conference*, pages 2229–2233.

YAMAKITA, M., SUGAHARA, M. I. Y., and FURUTA, K. (1995). Robust swing up control of a double pendulum. In *Proceedings of 1995 American Control Conference*, pages 290–295.

ZHAO, J., and SPONG, M. W. (2001). Hybrid control for global stabilization of the cart-pendulum system. *Automatica*, 37(12):1941–1951.